REPORT CDOT-2023-06 May 2023

# Rehabilitation and Load Rating of Deteriorated Timber Bridges in Colorado: Parametric Investigations and Implementation

APPLIED RESEARCH & INNOVATION BRANCH

Yail Jimmy Kim

COLORADO
Department of Transportation

The contents of this report reflect the views of the author(s), who is(are) responsible for the facts and accuracy of the data presented herein. The contents do not necessarily reflect the official views of the Colorado Department of Transportation or the Federal Highway Administration. This report does not constitute a standard, specification, or regulation.

**Technical Report Documentation Page**

| 1. Report No.<br>CDOT-2023-06 | 2. Government Accession No. | 3. Recipient's Catalog No. |
|---|---|---|
| 4. Title and Subtitle<br>Rehabilitation and Load Rating of Deteriorated Timber Bridges in Colorado: Parametric Investigations and Implementation | | 5. Report Date<br>May 2023<br>6. Performing Organization Code |
| 7. Author(s)<br>Yail Jimmy Kim | | 8. Performing Organization Report No.<br>CDOT-2023-06 |
| 9. Performing Organization Name and Address<br>University of Colorado Denver<br>1200 Larimer St., Denver, CO 80217 | | 10. Work Unit No. (TRAIS)<br>11. Contract or Grant No. |
| 12. Sponsoring Agency Name and Address<br>Colorado Department of Transportation - Research<br>2829 W. Howard Pl.<br>Denver, CO 80204 | | 13. Type of Report and Period Covered<br>14. Sponsoring Agency Code |
| 15. Supplementary Notes<br>Prepared in cooperation with the US Department of Transportation, Federal Highway Administration | | |


16. Abstract

This report presents three major aspects that are related to the evaluation of timber bridges with and without repair: i) laboratory testing, ii) finite element modeling, and iii) load ratings. In addition, worked examples are provided to demonstrate the implementation of research findings. The first part of the report explores the effectiveness of various retrofit techniques in improving the flexural behavior of structural timber. The second part presents the behavior of a timber bridge strengthened with lag bolts, carbon fiber reinforced polymer (CFRP) sheets, and hollow structural sections (HSS). The third part discusses load ratings for timber bridges repaired with HSS. A mechanics-based rating approach is proposed to holistically rate these bridges before and after the repair. The capacity of the girders with the steel beams is as high as 2.56 times that of the control girders. Likewise, the allowable stress of the timber is improved by a factor of 1.39 and 2.09 for flexure and shear, respectively. The effectiveness of the repair becomes pronounced when the deterioration level of the timber girders rises, and the geometric properties of the steel beams are a crucial consideration that alters the rating of the repaired girders. The placement of grouped steel beams is recommended to raise the efficacy of the repair system.

Implementation

A new rating method is proposed for constructed timber bridges repaired with and without steel beams.


| 17. Keywords | 18. Distribution Statement |
|---|---|
| bridges; development; field-testing; live load distribution factor; modeling; rating; repair; timber | This document is available on CDOT's website http://www.coloradodot.info/programs/research/pdfs |

| 19. Security Classif. (of this report) | 20. Security Classif. (of this page) | 21. No. of Pages | 22. Price |
|---|---|---|---|
| Unclassified | Unclassified | | |

## ACKNOWLEDGMENTS

The research team would like to acknowledge valuable guidance and thought-provoking comments provided by the study panel members: Natasha Butler (Staff Bridge, CDOT), Trever Wang (Staff Bridge, CDOT, Retired), Jacob O'Brien (Staff Bridge, CDOT), Scott Husen (Staff Bridge, CDOT), Hoang Bui (Staff Bridge, CDOT), Nick Chavez (Staff Bridge, CDOT), Ahmed Ibraheem (Staff Bridge, CDOT), and Spencer Tucker (Federal Highway Administration). The research team is also grateful to Thien Tran (Applied Research and Innovation Branch, CDOT) for his comprehensive support and administrative assistance.

## Executive Summary

This report presents three major aspects that are related to the evaluation of timber bridges with and without repair: i) laboratory testing, ii) finite element modeling, and iii) load ratings. In addition, worked examples are provided to demonstrate the implementation of research findings. The first part of the report explores the effectiveness of various retrofit techniques in improving the flexural behavior of structural timber. For realistic representation with regard to site application, timber girders are salvaged from a decommissioned highway bridge that has been in service over several decades and are strengthened using lag bolts, carbon fiber reinforced polymer (CFRP) sheets, and hollow steel sections (HSS): the retrofitted girders are referred to as Bolt, CFRP, and HSS, respectively. Each category is repeated three times, and the responses of the 12 unstrengthened and strengthened girders are comparatively evaluated. From a load-carrying capacity point of view, lag bolting is not effective; however, CFRP and HSS result in a capacity increase of up to 156.2% relative to the control girder (Cont). Regarding the load-displacement relationship of these girders, the retrofit systems alter the post-peak behavior of the timber; for instance, the lag bolts periodically embedded along the specimens bring about pseudo-yield plateaus, which preclude the abrupt failure of the Bolt girder. In addition, the amount of dissipated energy increases in all upgraded girders owing to the presence of the retrofit systems. The failure modes of the individual girders are unique, depending upon the type of retrofit. Except for the HSS girder, the effective elastic moduli of the Cont, CFRP, and HSS girders agree with those measured by a stress wave timer. Parameter estimation theoretically infers the possible range of the experimental findings and ensures the adequacy of the test program.

The second part presents the behavior of a timber bridge strengthened with lag bolts, carbon fiber reinforced polymer (CFRP) sheets, and hollow structural sections (HSS). The 83-old bridge is composed of three spans, supported by 14 Douglas Fir girders, and is tested employing truck loadings of 28 kips and 60 kips. Three-dimensional finite element models are formulated to study the flexural response of the bridge with and without the retrofit options. The magnitude of the truck load dominates the degree of dispersion in girder deflections and alters the shape of probability density functions, which are associated with behavioral uncertainty. The effectiveness of strengthening is apparent in terms of reducing the exceedance probability of deflection limits and increasing reliability indices above the design threshold of $\beta$ = 3.5,

stipulated in bridge specifications. Among the three methods, the stiffening efficiency of the HSS option is higher at the system level; however, the use of CFRP is most efficient at the member level. Live load distribution factors are examined and implementable recommendations are provided for practice. Parametric investigations clarify the efficacy of variable HSS sizes and the ramifications of a permit truck weighing 100 kips.

The third part discusses load ratings for timber bridges repaired with hollow steel sections (HSS) made of ASTM A500C. Two bridges are selected (F-22-V and H-20-T built in 1938 and 1935, respectively) and upgraded with HSS steel beams. For numerical analysis, finite element models are formulated and validated. The model is then employed to investigate the behavior of the bridges under 17 live loads specified in the manual of a transportation agency. A mechanics-based rating approach is proposed to holistically rate these bridges before and after the repair. The configuration and position of the live loads affect the bending moment and shear force of the bridges; especially, the spacing of axles plays a role in increasing deflections. The capacity of the girders with the steel beams is as high as 2.56 times that of the control girders. Likewise, the allowable stress of the timber is improved by a factor of 1.39 and 2.09 for flexure and shear, respectively. The effectiveness of the repair becomes pronounced when the deterioration level of the timber girders rises, and the geometric properties of the steel beams are a crucial consideration that alters the rating of the repaired girders. The placement of grouped steel beams is recommended to raise the efficacy of the repair system. Owing to the repair, the failure probability of the bridges is reduced by up to 99.2%.

**Implementable Outcomes**: The research suggests a new rating method for repaired timber bridges. Current rating methodologies stated in the CDOT Bridge Rating Manual are incomplete and inconsistency is noticed before and after repair. By adopting the proposed methodologies, consistent rating outcomes are expected. Additionally, refined live load distribution factors are suggested to enhance the rating process of constructed timber bridges.

**Keywords**: bridges; development; field-testing; live load distribution factor; modeling; rating; repair; timber

## List of Tables

## List of Figures

## Table of Contents

**Part II: Structural Strengthening of a Constructed Timber Bridge**



**Part III: Rating of Constructed Timber Bridges Repaired with Steel Beams**

# Part I: Retrofit of Salvaged Timber Girders Using Various Techniques

## I.1. INTRODUCTION

Although steel and concrete are the major materials for the construction of highway bridges, reliance on timber is still noteworthy especially in nonurban areas. Several advantages of using wood include the abundance of materials, light weight, expedient fabrication, natural appearance, resistance to deicing chemicals, and affordable cost (Ou and Weller 1986). The number of timber bridges in the United States is counted to be 48,759 (24,267 for all timber superstructures and 24,492 for timber decks on steel stringers) and a considerable amount of them have been erected in Midwestern states such as Illinois, Nebraska, Oklahoma, and Texas (Brashaw et al. 2013). Like other structural types, timber elements deteriorate over time. The sources of strength degradation involve biological decay, weathering, ultraviolet rays, trapped moisture, heat, and over loading (Asif 2009; Mahini et al. 2016; Nasir et al. 2021). Of particular concern is an increase in live load that raises unfavorable distress (Peterson and Gutkowski 1999). In many circumstances, the service life of timber bridges is estimated from 20 years to 100 years alongside proper maintenance (Ou and Weller 1986; Peterson and Gutkowski 1999; Brashaw et al. 2013). A case study reports that extensive decay, outdated technical actions, and improper decisions brought about the collapse of a 6-span timber bridge in the state of Oregon (Dethlefs and Martin 2009). A demand for improving the load-bearing capacity of timber bridges is thus prevalent in the infrastructure community; in other words, opportune activities are essential to alleviate the likelihood of catastrophic events and to prolong the intended functionality within the boundary of a budgetary appropriation. Specifically, timely inspections and strengthening are crucial components to warrant the safe operation of aged timber elements.

Structural rehabilitation is continually evolving technology that can address the immoderate challenges of reconstruction, stemming from finance and traffic interruption. Identifying a suitable retrofit method helps practitioners better manage deficient highway bridges. Structural timber may be upgraded by conventional and emerging approaches. The use of metals has been a routine practice and existing efforts may be subdivided into two categories: connection details and supplementary members. Franke et al. (2015) described a way to reinforce timber girders with mechanical bolts. The members embedded with inclined bolts at $45^{o}$

outperformed those with vertically installed ones in terms of capacity and ductility. Schiro et al. (2018) examined the behavior of timber elements connected with assorted bolt types. The relative stiffness of the adjoined elements was critical for the development of interfacial strength, and the geometric configuration of the bolts was a predominant factor influencing the failure plane of the connections. Kode et al. (2021) tested wooden diaphragms fastened to chord members using lag bolts as part of a repair project for rural timber bridges. The connection of the members was vulnerable to cyclic loading, and the excessive shear displacement of the bolted regions precipitated the structural system's failure. Dahlberg et al. (2015) provided guidance to repairing timber bridges with steel channels and plates. These subsidiary elements can be mounted mechanically and increase the capacity of primary members. Corradi et al. (2019) compiled repair techniques pertaining to conjoining steel profiles. The attached steel sections enabled partial composite action and resisted flexural stresses. A representative non-traditional rehabilitation material is carbon fiber reinforced polymer (CFRP). This advanced composite, consisting of carbon fibers and a resin matrix, offers notable benefits, namely, noncorrosiveness, high strength and modulus, negligible thermal expansion, light weight, minimal labor, and satisfactory long-term durability (ACI 2017). Externally bonded CFRP sheets have been successfully used for strengthening concrete structures (Naser et al. 2019) and, albeit uncommon, the non-metallic composites were often chosen as an alternative for retrofitting timber structures (Zhang et al. 2022). Vahedian et al. (2019) studied the response of timber beams strengthened with CFRP sheets. The bonded width, length, and layers of CFRP controlled the maximum bending moment, elastic modulus, and displacement of the beams. A correlation was found between the bond properties and ductility of the beams at failure. Isleyen et al. (2021) carried out an experimental program with CFRP-retrofitted timber beams incorporating anchorage. The beams were predrilled to install fan-type anchors at multiple locations. Compared with control beams, the behavior of the upgraded beams was enhanced, and the anchors positioned near the termination of the CFRP sheets were beneficial for ductility. Other significant subjects available in literature are the bond-slip of a CFRP-timber interface (Biscaia et al. 2016), CFRP stress on a timber substrate (Jesus et al. 2012), hybrid CFRP layouts (Rescalvo et al. 2019), damage evolution in CFRP-retrofitted timber (Khelifa et al. 2015), field demonstration (Meier 2000), and structural health monitoring of CFRP-bonded timber beams (Rescalvo et al. 2018).

Notwithstanding a plethora of knowledge on respective retrofit techniques, there still is a dearth of synthetic endeavors to comparatively elucidate the operational mechanisms in relation to the preservation of timber structures aged under actual service environments. Consequently, bridge engineers tend to select a strengthening method on the basis of previous experience, rather than a systematic process of gathering relevant information. Furthermore, most published papers dealt with timber elements that had not been exposed to detrimental load effects (Bhat 2021; Dar et al. 2021; Silwa-Wieczorek et al. 2021), so that experimental findings may not realistically represent the efficaciousness of retrofit methodologies. This part presents holistic investigations into the performance of the foregoing retrofit techniques. Timber girders salvaged from a decommissioned bridge that has been in service over several decades are strengthened with lag bolts, CFRP sheets, and steel sections and tested to establish an organized strategy for translating research into practice. Statistical modeling estimates the possible ranges of parameter values at the population level, which can theoretically generalize technical findings.

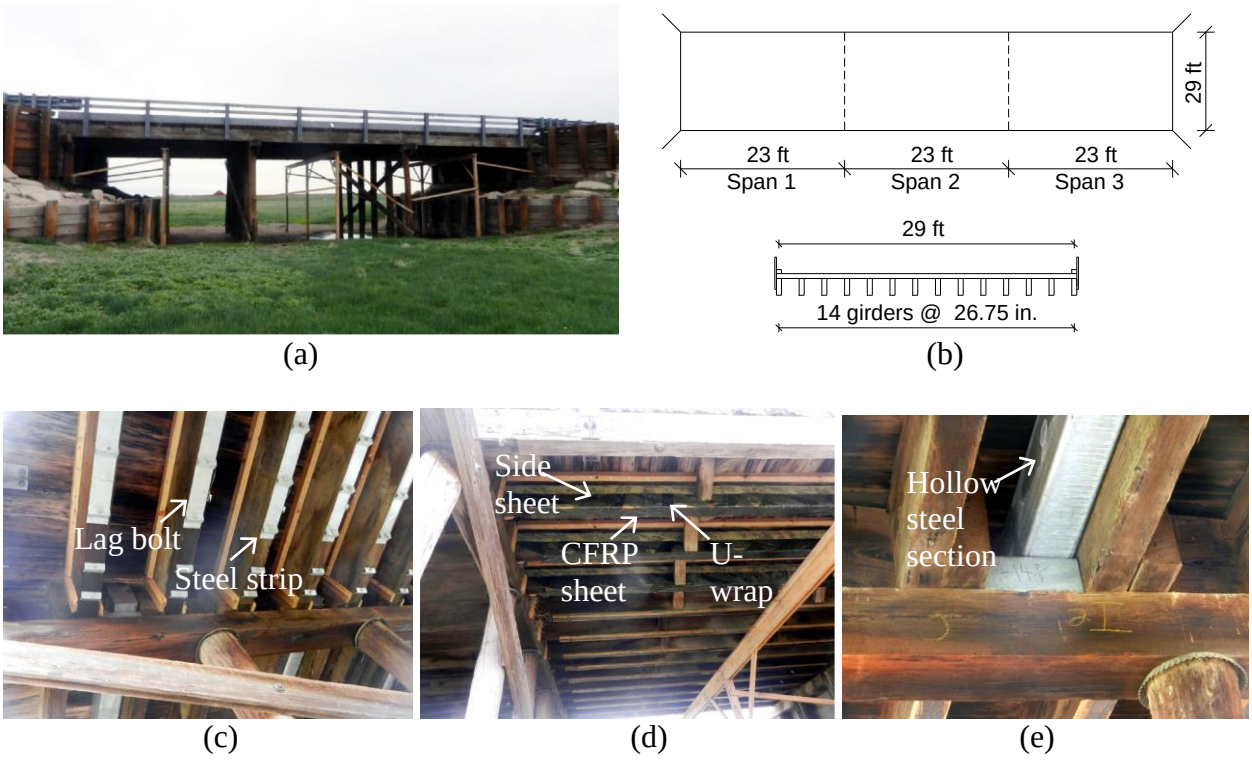


**Fig. I.1**. F-22-V Bridge: (a) overview; (b) dimensions; (c) retrofit with lag bolts; (d) retrofit with CFRP sheets; (e) retrofit with hollow steel section

## I.2. BACKGROUND

The F-22-V Bridge situated in Washington County, Colorado, USA, was constructed in 1938 with Douglas Fir lumber (Fig. I.1(a)). The load-bearing system was composed of 3 spans and 14 girders (23 ft long, each), as depicted in Fig. I.1(b). Due to aging and deterioration, the superstructure of the bridge was rated to be 4 (*Poor Condition*, FHWA 1995) and the Owner (Colorado Department of Transportation) decided to strengthen the girders using three approaches in each span (Figs. I.1(c) to (e)): lag bolting, CFRP, and hollow steel section (HSS). The size of the bolts was 0.75 in. in diameter, which was embedded every 16 in. at an angle of $45^o$ with steel strips (Fig. I.1(c)). The CFRP sheets were bonded to the bottom and sides of the girders (Fig. I.1(d)). The rectangular HSS beams, 12 in. deep by 8 in. wide by 0.31 in. thick, were mounted adjacent to the girders and mechanically fastened (Fig. I.1(e)). Details of these applications (e.g., material properties and installation procedures) are described in the next section. To confirm the effectiveness of the individual approaches, girders were taken out of a decommissioned bridge having similar characteristics to the retrofitted bridge and were tested in the laboratory.

## I.3. EXPERIMENTAL PROCEDURE

Timber girders taken from a constructed bridge are tested under flexural loading. Below is a summary of materials, specimens, retrofit systems (lag bolting, CFRP, and HSS, as enumerated in Table I.1), and evaluation methods.

**Table I.1**. Girder details

| Girder | Retrofit | Ultimate load (kip) | | Modulus of rupture (psi) | |
|---|---|---|---|---|---|
| | | Individual | Average | Individual | Average |
| Cont-1 | None | 9.26 | 8.72 | 5,482 | 5,154 |
| Cont-2 | None | 8.00 | | 4,728 | |
| Cont-3 | None | 8.88 | | 5,250 | |
| Bolt-1 | Lag bolts | 6.68 | 7.01 | 3,945 | 4,143 |
| Bolt-2 | Lag bolts | 7.06 | | 4,177 | |
| Bolt-3 | Lag bolts | 7.28 | | 4,307 | |
| CFRP-1 | CFRP | 9.33 | 9.55 | 5,526 | 5,647 |
| CFRP-2 | CFRP | 10.07 | | 5,961 | |
| CFRP-3 | CFRP | 9.24 | | 5,453 | |
| HSS-1 | Steel beam | 22.41 | 22.35 | 13,256 | 13,223 |
| HSS-2 | Steel beam | 20.30 | | 12,009 | |
| HSS-3 | Steel beam | 24.35 | | 14,402 | |

### I.3.1. Materials

The nominal dimension of the salvaged Douglas Fir girders was 6 in. wide by 20 in. deep by 24 ft long and each one weighed approximately 507 lb. After transporting to the laboratory, the girders were sawcut (6 in. wide by 6.7 in. deep by 130 in. long), considering the space of the test site and the capacity of an actuator (Fig. I.2(a)). According to the USDA Wood Handbook (USDA 2010), the elastic modulus of those girders in the parallel-to-grain direction was expected to be $E_w$ = 1,566 ksi to 1,943 ksi with a specific gravity of 0.45 to 0.50. The diameter of threaded steel bolts was $d_b$ = 0.75 in. and their grade was ASTM A354 BC (yield strength = 109 ksi, ASTM 2018). Unidirectional CFRP sheets had the succeeding nominal properties based on a thickness of $t_f$ = 0.013 in.: elastic modulus ($E_f$) = 34,084 ksi, tensile strength ($f_{fu}$) = 550 ksi, and rupture strain ($\varepsilon_{fu}$) = 1.5%. The bonding agent for CFRP was a two-part epoxy: a resin and a hardener were blended at a mass ratio of 4:1 for about 5 min. until a homogeneous mixture was obtained. The manufacturer-reported tensile strength and elastic modulus of the 7-day-cured epoxy were $f_{eu}$ = 4,931 psi and $E_e$ = 508 ksi, respectively. The size of a hollow steel section (HSS) was 2 in. wide by 6 in. deep with a wall thickness of 0.25 in. The cold-formed rectangular HSS possessed an elastic modus of $E_s$ = 29,000 ksi and a yield strength of $f_y$ = 45,686 psi (ASTM A500 Grade B, ASTM 2021a).

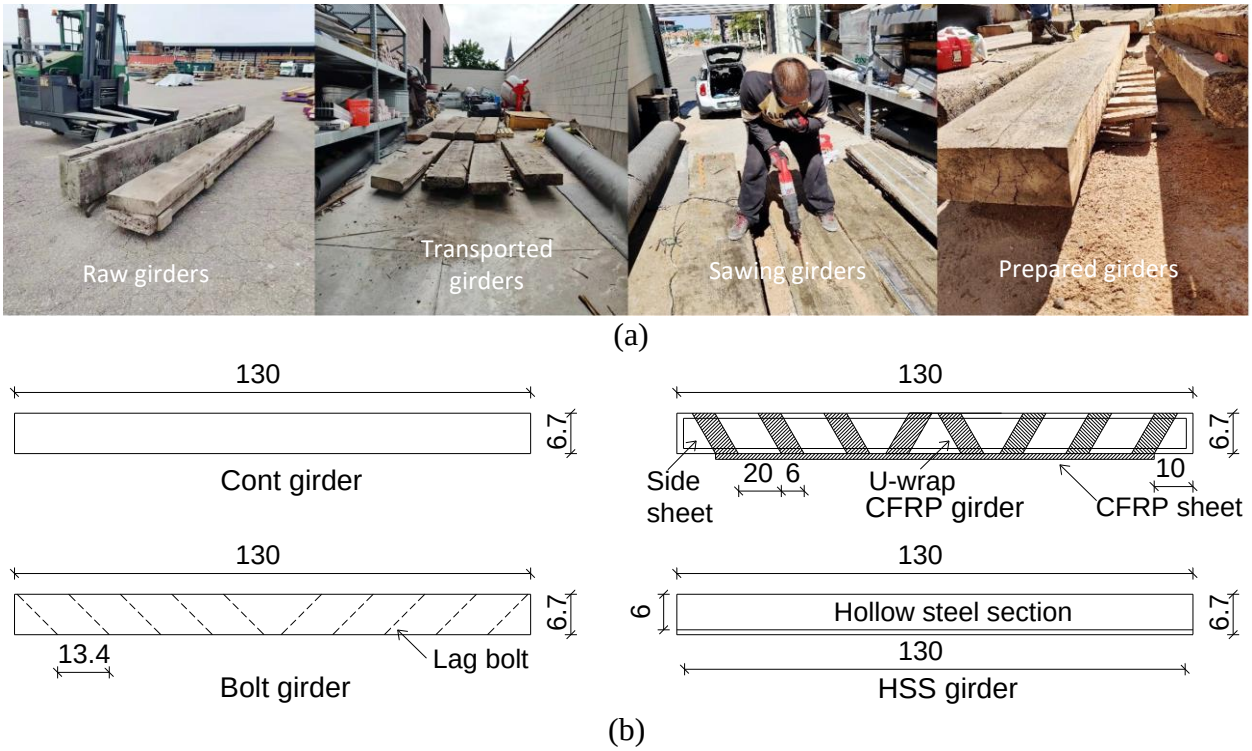


**Fig. I.2**. Preparation for laboratory testing: (a) salvaged timber girders; (b) control and retrofitted girders (units in in.)


(a)


(b)


(c)

**Fig. I.3**. Retrofit procedure: (a) Bolt; (b) CFRP; (c) HSS

### I.3.2. Retrofit Schemes

Conforming to the rehabilitation of the F-22-V Bridge, the prepared girders were retrofitted (Fig. I.2(b)). It should be noted that the laboratory application was scaled (Fig. I.3) as per the ratio of the salvaged and prepared girders; scilicet, the number of bolts, width of CFRP, and size of HSS were adjusted in accordance with the reduced size of the girders. It is noted that the steel strips installed underneath the in-situ girders (Fig. I.1(c)) were not used because these were not available in the repository of CDOT. For those to be upgraded with the lag bolts (Fig. I.3(a)), holes (dia. = 0.75 in.) were predrilled to a depth of 9.0 in. at an angle of 45$^{o}$; then, the threaded bolts were inserted using an impact wrench and extruded portions were cut out. This process was repeated along the girder at hole spacings of 13.4 in. Regarding CFRP-strengthened girders (Fig.

I.3(b)), the bottom and sides were cleansed with a wet towel and fully dried to eliminate unnecessary residues on the surface; next, the epoxy was evenly pasted on the bottom for bonding a single layer of the CFRP sheet (4 in. wide, left of Fig. I.3(b)). To prevent premature debonding failure, U-wrap CFRP sheets (one layer with 6 in. in width) were bonded at an angle of 30$^o$ as in the procedure of the longitudinal sheet (middle of Fig. I.3(b)). Finally, for the preservation of the CFRP system, one more layer of the sheets (4 in. wide) was bonded along both sides of the girders (right of Fig. I.3(b)). The retrofitted girders were cured at room temperature for 7 days. The HSS beams, precut to a length of 130 in., were drilled in the middle and near the ends (left of Fig. I.3(c)). After pairing with the timber girder (middle of Fig. I.3(c)), fasteners (dia. = 0.4 in.) were installed with washers and nuts (right of Fig. I.3(c)).

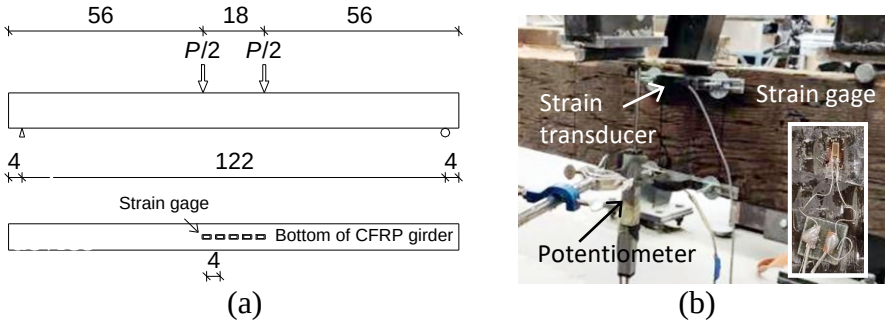


**Fig. I.4**. Test setup: (a) flexural loading (units in in.); (b) instrumentation

### I.3.3. Test Approaches

#### I.3.3.1. Flexural loading

The control and retrofitted girders were simply supported (Fig. I.4(a)) and monotonically loaded at a rate of 0.039 in./min until failure occurred. Each of the Cont, Bolt, CFRP, and HSS categories (Table I.1) was replicated three times (12 girders in total) to address possible uncertainties that could be associated with in-situ deterioration. A load cell and a linear potentiometer were positioned at midspan to record the load and the displacement, respectively (Fig. I.4(b)). The strain transducers, placed 0.8 in. from the top and bottom of the girders, logged compressive and tensile strains under the flexural loading. For the CFRP girders, 5 strain gages were bonded along the bottom at spacings of 4 in. (Fig. I.4(a)). To visually assess the initiation and progression of damage in all girders, a digital image correlation (DIC) technique was utilized. A camera (5 mega pixels) equipped with an automatic macro lens at a maximum aperture of 2.8

monitored the midspan deformation of the girders. The quality of digital images was enhanced by painting the constant moment zone of the girders in white. A computerized multichannel Ethernet system collected all test data.

## I.4. TEST RESULTS

Experimental data are collected and analyzed with a focus on the flexural behavior of control and retrofitted girders, including capacity, displacement, energy, strain, and failure. The applicability of non-destructive testing is studied against the mechanical response of those girders.

### I.4.1. Load-Carrying Capacity

Figure I.5(a) charts the average ultimate loads of the test girders. Contrary to expectations, the flexural capacity of the retrofitted girder using lag bolts ($P_u$ = 7.01 kips) did not reach the capacity of the control girder ($P_u$ = 1.53 kips). This observation is attributable to the fact that the embedded bolts caused geometric discontinuities along the grains and prompted the local failure of the girder (details will be elaborated). A capacity increase of 9.5% and 156.2% was noticed for the CFRP and HSS girders ($P_u$ = 9.55 kips and 3.91 kips, respectively) relative to the Cont girder. To appraise the performance safety of these girders against the required safety of the American Association of State Highway and Transportation Officials (AASHTO) Load and Resistance Factor Design (LRFD) Bridge Design Specifications (BDS) (AASHTO 2021), a reliability index ratio ($\beta_{\text{ratio}}$) is defined as

$$\beta_{ratio} = \frac{\beta(Experimental)}{\beta(AASHTO)} \tag{I.1}$$

$$\beta(Experimental) = \frac{R - E}{\sqrt{\sigma_R^2 + \sigma_E^2}} \tag{I.2}$$

where $\beta(Experimental)$ and $\beta(AASHTO)$ are the reliability indices from the test and AASHTO LRFD BDS ($\beta(AASHTO)$ = 3.5), respectively; $R$ is the flexural resistance of the control or retrofitted timber girder (equivalent to $P_u$ in the experimental program); $E$ is the applied service load; and $\sigma_R$ and $\sigma_E$ are the standard deviations of the flexural resistance and the service load,

respectively. For the calculation of Eq. I.1, $E$ was assumed to be 50% of the control girder's capacity and $\sigma_E$ = 0.18 was taken from literature (Barker and Puckett 2021). As shown in Fig. I.5(b), the performance safety of the Cont girder ($\beta_{ratio}$ = 1.2) exceeded the demand of AASHTO LRFD BDS ($\beta_{ratio}$ = 1.0). Contemplating that the $\beta$ index measures the degree of safety to a failure state, the performance of the salvaged control girders is believed adequate under typical service loading. However, such a member-level assessment does not necessarily mean that the global performance of the decommissioned bridge was satisfactory when loaded with rating trucks: the Allowable Stress Rating (ASR) method is customarily used for timber bridges (AASHTO 2017). The $\beta_{ratio}$ of the Bolt girder was below unity due to the reduced capacity; by contrast, the ratios of the CFRP and HSS girders were 1.6 and 2.4, respectively. Although the number of specimens was limited, the CFRP and HSS retrofit methods are recommended for enhancing the flexural capacity and performance reliability of timber girders.

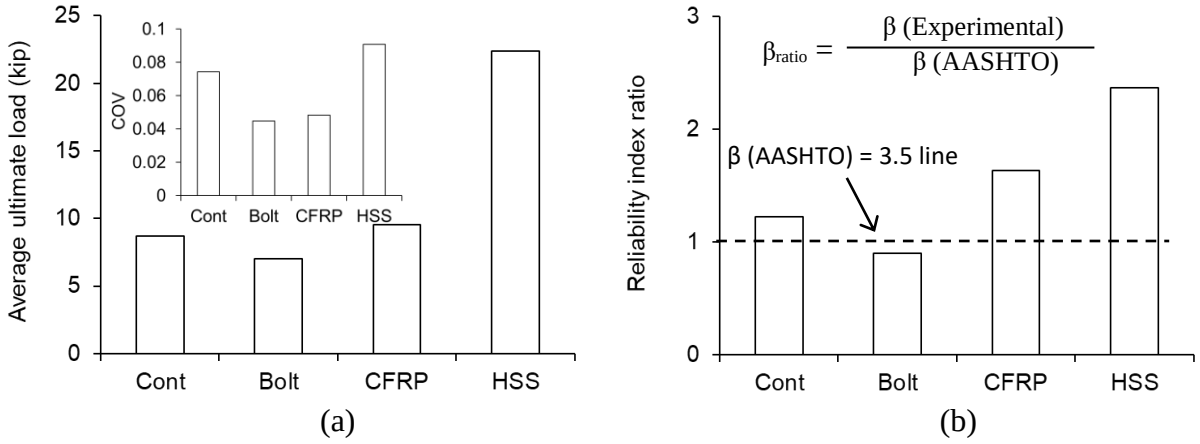


**Fig. I.5**. Flexural capacity: (a) average capacities; (b) performance safety

### I.4.2. Flexural Behavior

#### I.4.2.1. Load-displacement relationship

Given in Fig. I.6 are the load-displacement curves of the girders. The control girders revealed consistent responses up to a load of 6.74 kips at which the behavior of one girder (Cont-2) deviated from the linear propensity on account of the early rupture of the tensile grains near midspan (Fig. I.6(a)). A linearly increasing relationship was also visible in the Bolt girders, followed by pseudo-yield plateaus (Fig. I.6(b)). The efficacy of the lag bolts can, thus, be found in the remarkably improved post-peak behavior. Mechanically saying, the vertical force

component of the diagonally inserted bolts resisted the downward displacement of the girders and, in addition, the thread engagement with the substrate timber enabled the progressive splitting of the grains, as substantiated by the jagged responses in the plateau region. The gradual failure of the CFRP girders (Fig. I.6(c)) implies that the U-wraps and side sheets restrained the deformation of the girders within the retrofitted areas without delamination. The elevating slope of the HSS girders altered when the steel beam yielded (Fig. I.6(d)), and abrupt load drops were noted with the fracture of the tensile grains. The degraded performance of HSS-2 was ascribed to the spontaneous local imperfections that weakened the load-bearing ability of the girder.

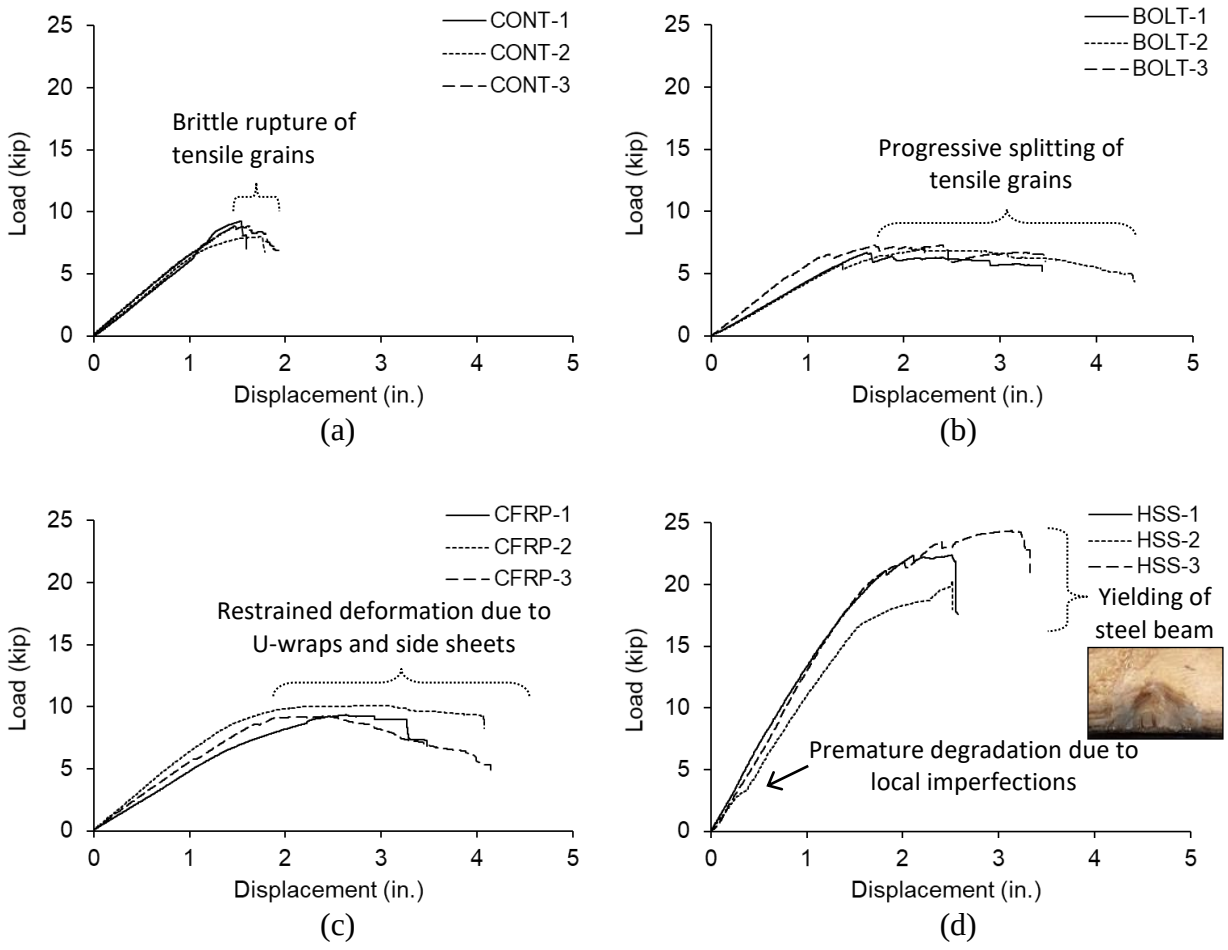


**Fig. I.6**. Load-displacement: (a) control; (b) lag bolts; (c) CFRP; (d) hollow steel section

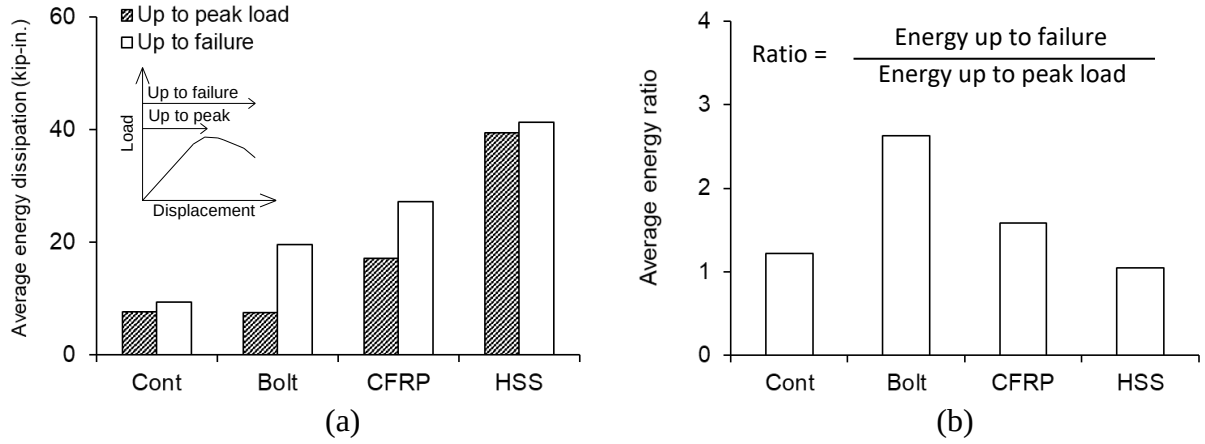


**Fig. I.7**. Energy dissipation: (a) up to peak and failure states; (b) average energy ratio

### I.4.2.2. Energy dissipation

The dissipated energy of the girders was acquired by numerically integrating the load-displacement curves and is graphed in Fig. I.7(a). For measuring ductility characteristics, two energy levels were classified up to the peak load and to the failure (termination of the test owing to the physical disintegration of the specimens). Even if the energy levels up to the peak loads of the Cont and Bolt girders were alike (7.72 lb-in. and 7.49lb-in., respectively), the levels up to the failure differed substantially (9.42 lb-in. and 19.69 lb-in., respectively). By bonding the CFRP sheets, both of these energy levels were further ameliorated over 224% (peak) and 290% (failure) relative to those of the Cont girder. As far as the HSS girder is concerned, a remarkable increase was observed in consequence of sharing the applied load with the steel beam. Figure I.7(b) exhibits a ratio between the energy values dissipated up to the failure and the peak load of the girders, which is useful to characterize the imminent loss of load-bearing ability passing through the maximum resistance. The Cont and HSS girders showed the ratios of 1.22 and 1.05, respectively. These point out that care should be taken when timber girders are retrofitted with steel sections and subjected to a load significantly heavier than ordinary service vehicles (e.g., nonstandard trucks requiring special permit), which may lead to a sudden collapse of the bridge system. The high energy ratio of 2.63 in the Bolt girder suggests the potential of a hybrid retrofit scheme using lag bolts to extend the post-peak energy dissipation of upgraded members. The ratio of 1.58 in the CFRP girder, positioned midway between those of the Bolt and HSS girders, was overall satisfactory and such a strengthening method is implementable for practice.

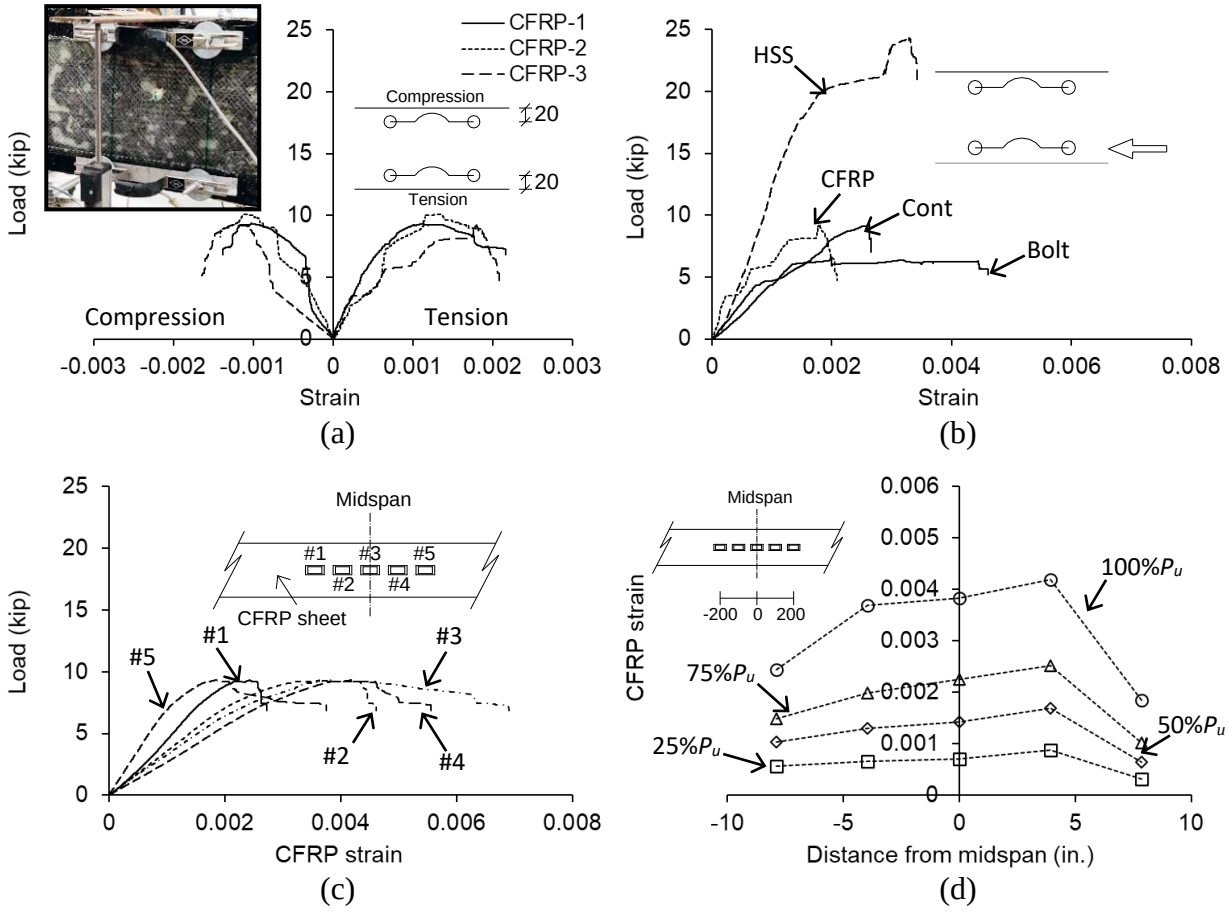


**Fig. I.8**. Load-strain: (a) tensile and compressive strains of CFRP girders; (b) comparison of tensile strains; (c) strains along CFRP sheet; (d) incremental CFRP strains

### I.4.2.3. Strain development

The strains of the test girders were reasonably repeated in each test (Fig. I.8(a)), which are acceptable in light of their random deterioration in the field. The magnitude of the tensile strains across the board was greater than that of the compressive strains. These asymmetric responses denote that the wood fibers below the neutral axis were more responsive to the flexural loading. Given that the modulus of rupture dominates the flexural capacity of timber elements, the tensile strains of the control and retrofitted girders are evaluated in Fig. I.8(b). The initial slope of the retrofitted girders seemed somewhat stiffer due to the contribution of the strengthening materials. The strain of the Bolt girder was lengthened beyond 0.004 in line with the aforementioned progressive splitting of the grains; contrarily, the strain of the CFRP girder was 0.0021 at failure. The strain development of the HSS girder was steady until the engaged steel beam yielded. Figure I.8(c) displays the strains of CFRP in the longitudinal direction. Complying with the

degree of curvature, the gages near midspan (#2, #3, and #4) recorded higher strains than others (#1 and #5). Considering the rupture strain of $\varepsilon_{fu}$ = 0.015, the application of multiple CFRP layers was figured out to be conservative (i.e., the maximum usable strain was 46% of the ultimate strain). The incremental strain profiles of the longitudinal CFRP sheet are presented in Fig. I.8(d). The flat shape at 25%$P_u$ became concave down with an increase in the load level under the nonuniform curvature along the span, and the sign of debonding was not detected (a spike-like strain variation is observed if local debonding takes place, Lam et al. 2007).

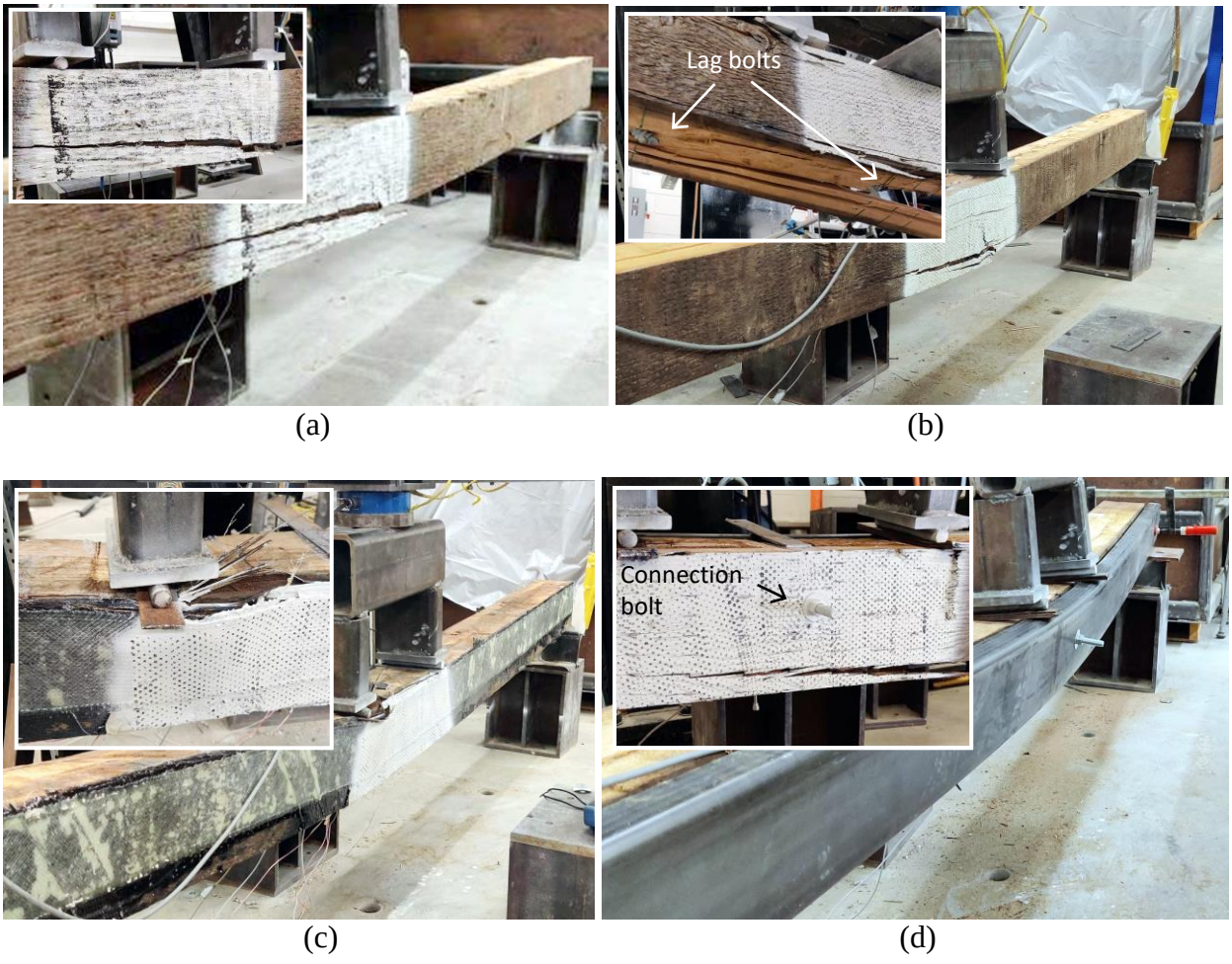


**Fig. I.9**. Failure mode: (a) Cont; (b) Bolt; (c) CFRP; (d) HSS

### I.4.3. Failure Mode

#### I.4.3.1. Cause of failure

Pictured in Fig. I.9 are the failure modes of selected girders (the inset photos were taken immediately after failure). For the Cont girder (Fig. I.9(a)), grain-splitting initiated in the tension

zone right below a loading point and advanced in the horizontal direction at an angle of 30°. While the Bolt girder revealed a splitting pattern similar to the control (Fig. I.9(b)), the fractured segments were not localized because the lag bolts interfered with the progression of the splits and distributed stresses (Fig. I.9(b), inset). Unlike these girders, no perceivable damage was noticed in the CFRP girder except for the crushed grains underneath the loading point (Fig. I.9(c)). The pristine CFRP sheets at the global level confirm the adequacy of the strain-based bond assessment that was discussed in Fig. I.8(d). The bending of the timber-steel assembly was apparent, as shown in Fig. I.9(d), and their integrity was well preserved even with three connection bolts. The yielded steel beam demonstrated permanent plastic deformations and the timber girder suffered grain fractures (Fig. I.9(d), inset). No physical impairment was observed in the vicinity of the connection bolt, justifying the feasibility of the HSS retrofit method on site.

### I.4.3.2. Vision-based appraisal

Sequential images describing the failure of the test girders are provided in Fig. I.10. The scanned surface of the Cont girder clarified that no splitting occurred at 20%$P_u$ and 40%$P_u$ (Fig. I.10(a)); on the other hand, a wood check was captured at 80%$P_u$ and widened through 100%$P_u$. At a load level of 20%$P_u$ in the Bolt girder (Fig. I.10(b)), an abnormality was identified at the location of an embedded lag bolt, which served as the weak link of the retrofitted girder. Guided by the direction of the lag bolt, the formed damage was conspicuous and the flexural loading resulted in the horizontal grain split (40%$P_u$ to 100%$P_u$). The CFRP girder did not exhibit noticeable deterioration up to 40%$P_u$, other than the concentrated stress beneath the loading point (Fig. I.10(c)). The inclined vertical distress represented by the reddish contours at 80%$P_u$ and 100%$P_u$ accounts for the compression failure of the CFRP girder (Fig. I.10(c)). It is worth reporting that marginal surface-level flaws were discernible along the bond-line of the side sheet (80%$P_u$ and 100%$P_u$), indicating the enlarged mismatch with the substrate that was induced by shear slipping. For the HSS girder (Fig. I.10(d)), anomalous deformations were not seen around the connection bolt and the grain splits led to the failure of the specimen.

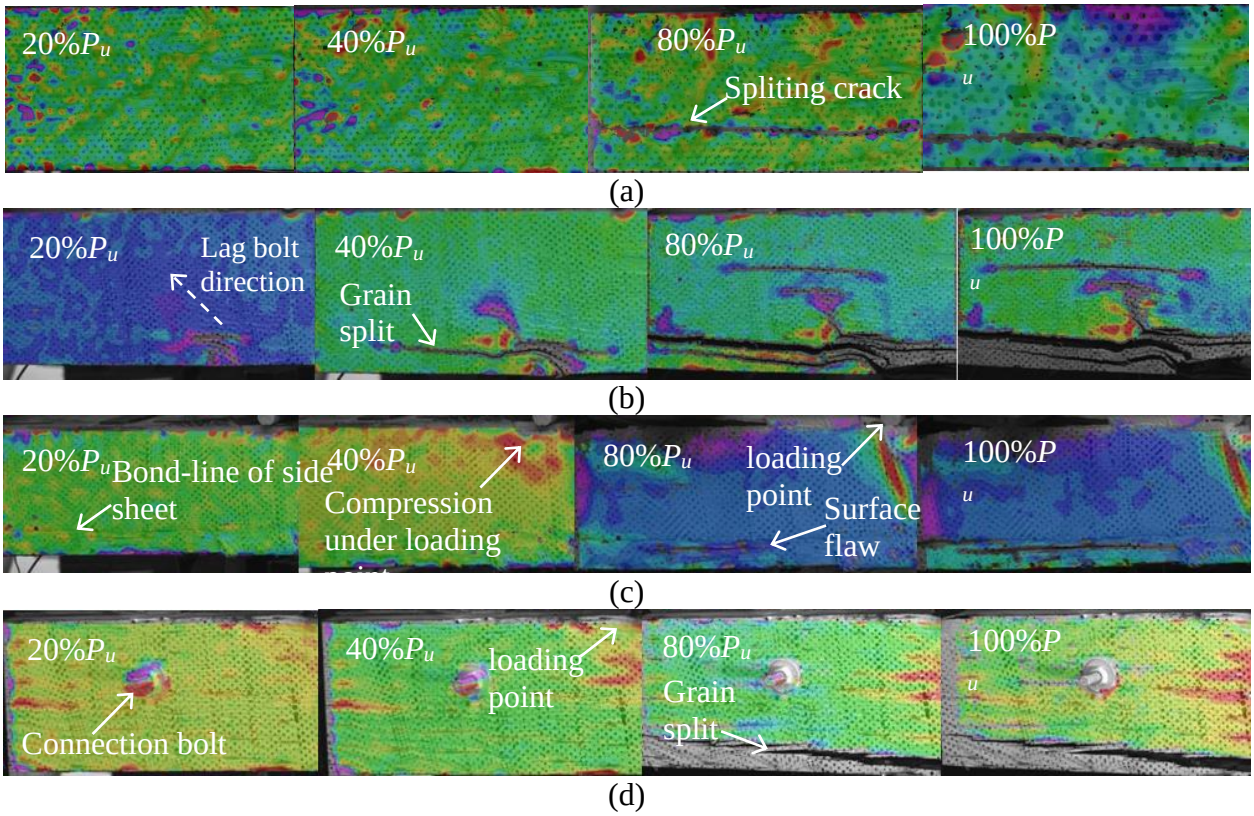


**Fig. I.10**. Sequential failure: (a) Cont; (b) Bolt; (c) CFRP; (d) HSS

### I.4.4. Effective Elastic Modulus

The effective elastic modulus of all specimens was mechanically determined by referring to ASTM D198 (ASTM 2021b, Eq. I.3) and ASTM D3043 (ASTM 2017, Eq. I.4)

$$E = \frac{Pa\left(3L^2 - 4a^2\right)}{4bh^3\Delta} \tag{I.3}$$

$$E = \frac{a\left(3L^2 - 4a^2\right)}{2bh^3}\left(\frac{P_{50\%} - P_{10\%}}{\Delta_{50\%} - \Delta_{10\%}}\right) \tag{I.4}$$

where $P$ are $\Delta$ are the applied load and the midspan displacement, respectively, under four-point bending (a load level of 60%$P_u$ was employed); $L$ is the span length; $a$ is the distance between the loading points; and $b$ and $h$ are the width and depth of the girder, respectively. The percentage in Eq. I.4 means a fraction of the ultimate load. As shown in Figs. I.11(a) and (b), Eqs.

I.3 and I.4 generated insignificant differences. The average elastic moduli of the control girders ($E$ = 1,566 ksi and 1,580 ksi from Eqs. I.3 and I.4, respectively) were close to the modulus obtained from the stress wave timer ($E$ = 1,348 ksi). Likewise, the moduli of the girders retrofitted with the bolts and CFRP were comparable between the outcomes of the destructive and non-destructive test methods. The average effective modulus of rupture (MOR) was 5,419 psi for the Cont girder and those for the Bolt, CFRP, and HSS girders were 4,148 psi, 5,642 psi, and 13,227 psi, respectively (Fig. I.11(c)). These discrepancies were attributed to their different failure characteristics. The relationship between the effective modulus of rupture and the elastic modulus is given in Fig. I.11(d). Irrespective of the retrofit method, the mutual dependency was linear with a determination coefficient of $R^2$ = 0.9486 (Fig. I.11(d), inset). Practically saying, the effective modulus of rupture for the strengthened timber can be conveniently estimated using the effective elastic modulus.

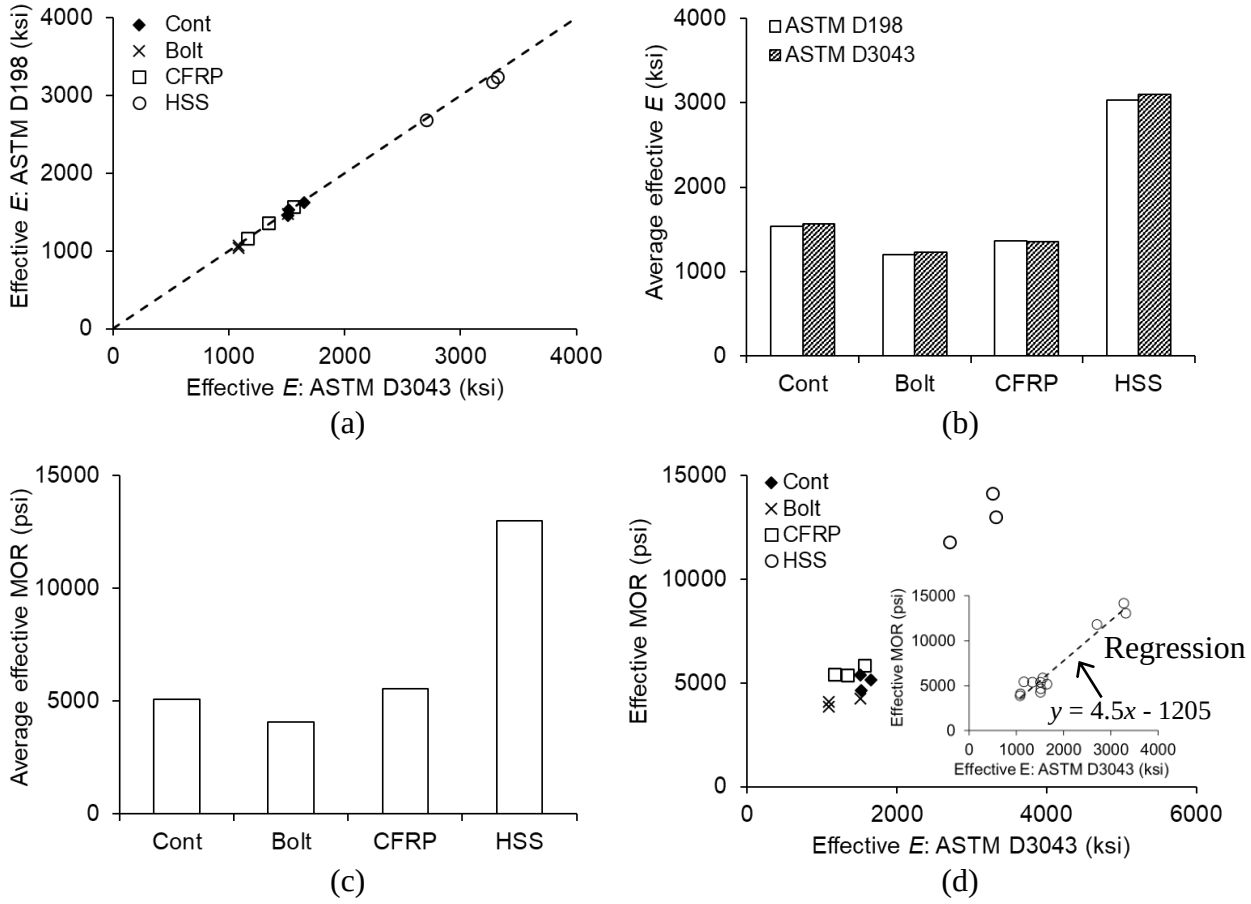


**Fig. I.11**. Determination of effective elastic modulus: (a) comparison between approaches; (b) average effective elastic modulus; (c) average effective modulus of rupture; (d) modulus rupture vs. elastic modulus

## I.5. STATISTICAL ESTIMATION

To overcome potential restrictions resulting from the limited number of test data, statistical techniques are adopted for estimating the probable range of capacity variations. Outlined below are the methodologies and implementation that can impart practical knowledge to assist bridge engineers.

### I.5.1. Estimation

The above-explained load-carrying capacities of the timber girders may not fully encompass in-situ application, and the true mean values of the individual categories are unknown at the population level. By calculating a theoretically achievable interval of the capacities, the effectiveness of the retrofit methods is properly delineated. The possible ranges of the mean (Eq. I.5) and variance (Eq. I.6) may be predicted using (Singh et al. 2007)

$$L_{lo} \le \frac{\mu - m}{s/\sqrt{n}} \le L_{up} \tag{I.5}$$

$$\frac{(n-1)s^2}{\chi^2_{\alpha/2}} \le \sigma^2 \le \frac{(n-1)s^2}{\chi^2_{(1-\alpha/2)}} \tag{I.6}$$

where $L_{lo}$ and $L_{up}$ are the lower and upper limits of the estimated parameter $m$ at a specific confidence interval, respectively; $\mu$ and $s$ are the sample mean and standard deviation, respectively; $n$ is the number of the samples or the degree of freedom; $\chi^2$ is the Chi-square; and $\alpha$ is the significance level.

**Table I.2**. Estimated limits of flexural capacity of girders

| Girder | Confidence interval | $z(\alpha/2)$ | Limit (kip) | |
|---|---|---|---|---|
| | | | Lower | Upper |
| Cont | 90% | 1.64 | 8.09 | 9.33 |
| | 95% | 1.96 | 7.98 | 9.42 |
| | 99% | 2.58 | 7.76 | 9.67 |
| Bolt | 90% | 1.64 | 6.70 | 7.31 |
| | 95% | 1.96 | 6.70 | 7.35 |
| | 99% | 2.58 | 6.54 | 7.46 |
| CFRP | 90% | 1.64 | 9.11 | 9.98 |
| | 95% | 1.96 | 9.02 | 10.07 |
| | 99% | 2.58 | 8.86 | 10.23 |
| HSS | 90% | 1.64 | 20.44 | 24.26 |
| | 95% | 1.96 | 20.05 | 24.64 |
| | 99% | 2.58 | 19.33 | 25.36 |

### I.5.2. Implementation

In compliance with traditional statistics (Holmes et al. 2017), three levels of confidence (90%, 95%, and 99%) were set and corresponding limits were calculated (Table I.2). Illustrated in Fig. I.12(a) are the upper and lower limits of the flexural capacity at a confidence interval of 95%. The theoretically inferred range completely encompassed the test data, corroborating the reliance of the capacity on the retrofit method. The interrelationship between the limits is shown in Fig. I.12(b), contingent upon the confidence interval. The theoretical capacity ratios of the Bolt and CFRP girders were analogous, which were positioned higher than those of the Cont and HSS girders. The low capacity ratios signify the increased extent of uncertainty, as confirmed by the standard deviations predicted by Eq. I.6 (Fig. I.12(c)). The ratio of the inferred standard deviations declined with the raised confidence interval, whereas the ratio was independent of the retrofit scheme (Fig. I.12(d)).

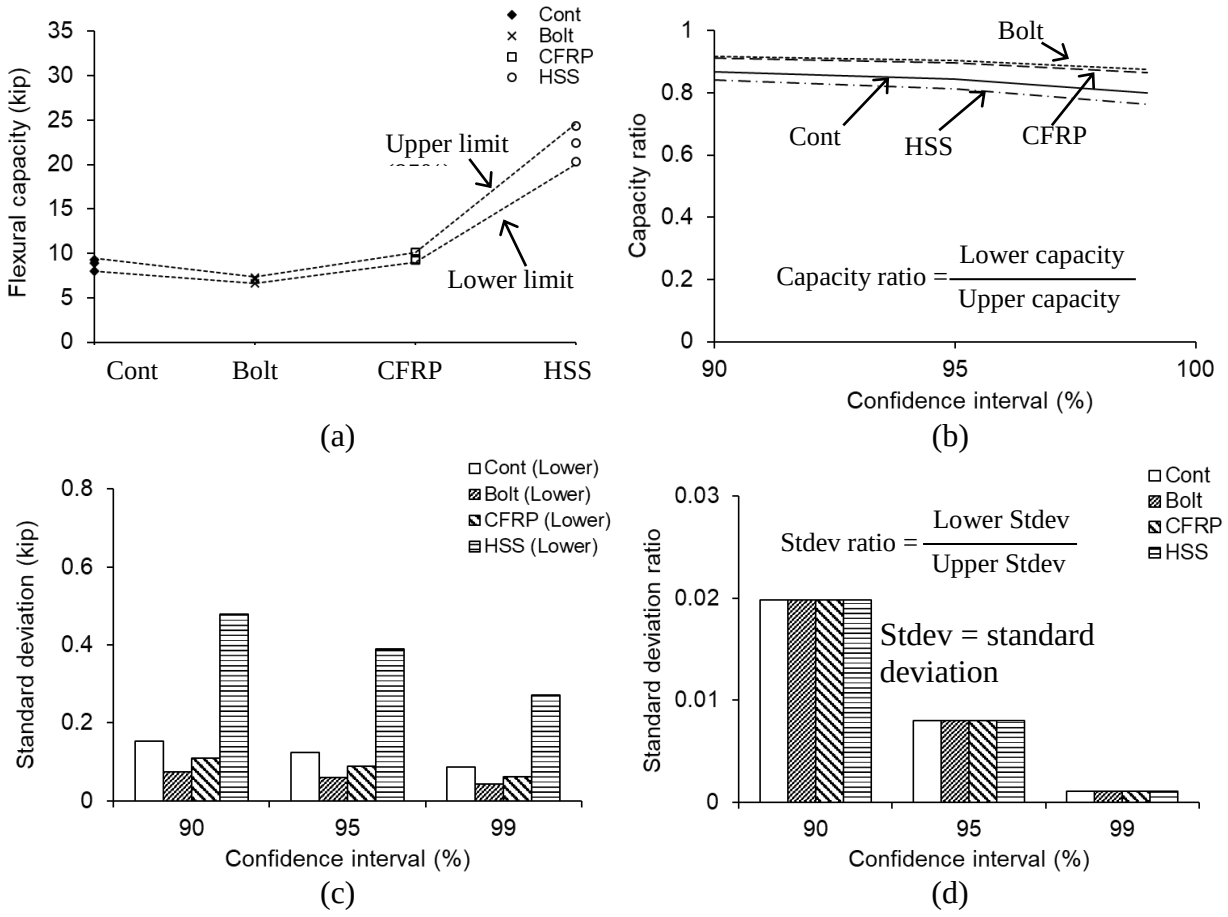


**Fig. I.12**. Parameter estimation: (a) limit lines encompassing test data; (b) capacity ratio; (c) lower limit of standard deviation; (d) standard deviation ratio

## I.6. SUMMARY AND CONCLUSIONS

This part has explored the behavior of salvaged timber girders retrofitted with lag bolts, CFRP sheets, and HSS. A total of 12 girders were tested and flexural responses were examined. The capacities of the control (Cont) and upgraded (Bolt, CFRP, and HSS) girders were compared and other structural aspects were also of interest: energy, displacement, strain, and failure characteristics. By means of a stress wave timer, the mechanical properties of the girders were quantified non-destructively. To handle the possible restrictions of the experimental findings in practice, parameter estimation was conducted. The following conclusions are drawn:

- In conformity with the linearly varying relationship between the transit time and transducer distance of stressed waves, the ramifications of the retrofit methods were

characterized. The dynamic disturbance of the Cont, Bolt, and HSS girders was almost identical; however, due to the polymeric nature of the composite sheets, the wave transmission of the CFRP girder was relatively decelerated. In like manner, the bulk moduli of these girders were classified into two groups. The wave-based effective elastic moduli of the retrofitted girders were lower than that of the control girder.

- The embedded lag bolts incurred geometric discontinuities and initiated local failure, thereby lowering the load-carrying capacity of the Bolt girder below the level of the control girder by 19.6%. On the contrary, the capacities of the CFRP and HSS girders were 9.5% and 156.2% higher than the capacity of the control. From a performance-safety point of view, the reliability index ratio of the Cont, CFRP, and HSS girders went over the requirement of AASHTO LRFD BDS.
- The installation of the retrofit systems changed the linear load-displacement curve of the unstrengthened control girders. The pseudo-yield plateau of the Bolt girder appreciably enhanced the post-peak behavior by virtue of the vertical force component and the thread engagement that resisted the splitting of the grains. The U-wraps and side sheets led to the gradual failure of the CFRP girder. The yielding of the steel beam, followed by the grain fracture, governed the flexural response of the HSS girder. After retrofitting, the amount of dissipated energy increased in all timber girders. Lag bolting was advantageous to extending the development of tensile strains.
- The splitting of grains was responsible for the failure of the Cont girder. While the weak link of the Bolt girder formed through the embedded lag bolts, the bolts interacted with the grain-splitting and distributed flexural stresses. The CFRP sheets maintained the role as a strengthening material without premature debonding. Despite the permanent deformation of the steel beam, the connection between the beam and the timber was not impaired until the HSS girder failed. The mechanically determined effective elastic moduli of the test girders agreed with those measured using the stress wave timer, except for the HSS girder.
- The theoretically inferred capacities of the girders enveloped the experimental data, supporting the adequacy of the test program. The ratio of the estimated upper and lower standard deviations decreased as the confidence interval rose, and the ratio was not a function of the retrofit methods.

## I.7. REFERENCES

AASHTO. 2017. The manual for bridge evaluation (3rd Edition), American Association of State Highway and Transportation Officials, Washington, D.C.

AASHTO. 2021. AASHTO LRFD bridge design specifications (9th Edition), American Association of State Highway and Transportation Officials, Washington, D.C.

ACI. 2017. Guide for the design and construction of externally bonded FRP systems for strengthening concrete structures (ACI 440.2R-17), American Concrete Institute, Farmington Hills, MI.

Adam, J.A. 2017, Rays, waves, and scattering, Princeton University Press, Princeton, NJ.

Asif, M. 2009, Sustainability of timber, wood and bamboo in construction, Sustainability of Construction Materials, Woodhead Publishing Series in Civil and Structural Engineering, 31-54.

ASTM. 2017. Standard test methods for structural panels in flexure (ASTM D3043-17), ASTM International, West Conshohocken, PA.

ASTM. 2018. Standard specification for quenched and tempered allow steel bolts, studs, and other externally threaded fasteners (ASTM A354), ASTM International, West Conshohocken, PA.

ASTM. 2021a. Standard specification for cold-formed welded and seamless carbon steel structural tubing in rounds and shapes (ASTM A500), ASTM International, West Conshohocken, PA.

ASTM. 2021b. Standard test methods of static tests of lumber in structural sizes (ASTM D198-21), ASTM International, West Conshohocken, PA.

Barker, R.M. and Puckett, J.A. 2021. Design of highway bridges: an LRFD approach (4th Edition), Wiley, Hoboken, NJ.

Bhat, J.A. 2021. Effect of CFRP-Reinforcement variation on the strength parameters of different timber beams, Materials Today: Proceedings, 44, 2785-2791.

Biscaia, H., Cruz, D., and Chastre, C. 2016. Analysis of the debonding process of CFRP-to-timber interfaces, Construction and Building Materials, 113, 96-112.

Brashaw, B.K., Wacker, J., and Jalinoos, F. 2013. Field performance of timber bridges: a national study, International Conference on Timber Bridges, Las Vegas, NV, 12 pp.

Corradi, M., Osofero, A.I., and Borri, A. 2019. Repair and reinforcement of historic timber structures with stainless steel-a review, Metals, 9(1), 106.

Dahlberg, J., Phares, B., and Klaiber, W. 2015. Development of cost-effective timber bridge repair techniques for Minnesota, Final Report 2015-45A, Bridge Engineering Center and National Center for Wood Transportation Structures, Iowa State University, Ames, IA.

Dar, M.A., Subramanian, N., Anbarasu, M., Carvalho, H., and Dar, A.R. 2021. Effective strengthening of timber beams: experimental investigation, Practice Periodical on Structural Design and Construction, 26(1), 04020042.

Dethlefs, R. and Martin, Z. 2009. Collapse of the Wimer covered timber bridge, Forensic Engineering Congress, ASCE, 133-142.

Fakopp. 2022. FAKOPP microsecond timer: user's guide, Fakopp Enterprise, Agfalav, Hungary.

FHWA. 1995. Recording and coding guide for the structure inventory and appraisal of the nation's bridges, Federal Highway Administration, U.S. Department of Transportation, Washington, D.C.

Franke, S., Franke, B., and Harte, A.M. 2015. Failure modes and reinforcement techniques for timber beams- state of the art, Construction and Building Materials, 97, 2-13.

Holmes, L., Illowsky, B., and Dean, S. 2017. Introductory business statistics, OpenStax, Houston, TX.

Isleyen, U.K., Ghoroubi, R., Mercimek, O., Anil, O., Togay, A., and Erdem, R.T. 2021. Effect of anchorage number and CFRP strips length on behavior of strengthened glulam timber beam for flexural loading, Advances in Structural Engineering, 24(9), 1869-1882.

Jesus, A.M.P.D., Pinto, J.M.T., and Morais, J.J.L. 2012. Analysis of solid wood beams strengthened with CFRP laminates of distinct lengths, Construction and Building Materials, 35, 817-828.

Khelifa, M., Auchet, S., Meausoone, P.-J., and Celzard, A. 2015. Finite element analysis of flexural strengthening of timber beams with carbon fibre-reinforced polymers, Engineering Structures, 101, 364-375.

Kode, A., van de Lindt, J.W., and Amini, M.O. 2021. Investigation of cross timber bridge decks as a sustainable solution for repair of deficient rural wood bridges, Report No. MPC 21-437, Mountain-Plains Consortium, University Transportation Center, Fargo, ND.

Lam, A.C.C., Cheng, J.J.R., and Kennedy, G.D. 2007. Repair of steel structures by bonded carbon fibre reinforced polymer patching: experimental and numerical study of carbon fibre reinforced polymer- steel double-lap joints under tensile loading, Canadian Journal of Civil Engineering, 34, 1542-1553.

Mahini, S.S., Moore, J.C., and Glencross-Grant, R. 2016. Monitoring timber beam bridge structural reliability in regional Australia, Journal of Civil Structural Health Monitoring, 6, 751-761.

Meier, U. 2000. Composite materials in bridge repair, Applied Composite Materials, 7, 75094.

Naser, M.Z., Hawileh, R.A., and Abdalla, J.A. 2019, Fiber-reinforced polymer composites in strengthening reinforced concrete structures: A critical review, Engineering Structures, 198, 109542.

Nasir, V., Fathi, H., and Kazerirad, S. 2021. Combined machine learning–wave propagation approach for monitoring timber mechanical properties under UV aging, Structural Health Monitoring, 20(4), 2035-2053.

Ou, F.L. and Weller, C. 1986. An overview of timber bridges, Transportation Research Record 1053, Transportation Research Board, Washington, D.C., 12 pp.

Peskin, M.E. 2019. Concepts of elementary particle physics, Oxford University Press, Oxford, UK.

Peterson, M.L. and Gutkowski, R.M. 1999. Evaluation of the structural integrity of timber bridges, NDT&E International, 32, 43-48.

Rescalvo, F., Suarez, E., Valverde-Palacios, I., Santiago-Zaragoza, J.M., and Gallego, A. 2018. Health monitoring of timber beams retrofitted with carbon fiber composites via the acoustic emission technique, Composite Structures, 206, 392-402.

Rescalvo, F.J., Suarez, E., Abarkane, C., Cruz-Valdivieso, A., and Gallego, A. 2019. Experimental validation of a CFRP laminated/fabric hybrid layout for retrofitting and repairing timber beams, Mechancis of Advanced Materials and Structures, 26(22), 1902-1909.

Schiro, G., Giongo, I., Sebastian, W., Riccadonna, D., and Piazza, M. 2018. Testing of timber-to-timber screw-connections in hybrid configurations, Construction and Building Materials, 171, 170-186.

Silwa-Wieczorek, K., Ostrowski, K.A., Jaskowska-Lemanska, J., and Karolak, A. 2021. The Influence of CFRP Sheets on the Load-Bearing Capacity of the Glued Laminated Timber Beams under Bending Test, Materials, 14(14), 4019.

Singh, V.P., Jain, S.K., and Tyagi, A. 2007. Risk and reliability analysis, American Society of Civil Engineers, Reston, VA.

Ugural, A.C. and Fenster, S.K. (1995). Advanced Strength and Applied Elasticity, 3rd Ed., Prentice-Hall, Hoboken, NJ.

USDA. 2010. Wood handbook: wood as an engineering material (centennial edition), United States Department of Agriculture, Madison, WI.

Vahedian, A., Shrestha, R., and Crews, K. 2019. Experimental and analytical investigation on CFRP strengthened glulam laminated timber beams: full-scale experiments, Composite Part B, 164,377-389.

Zhang, C., Chun, Q., Wang, H., Lin, Y., and Shi, J. 2022, Experimental study on the flexural behaviour of timber beams strengthened with high ductility and low cost hybrid fibre sheets, Construction and Building Materials, 322, 126514.

# Part II: Structural Strengthening of a Constructed Timber Bridge

## II.1. INTRODUCTION

Timber is an abundant material and has been used exclusively for bridges and trestles until the early 20$^{th}$ century (Ou and Weller 1986). The advantages of timber construction are found in its convenient set of fabrication procedures, light weight, environmental friendliness, versatility, and aesthetically pleasing impressions; at the same time, it also involves drawbacks (e.g., anisotropic properties, irregular grains, and frequent maintenance) (Balendra et al. 2010; Breyer and Cobeen 2019; Zhu et al. 2021; Palanti and Terziev 2022). In light of the fact that timber comprises organic cellulose fibers, performance degradation is unavoidable with time. A wide variety of defects in timber elements increase the extent of uncertainty and precipitate the need for an intricate operations program to warrant the safety of bridge systems. There are numerous causes of deterioration, namely, moisture, fungi, insects, temperature, ultraviolet rays, wearing, and mechanical distress (Ou and Weller 1986; Rashidi et al. 2021; Ribas and Molina 2021). The degenerated strength and modulus of timber can possibly lead to a catastrophic collapse of bridge structures (Dethlefs and Martin 2009; Rashidi et al. 2021). Owing to a unique decay mechanism differing from those of concrete and steel, the maintenance and rehabilitation of timber bridges necessitate special efforts and extra budgets (Dunker and Rabbat 1993; Kleppe et al. 2013): it is not uncommon to spend more dollars for the preservation of intended condition states compared with initial erection expense (Ranjith et al. 2013). As a result, transportation authorities are eager for sustainable and cost-effective solutions to extend the longevity of aging timber bridges.

The functional level of decrepit timber bridges may be improved by alleviating vehicular loads, inserting deformation restrainers, driving nails, injecting epoxies, and adhering external reinforcement. Insufficient funds, however, often bring about a scarcity of attention and a lack of investment when administering such bridges (McCutcheon et al. 1986). Therefore, apposite methodologies should be selected in line with spatial and financial restrictions, which can minimize the likelihood of exacerbation and retard the progression of chronic damage. Routine practices without an in-depth understanding of underlying principles and physical engagement between multiple constituents cannot establish the practical competency of promising rehabilitation strategies. Even if innumerable retrofit projects were conducted for timber bridges,

documented data are sparse and thus scientific assessments on the effectiveness are not achieved (Dahberg et al. 2012). Besides, pertinent guidance is rarely attainable when upgrades are necessary due to the empirical and case-specific nature of site work (Phares 2015).

This part discusses strengthening techniques for ameliorating the performance of a deficient timber bridge. The aim of the present case study is to explore the applicability of retrofit schemes employing lag bolts, carbon and glass fiber reinforced polymer (CFRP and GFRP, respectively) sheets: CFRP is the primary strengthening material, and steel sections, which can support a decision-making process when addressing structural faults. In tandem with field testing, finite element modeling is undertaken to predict the response of the bridge. Technical interests lie in girder deflections, reliability, efficiency, load distribution factors, and sensitivity analysis.

## II.2. RESEARCH SIGNIFICANCE

The deterioration of built-environments is a pressing issue facing the infrastructure community. Despite the significance of timber bridges in a highway system, the value is frequently underrated as evidenced by the exclusion from the Long-Term Bridge Performance Program of the Federal Highway Administration (FHWA 2013). In consequence, scant information is available on the retrofit of timber bridges and a well-organized strategy should be developed to properly guide engineering professionals who are in charge of managing constructed facilities. The objective of this research is to holistically comprehend the ramifications of various strengthening methods for the behavior of timber girders subjected to flexural loading via a real-world context.

## II.3. RETROFITTED BRIDGE

A strengthening project is carried out to elevate the performance of an 83-old timber bridge. The background of bridge configurations and implementation procedures are outlined. To quantify the efficaciousness of the retrofit, the bridge is loaded using a truck with known weights and its flexural responses are logged.

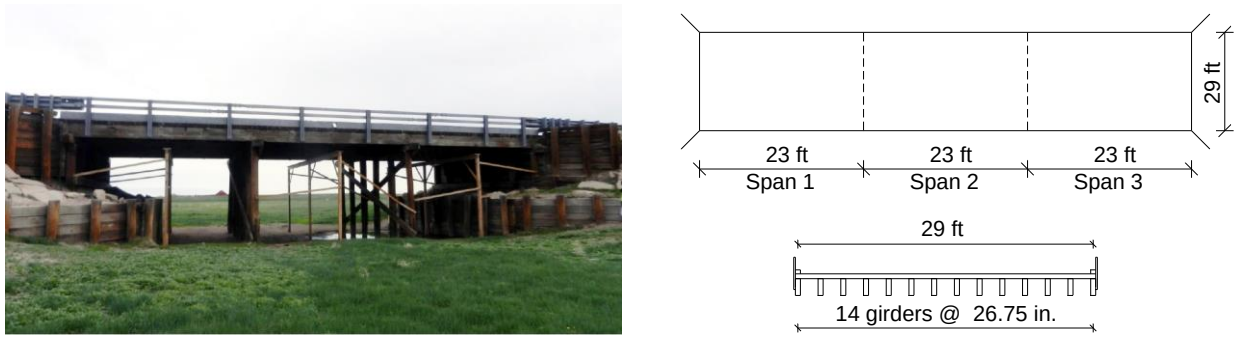


(a) (b)

**Fig. II.1**. The F-22-V Bridge: (a) overview of site; (b) structural configuration

**Table II.1**. Material properties of Douglas Fir used for modeling the F-22-V Bridge

| | $E_L$ (ksi) | $E_T$ (ksi) | $E_R$ (ksi) | $G_{LT}$ (ksi) | $G_{TR}$ (ksi) | $G_{LR}$ (ksi) | $\mu_{LT}$ | $\mu_{TR}$ | $\mu_{LR}$ |
|---|---|---|---|---|---|---|---|---|---|
| Value | 1,570 | 80 | 110 | 120 | 11 | 100 | 0.029 | 0.374 | 0.292 |

$E$ = elastic modulus; G = shear modulus; $\mu$ = Poisson's ratio; $L$ = longitudinal; $T$ = tangential; $R$ = radial

### II.3.1. Description

The F-22-V Bridge in Washington County, Colorado, USA, was built with Douglas Fir in 1938. As depicted in Figs. II.1(a) and (b), the three-span skewless bridge ($L$ = 23 ft @ 3 = 69 ft) was supported by 14 girders (6 in. wide by 20 in. deep, each) at spacings of 26.75 in. to accommodate two lanes. The design load used at the time of construction was H15 (a two-axle single unit truck of 15 tons) and the average daily traffic was measured to be 720 vehicles in 2011. Pursuant to the USDA Wood Handbook (USDA 2010), the orthogonal properties of the lumber were determined as listed in Table II.1. The modulus of rupture was MOR = 7,690 MPa. The condition of the deck, superstructure, and substructure was rated as 6, 4, and 6, respectively, in 2019: Scale 6 = *Satisfactory Condition*: *structural elements show some minor deterioration* and Scale 4 = *Poor Condition*: *advanced section loss, deterioration, spalling or scour* (FHWA 1995). For enhancing the performance of the bridge, the Colorado Department of Transportation (CDOT) decided to strengthen the superstructure with three different methods in each span (Fig. II.2(a): selected girders were retrofitted as per site condition), so that their individual performance was evaluated:

- CFRP sheets (Fig. II.2(b)): Two layers of 4-in. wide unidirectional CFRP sheets were bonded with an epoxy adhesive along the bottom of the girders in conjunction with pressure-treated lumber strips (2 in. thick by 6 in. wide), followed by bonding diagonal CFRP U-wraps with a single layer of 6 in. in width at spacings of 20 in. The nominal tensile strength, elastic modulus, and thickness of the sheets were $f_{fu}$ = 550 ksi, $E_f$ = 34,000 ksi, and $t_f$ = 0.013 in., respectively, at a rupture strain of $\varepsilon_{fu}$ = 1.5%. The Poisson's ratio of CFRP was assumed $v_f$ = 0.3 (Chandrathilaka et al. 2019). To preclude the premature delamination of the diagonal sheets, general purpose GFRP sheets (0.044 in. thick by 5 in. by 6 in. wide) were additionally bonded to the sides of the girders.
- Steel beams (Fig. II.2(c)): Next to the existing timber girders, hollow structural sections (HSS) were positioned on top of precut bearing steel blocks (9 in. by 7 in.). The steel HSS beam (12 × 8 × 5/16), 12 in. deep by 8 in. wide by 0.29 in. thick by 23 ft long, was made of ASTM A500 Grade C (elastic modulus: $E_s$ = 29,000 ksi, yield strength: $f_y$ = 50 ksi, and Poisson's ratio = 0.3) and was mechanically fastened with the timber at both ends and midspan using threaded rods (0.63 in. in diameter).
- Lag bolts (Fig. II.2(d)): ASTM A354 Grade BC threaded bolts (yield strength = 110 ksi, tensile strength = 125 ksi, and average hardness = 31) were prepared as a retrofit material. Steel strips (0.19 in. thick by 5.5 in. wide by 17 ft long) were positioned underneath the girders, and the bolts (0.75 in. in diameter and 2.7 in. in length) were embedded through predrilled holes employing an impact wrench with spacings of 9 in. and 16 in. By welding 2-in. equilateral steel channels (0.374 in. in thickness) to the strips (inset of Fig. II.2(d)), an inclined angle of 45$^o$ was consistently maintained in all installed bolts.

Transverse timber bracings that connected adjacent girders were removed when placing the bolts and, then, reinstated after the retrofit work was completed.

These retrofit strategies can be categorized into two groups: i) enhanced performance of the respective timber girders by raising their resistance (lag bolts and CFRP) and ii) reduced magnitudes of live load by sharing applied distress (HSS beams). The actual cost ratio of the CFRP, steel beam, and lag bolt methods was 1.32: 1.0: 0.72, respectively, including materials and labor.

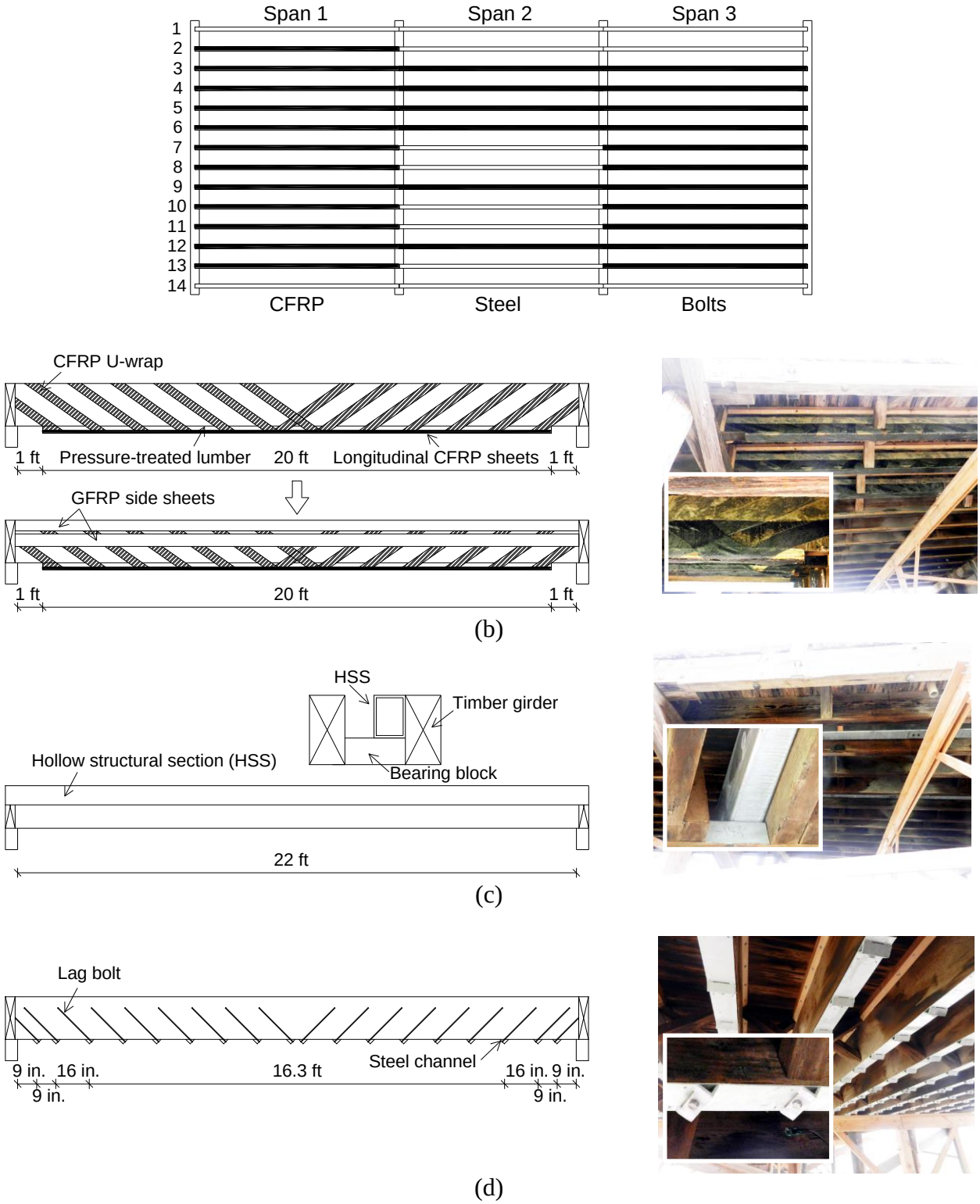


**Fig. II.2**. Strengthening methods: (a) plan view of girders (solid = retrofitted girder); (b) CFRP sheets; (c) HSS beams; (d) lag bolts

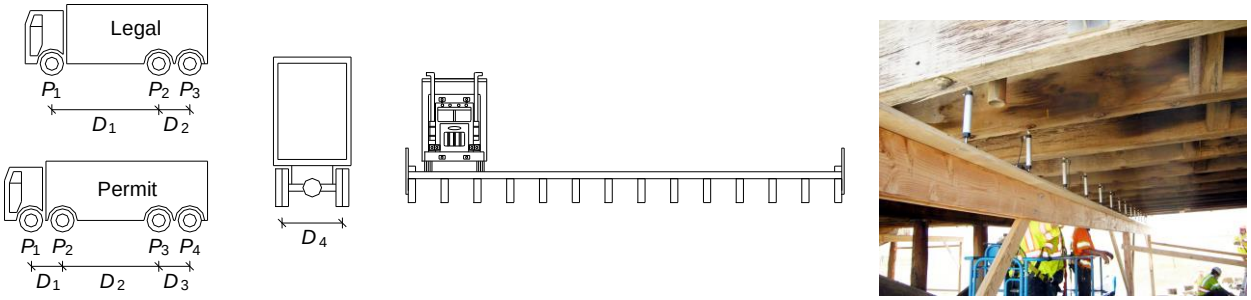


**Fig. II.3**. Live load: (a) Colorado Legal (Type 3) and Permit trucks ($D_4$ = 6 ft); (b) loading position; (c) instrumentation

### II.3.2. Load Test

In accordance with the CDOT Bridge Rating Manual (CDOT 2022), a Type 3 Legal Truck was prepared for load testing. The 267-kN truck consisted of three axles at spacings of $D_1$ = 13.5 ft and $D_2$ = 4 ft, as illustrated in Fig. II.3(a). Two scenarios were planned with i) an empty truck ($P_1$ = 13 kips, $P_2$ = 7.5 kips, and $P_3$ = 7.5 kips, a total of 28 kips: called *unloaded truck*) and ii) a full-weight truck ($P_1$ = 15.5 kips, $P_2$ = 22.25 kips, and $P_3$ = 22.25 kips, a total of 60 kips: called *loaded truck*). These stationary loadings were applied near the exterior girder (Fig. II.3(b): measured distance between the inside curb face and the rear axle outside tire during testing = 25.4 in., on average) at a location that generated the maximum bending moment of the superstructure in the longitudinal direction. To monitor downward deflections, linear variable displacement transducers (LVDTs) were placed underneath the girders at midspan (Fig. II.3(c)). The unloaded and loaded trucks were situated in each span and associated responses were recorded multiple times using a portable data acquisition system.

## II.4. FINITE ELEMENT MODELING

Three-dimensional finite element models are constructed using the commercial software package ANSYS. Described below are material representations, element details, a structural framework alongside boundary conditions, and failure criteria.

### II.4.1. Materials and Elements

Considering the direction-dependent properties of Douglas Fir, an orthogonal constitutive law was defined by linking a stress vector ($\{\sigma\} = \{\sigma_R \sigma_L \sigma_T \tau_{LR} \tau_{LT} \tau_{RT}\}^T$) with a strain vector ($\{\varepsilon\} = \{\varepsilon_R \varepsilon_L \varepsilon_T \gamma_{LR} \gamma_{LT} \gamma_{RT}\}^T$) through the stiffness matrix [*D*] requiring nine specific values that are enumerated in Table 1, where *R*, *L*, and *T* indicate radial, longitudinal, and tangential properties, respectively. Given that the response of the bridge was linear (to be discussed), the plasticity of the timber was not taken into account. Eight-node structural solid elements (SOLID185) represented the timber. Each node of the element was capable of translating in three-dimensional Cartesian space. The transverse bracings of the bridge superstructure, the steel strips coupled with the lag bolts, the HSS beams, the unidirectional CFRP sheets, and the pressure-treated lumber strips were simplified by spar elements (LINK180). This two-node element possessed three translational degrees of freedom per node, which would be ideal for simultaneously handling the timber elements (i.e., the nodal degrees of freedom were compatible with those of the superstructure elements). Figure II.4 shows the constitutive relationship of the materials. To avoid a potential loss in accuracy, full integration schemes were adopted in all simulations without reducing Gaussian points (Zienkiewicz et al. 2013).

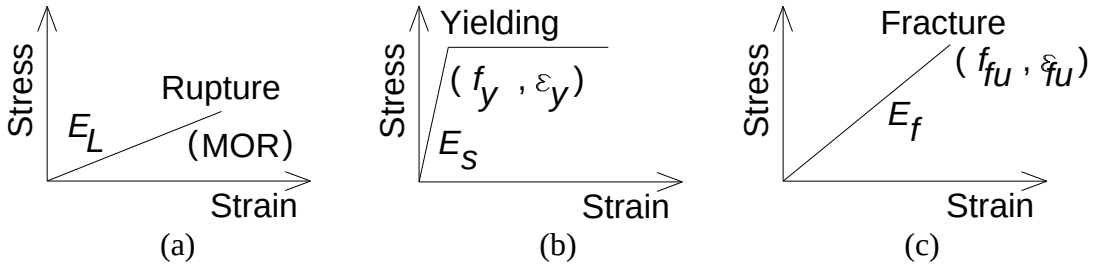


**Fig. II.4**. Stress-strain relationship: (a) timber; (b) steel; (c) CFRP

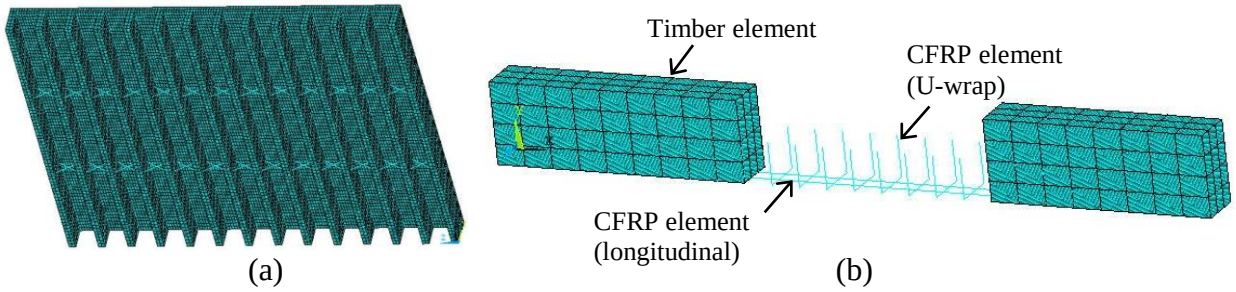


**Fig. II.5**. Model development: (a) full-scale bridge model; (b) laboratory-scale beam model (cut-away view)

### II.4.2. Formulation

Figure II.5(a) displays a single span of the full-scale F-22-V bridge model. In lieu of assuming simple composite action (perfect bond), individual load-bearing members were conjoined using a numerical procedure called *constraint equations* (Hook et al. 2002). Scilicet, all translational degrees of freedom were unified at nodes that were shared by the deck and girders in the vertical and transverse directions so as to ensure integrated motions, whereas their longitudinal degrees of freedom were not restrained to allow relative slips, which were appropriate for simulating local deformations in the timber elements joined by mechanical fasteners under truck loadings. The cross bracings and the girders were interconnected through the foregoing node-sharing technique with the coincident degrees of freedom in all directions. For the lag-bolt retrofit option, steel strip elements were generated along the tensile soffit of the girders and their translational degrees of freedom were tied with the bottom nodes of the girders to accomplish displacement compatibility resulting from the embedded bolts. Regarding the CFRP retrofit option, the

unidirectional spar elements were arranged as explained in the bridge description section. The insignificant bond-slip of a CFRP-timber interface at the structural scale was ignored (Brunetti et al. 2019), so that the degrees of freedom between the nodes of the timber and CFRP elements were coincided at a single location. As far as the HSS beams are concerned, the LINK180 elements were arrayed beside the girders and the constraint equations were applied at three locations (end and midspans) in compliance with the site implementation. The failure criteria of the numerical model were input as follows: i) the timber elements fracture when a tensile stress reaches the modulus of rupture ($\sigma_T$ = MOR) and ii) the CFRP elements rupture when a longitudinal strain equals the ultimate strain ($\varepsilon_f = \varepsilon_{fu}$).

**Table II.2**. Properties of timber beams used for validation of modeling approach

| Reference | Dimension | | | Material properties | | | | | | |
|---|---|---|---|---|---|---|---|---|---|---|
| | Width (in.) | Depth (in.) | Length (ft) | $E_L$ (ksi) | $E_T$ (ksi) | $E_R$ (ksi) | $G_{LT}$ (ksi) | $G_{TR}$ (ksi) | $G_{LR}$ (ksi) | MOR (ksi) |
| Gentile | 4 | 12 | 14.1 | 1,100 | 55 | 75 | 86 | 7.7 | 70.6 | 2.87 |
| Yang | 3 | 12 | 19.7 | 1,560 | 78 | 106 | 122 | 10.9 | 99.9 | 4.48 |
| Rescalvo | 3 | 6 | 4.3 | 1,740 | 86 | 118 | 135 | 12.2 | 111 | 4.32 |
| Nziengui | 2.3 | 7 | 13.3 | 2,850 | 142 | 193 | 222 | 19.9 | 182 | N/A* |
| Halicka | 5.5 | 8 | 11.2 | 1,190 | 60 | 81 | 93 | 8.4 | 76 | N/A** |

Gentile = Gentile et al. (2002); Yang = Yang et al. (2016); Rescalvo = Rescalvo et al. (2017); Nziengui = Nziengui et al. (2019); Halicka = Halicka and Slosarz (2021)
*: test was ceased at a load of 4.59 kN
**: average test capacity of 19.8 kips was given

**Table II.3**. CFRP properties used for validation of modeling approach

| Reference | $t_f$ (in.) | $f_{fu}$ (ksi) | $\varepsilon_{fu}$ (%) | $E_f$ (ksi) | $\nu$ |
|---|---|---|---|---|---|
| Rescalvo et al. (2017) | 0.047 | 320 | 1.22 | 26,110 | 0.3 |
| Halicka and Slosarz (2021) | 0.047 | 410 | 1.35 | 24,700 | 0.3 |

$t_f$ = thickness; $f_{fu}$ = tensile strength; $\varepsilon_{fu}$ = rupture strain; $E_f$ = elastic modulus; $\nu$ = Poisson's ratio

### II.4.3. Validation

The proposed modeling approach was validated against experimental results collected from published literature (Gentile et al. 2002; Yang et al. 2016; Rescalvo et al. 2017; Nziengui et al. 2019; Halicka and Slosarz 2021). Contemplating the availability of existing test data, the scope

of the validation encompassed two categories: plain control and CFRP-strengthened cases. All beams were Douglas Fir and simply supported for flexural loading. Table II.2 provides the dimensions and material properties of the specimens. Owing to the absence of necessary information in the references, a method shown in the USDA Wood Handbook (USDA 2010) was employed to determine the orthogonal properties of the timber and, in addition, Poisson's ratios were assumed to be the same as those given in Table II.1. The properties of CFRP are delineated in Table II.3. Figure II.5(b) exhibits a laboratory-scale model incorporating timber and CFRP elements. The aforementioned failure criterion of the timber was appraised in Fig. II.6(a), where the maximum usable strain of Douglas Fir was converted from the modulus of rupture. The load of the beam increased until computed strains at the extreme tension fiber went over the preassigned limit. The predicted and measured load-displacement and load-strain curves of the unstrengthened beams agreed (Figs. II.6(b) to (d)). On the CFRP-strengthened beams, marginal discrepancies were noticed in strains (Fig. II.6(e)) and deflections (Fig. II.6(f)). These are explained by the fact that strain gages bonded to the beam could be misaligned from the longitudinal axis and the placement of CFRP (wet-lay-up bonding) might be deviated from the specified drawings reported in the part, which can be justified by the inconsistent experimental responses in Figs. II.6(e) and (f).

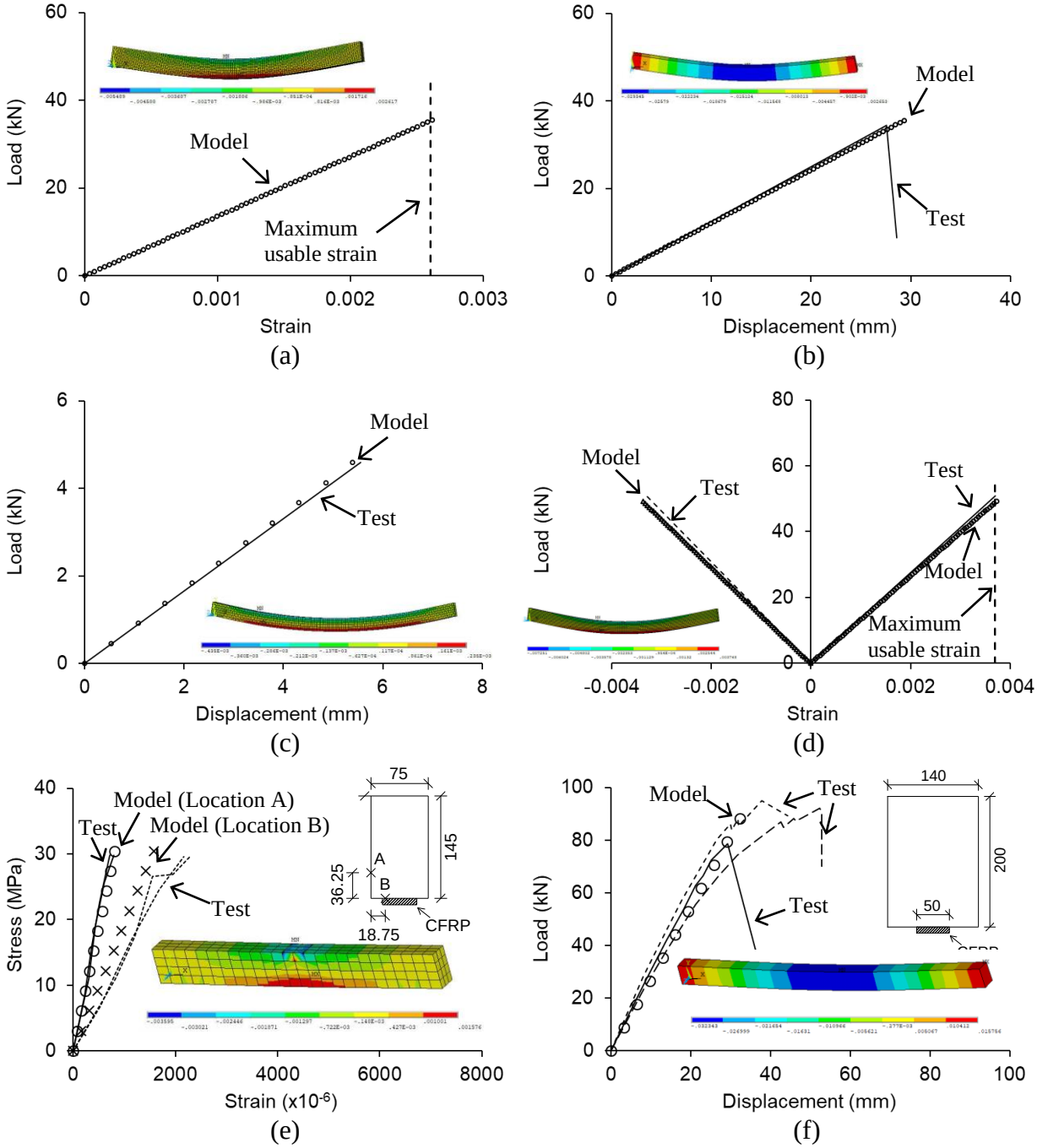


[1 kN = 0.224 kips; 1 mm = 0.0394 in.; 1 MPa = 145 psi]

**Fig. II.6**. Validation of modeling approach (drawing units in mm): (a) failure criterion of unstrengthened beam (Gentile et al. 2002); (b) load-displacement of unstrengthened beam (Gentile et al. 2002); (c) load-displacement of unstrengthened beam (Nziengui et al. 2019); (d) load-strain of unstrengthened beam (Yang et al. 2016); (e) load-strain of CFRP-strengthened beam (Rescalvo et al. 2017); (f) load-displacement of CFRP-strengthened beam (Halicka and Slosarz 2021)

## II.5. RESULTS AND DISCUSSION

The verified modeling approach is used to predict the behavior of the F-22-V Bridge with and without strengthening. Assorted subjects are of interest such as load-deflection, system reliability, stiffening efficiency, and live load distribution. The adequacy of the retrofit is further evaluated against design specifications.

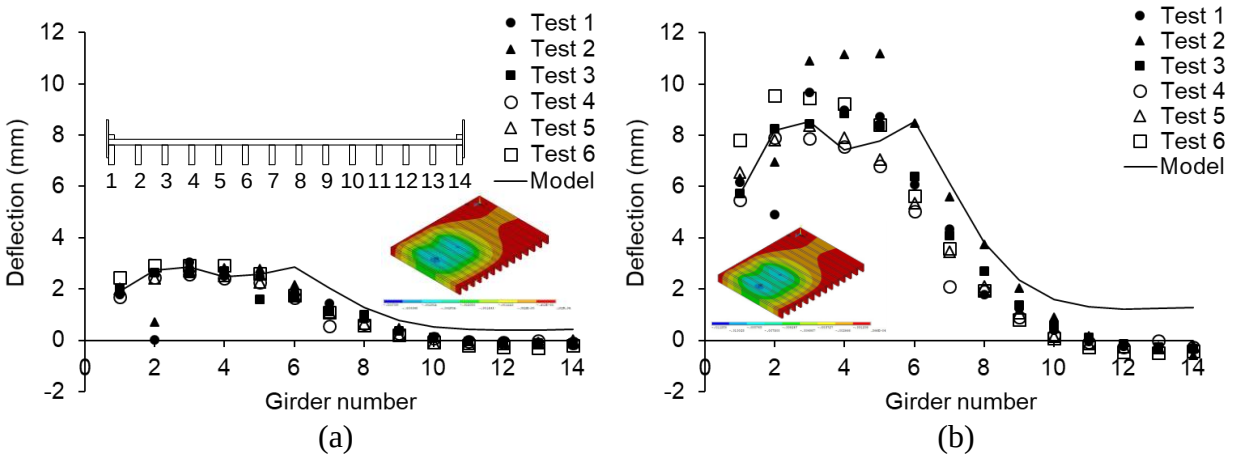


[1 mm = 0.0394 in.]

**Fig. II.7**. Deflection of bridge before strengthening: (a) under unloaded truck (Span 1); (b) under loaded truck (Span 1)

### II.5.1. Deflection

#### II.5.1.1. Unstrengthened case

The deflection of the unstrengthened bridge subjected to the unloaded and loaded trucks is graphed in Fig. II.7. Because the trucks were positioned near the exterior girder (Fig. II.3(b)), one side of the superstructure attracted more load than the other (insets in Figs. II.7(a) and (b)); that is, Girder Nos. 1 to 5 showed greater deflections than Girder Nos. 6 to 14. Whereas the responses of the in-situ bridge were relatively stable under the unloaded truck (Fig. II.7(a)), those under the loaded truck were accompanied by significant scatter (Fig. II.7(b)). These observations

can be ascribed to the fact that the position of the trucks was not the same when the tests were replicated six times in the field (coefficient of variation, COV = 0.343), and the implications of the load were amplified with the heavier truck. The predicted deflections were within the measured range of Girder Nos. 1 to 5, regardless of truck type; on the contrary, it overestimated deflections away from the loaded region (i.e., Girder Nos. 10 to 14): from a mechanics point of view, the bridge model better transferred the live load among the girders through the conjoined finite elements relative to the in-situ deck comprising discrete lumber pieces.

#### II.5.1.2. Strengthened case

Figure II.8 compares the deflections of the superstructure strengthened with the three retrofit methods. In the case with the lag bolts, good agreement was noticed between the prediction and measurement (Figs. II.8(a) and (b)). For the CFRP-strengthened span, albeit negligible, the model tended to generate higher deflections (Figs. II.8(c) and (d)). It is conjectured that the site work could be slightly different from the nominal bonding plan (Fig. II.2(b)). As shown in Figs. II.8(e) and (f), the predicted deflections of Girder Nos. 1 to 8 were almost symmetric because the HSS beams were evenly added between Girders 3 and 6; however, the measured deflections leaned toward Girder No. 2 possibly due to the formerly stated imperfect load transfer across the superstructure assembled with the beams.

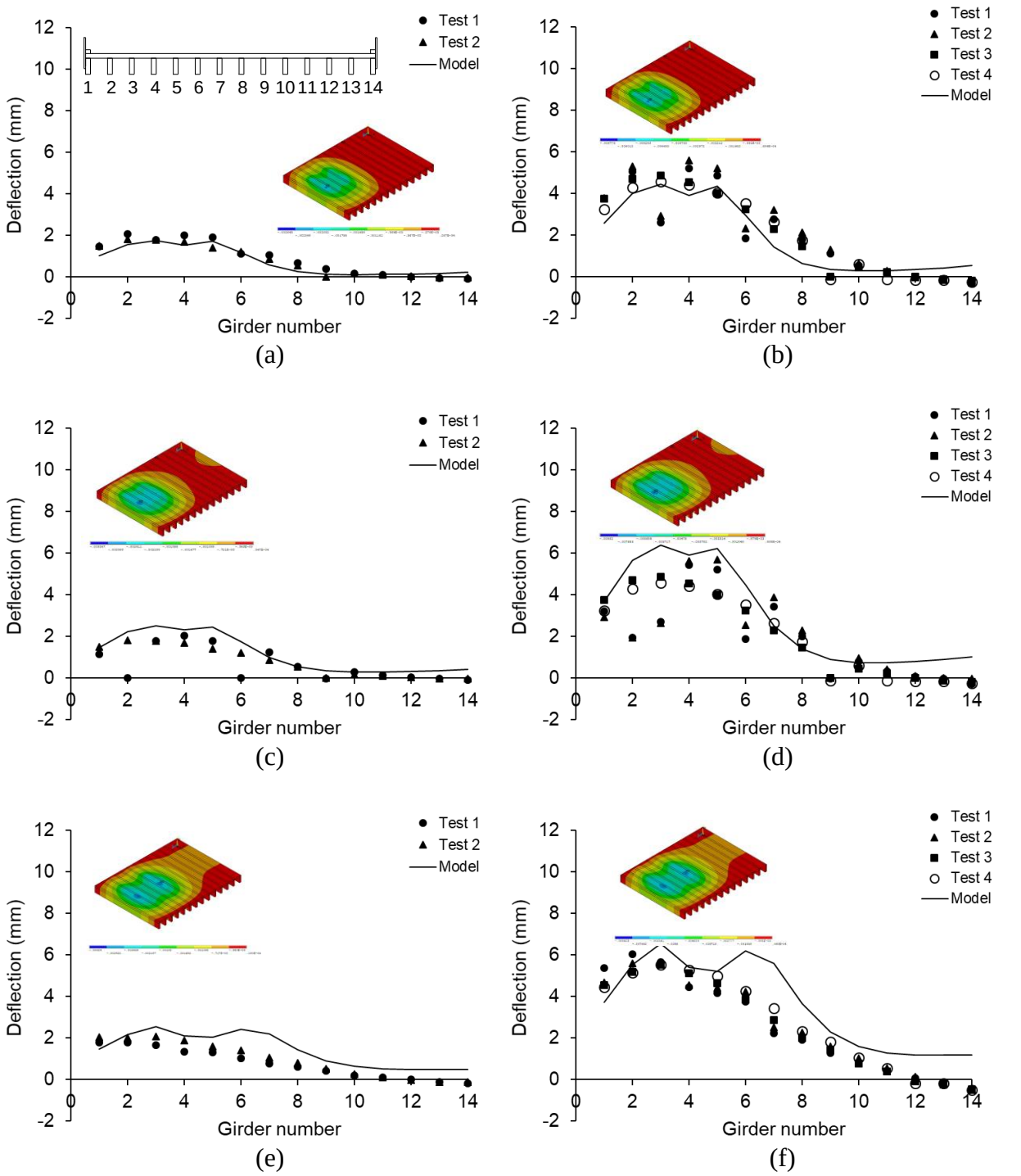


**Fig. II.8**. Deflection of bridge after strengthening: (a) under unloaded truck with lag bolts (Span 3); (b) under loaded truck with lag bolts (Span 3); (c) under unloaded truck with CFRP (Span 1); (b) under loaded truck with CFRP (Span 1); (e) under unloaded truck with HSS beams (Span 2); (f) under loaded truck with HSS beams (Span 2)

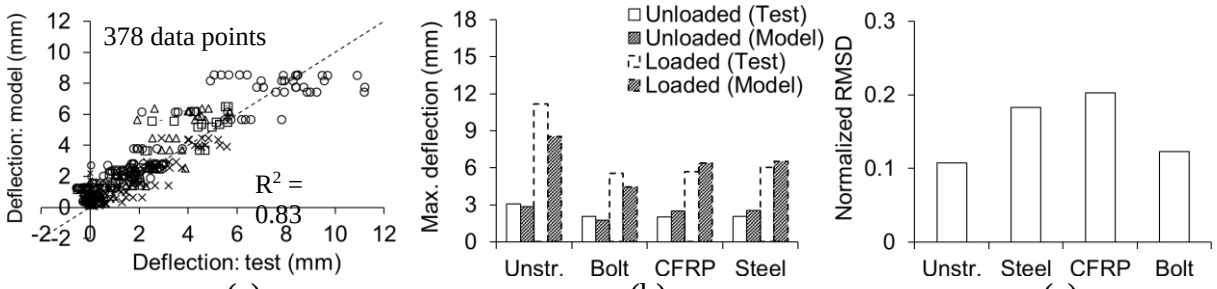


[1 mm = 0.0394 in.]

**Fig. II.9**. Comparison of flexural behavior: (a) comprehensive assessment (Circle: Unstrengthened; X: Lag bolts; Triangle: CFRP; Square: HSS beams); (b) maximum deflection; (c) normalized root mean square deviations

### II.5.1.3. Overall comparison

A comprehensive appraisal of the predicted and measured deflections is visible in Fig. II.9(a). A total of 378 data were plotted and an acceptable correlation was observed with a coefficient of determination of $R^2 = 0.83$. Shown in Fig. II.9(b) are the maximum deflections of each occasion with and without the retrofit. Except for the unstrengthened bridge under the loaded truck exhibiting a difference of 0.102 in. (0.037% of the span length), all others revealed a deflection difference of less than 0.043 in. (0.016% of the span length). In addition to these comparisons, the margin of the individual instances was calculated by the normalized root mean square deviation ($RMSD_{norm}$), which is a popular technique that quantifies estimation errors:

$$RMSD_{norm} = \frac{\sqrt{\sum_1^n \left(\delta_{test} - \delta_{predict}\right)^2} / n}{\left(\delta_{test-\max} - \delta_{test-\min}\right)} \qquad \text{(II.1)}$$

where $\delta_{test}$ and $\delta_{predict}$ are the measured and predicted deflections, respectively; $n$ is the number of observation times; and $\delta_{test\text{-}max}$ and $\delta_{test\text{-}min}$ are the maximum and minimum test deflections,

respectively. The rationale for using the normalized approach was that the root mean square deviation is size-dependent (Christie and Neill 2022). The lowest $RMSD_{norm}$ was 0.107 for the unstrengthened bridge (Fig. II.9(c)), followed by the bolt retrofit option ($RMSD_{norm}$ = 0.123), and the values of the HSS and CFRP cases were similar ($RMSD_{norm}$ = 0.183 and 0.203, respectively).

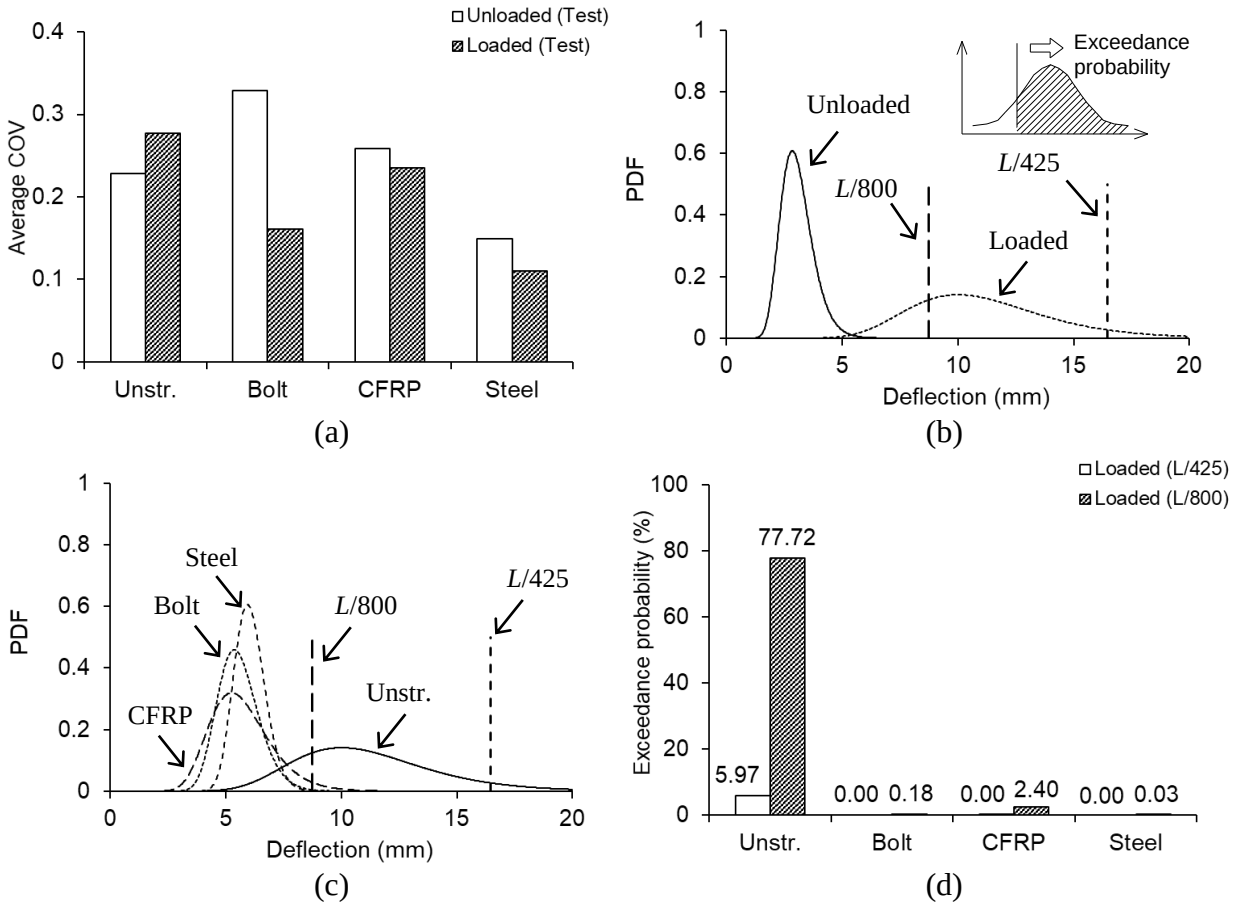


**Fig. II.10**. Probabilistic assessment: (a) average coefficient of variation; (b) probability density function of unstrengthened bridge; (c) probability density function of loaded cases; (d) exceedance probability against deflection limits

### II.5.2. Exceedance Probability

To assess serviceability in a holistic manner, the probability of exceeding the deflection limits stipulated in the American Association of State Highway and Transportation Officials

(AASHTO) Load and Resistance Factor Design (LRFD) Bridge Design Specifications (BDS) (AASHTO 2020) was examined. Figure 10(a) charts the average coefficients of variation (COV) obtained from the field-measured deflections of the girders. Although there is no absolute criterion, the values ranging from COV = 0.111 to 0.328 were acceptable, based on similar magnitudes reported by others (Nowak and Zhou 1990; Wu and Law 2009). The probability density function (PDF) of the unstrengthened bridge is drawn in Fig. II.10(b), including the AASHTO limits of $L/800$ and $L/425$ ($L$ = span length): the former is valid for general vehicular loads, while the latter is specifically for timber bridges. Because of the relatively large COV of 0.278 (Fig. II.10(a)), the distribution of the bridge subjected to the loaded truck was broader (Fig. II.10(b)) and its peak probability (PDF = 0.141) was lower in comparison with that of the bridge with the unloaded truck (PDF = 0.608). The inset of Fig. II.10(b) visually quantifies the probability of exceedance. In an analogous fashion, the probability density functions of the strengthened bridge under the loaded truck are compiled in Fig. II.10(c). The deflections of the strengthened bridge at the peak PDF values were apparently lower than the corresponding deflection of the unstrengthened state. Figure II.10(d) demonstrates the exceedance probability of the four categories. When the limit of $L/425$ was put into effect, the probability of the unstrengthened bridge was 5.97%; by contrast, with the general limit of $L/800$, the probability precipitously rose to 77.72%. The efficacy of the strengthening was substantiated by the negligible occurrence probabilities, spanning from 0.00% to 2.40%, irrespective of the deflection limit.

### II.5.3. Performance Reliability

The performance reliability of the bridge with and without strengthening may be quantified by (Barker and Puckett 2021)

$$\beta = \frac{LN\left(\delta_{\lim} / \delta_{actual}\right)}{\sqrt{\left(COV_{\lim}\right)^2 + \left(COV_{actual}\right)^2}} \quad \text{(II.2)}$$

where $\beta$ is the reliability index for lognormal distributions (bridge responses are lognormally distributed, Nowak and Taylor 1986); and $\delta_{lim}$ and $\delta_{actual}$ are the deflection limit and the measured or predicted deflection at each girder, respectively. The interactions between the multiple girders of the bridge formed the base of system reliability in the superstructure. Conforming to the preceding section, $\delta_{lim}$ was set to either $L$/800 or $L$/425. The COV of $\delta_{lim}$ was assumed to be that of typical live load (COV = 0.18)(Barker and Puckett 2021); on the other hand, the COV of $\delta_{actual}$ was adopted from the test results. Since the AASHTO limits are concerned with downward deflections under live load (AASHTO 2020), upward deflections logged during the field work were excluded. Figures II.11(a) and (b), respectively, describe the indices of the unstrengthened and strengthened bridges subjected to the loaded truck. The indices between the test and model agreed over the region under the truck load (so-called the zone of influence), which was supported by Girder No. 1 to No. 6, beyond which discrepancies were noted due to the negligibly small deflections that dramatically raised the $\beta$ values. The reliability level of the unstrengthened bridge directly under the live load (Fig. II.11(a)) was lower than the threshold value of $\beta$ = 3.5 stipulated in AASHTO LRFD BDS (AASHTO 2020), meaning that the degree of safety of the bridge system did not meet the design requirement. The reliability performance of the bridge strengthened with the lag bolts was improved and no single $\beta$ value

fell below the threshold limit (Fig. II.11(b)). As illustrated in Fig. II.11(c) where reliability indices appertaining to the predicted deflections are shown for brevity, all strengthening applications were satisfactory in terms of enhancing the system performance within the boundary of *L*/425. When the stringent limit of *L*/800 was executed, none of the strengthening methods were sufficiently efficacious for Girder No. 1 to No. 6 (Fig. II.11(d)). Nonetheless, these methods can still be useable on account of the fact that the serviceability demand linked with *L*/425 was particularly designated for timber bridges and that the primary purpose of structural strengthening was to increase the load-carrying capacity of the girders.

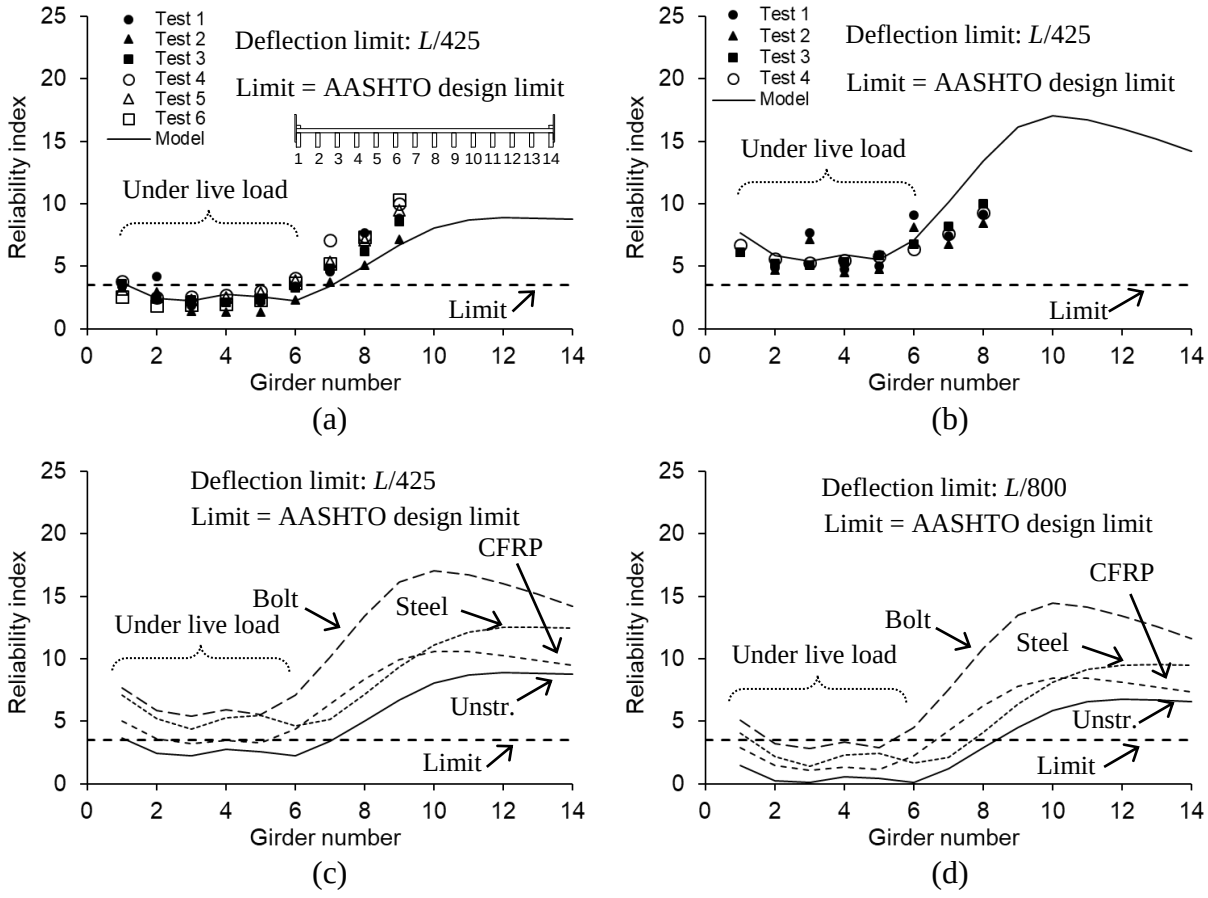


**Fig. II.11**. System reliability on girder deflection: (a) unstrengthened bridge under loaded truck; (b) strengthened bridge with lag bolts under loaded truck; (c) prediction under loaded truck against *L*/425 limit; (d) prediction under loaded truck against *L*/800 limit

### II.5.4. Stiffening Efficiency

To quantify the functionality of the strengthening methods, a stiffening efficiency index ($\psi$) was utilized (Shuraim et al. 2016)

$$\psi = \left(\frac{\delta_u}{\delta_s} - 1\right) / \left(\frac{(E_L I_t)_s}{(E_L I_t)_u} - 1\right) \quad \text{(II.3)}$$

where $\delta_u$ and $\delta_s$ are the deflections of the unstrengthened and strengthened girders, respectively, and their flexural rigidities are $(E_L I_t)_u$ and $(E_L I_t)_s$, in which $E_L$ is the elastic modulus of the timber in the longitudinal direction and $I_t$ is the moment of inertia of the transformed girder section. This index is intended to clarify how well each strengthening method works in terms of controlling girder deflections. Figures II.12(a) to (c) are the efficiency indices of the bridge strengthened with the lag bolts, CFRP, and HSS beams subjected to the loaded truck. As is the case for Fig. II.11, the indices belonging to Girder No. 1 to No. 6 under the live load hold practical significance. Notwithstanding the scatter caused by the large variations of the measured deflections (Figs. II.7 and 8), agreement was noted between the test- and model-based indices within the boundary of Girder No. 1 to No. 6. As corroborated in Fig. II.12(d) where the test averages are collated, the structural efficiency of CFRP was remarkably higher than that of the lag bolts and HSS beams. This trend was consistent in the indices based on the model prediction under the unloaded truck (Fig. II.12(e)). These are attributed to a change in the moment of inertia before and after the retrofit ($I_0$ and $I_t$, respectively), which dominated the girder deflections: the $I_t/I_0$ ratio of the girders with CFRP was 1.06; contrarily, the ratios with the lag bolts and HSS beams were 1.42 and 3.13, respectively. In other words, to reduce the deflections, the physical conformation of the girders was least altered by CFRP, whereas it was markedly modified by the

HSS beams; for this reason, among the three methods, the retrofit with CFRP was found to be the most efficient from a morphological standpoint.

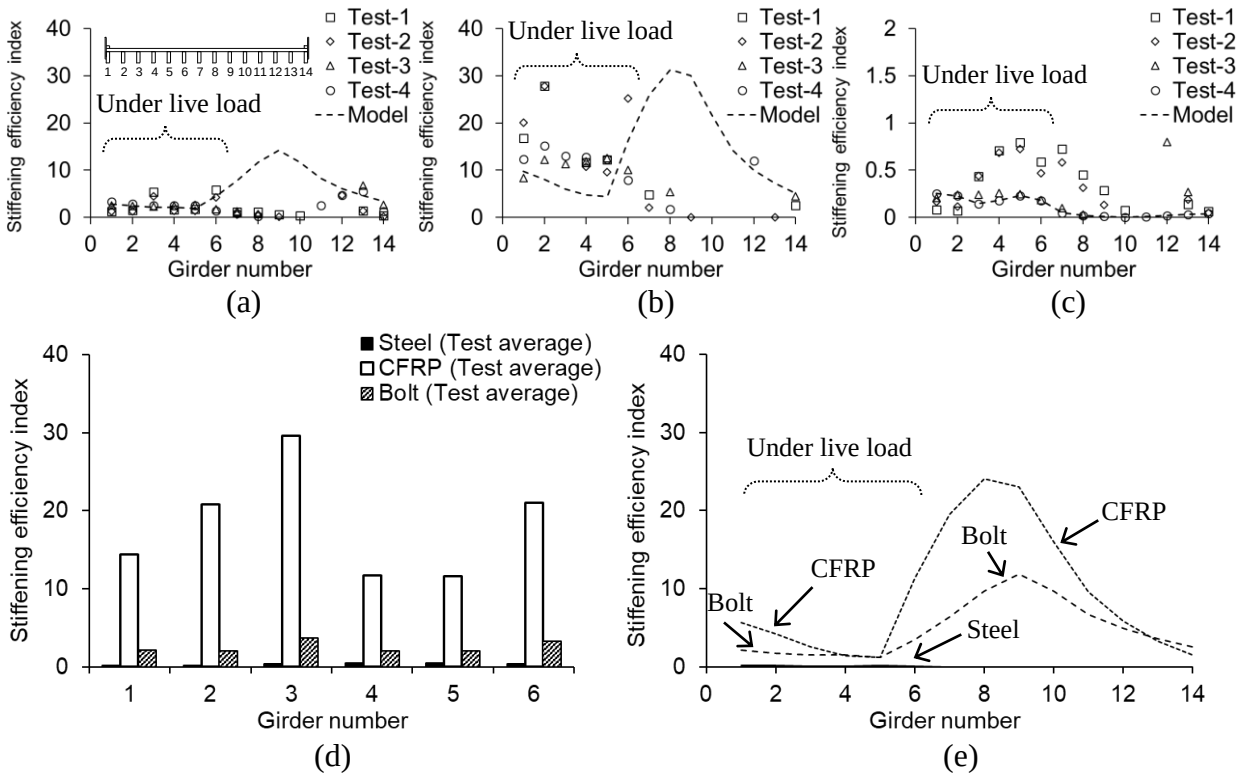


**Fig. II.12**. Assessment of stiffening efficiency: (a) under loaded truck with lag bolts; (b) under loaded truck with CFRP; (c) under loaded truck with HSS; (d) test average under loaded truck; (e) model responses under unloaded truck

### II.5.5. Live Load Distribution

The live load distribution factors of the bridge superstructure are given in Fig. II.13. The measured and predicted factors (marked as Test and Model, respectively) were attained by (Moses et al. 2006)

$$LDF_i = \frac{\varepsilon_i}{\sum_{i=1}^{i=n} \varepsilon_i} \qquad \text{(I.4)}$$

where $LDF_i$ is the load distribution factor of the $i^{th}$ girder; $n$ is the number of the girders; and $\varepsilon_i$ is the girder strain. The distribution factors of the AASHTO Standard Specifications (AASHTO 2002), used for the rating of timber bridges, were calculated by the lever rule (exterior girders) and $S/4$ (interior girder, $S$ = girder spacing) under the one-lane load. It should be noted that this traditional AASHTO formula is for wheel loadings, rather than for axle loadings that are prescribed in AASHTO LRFD BDS (AASHTO 2020), and associated multiple presence factors are unity. Fanous et al. (2011) calibrated live load distribution factors for timber bridges and proposed Eqs. II.5 to II.8 for the moment and shear (designated as $M$ and $S$, respectively) of the interior (*Int*) and exterior (*Ext*) girders

$$LDF_{Int}^{M} = \left(\frac{S}{D}\right)^{k_1}\left(\frac{S}{L}\right)^{k_2}\left(\frac{W_c}{N_g}\right)^{k_3} \quad \text{(II.5)}$$

$$LDF_{Ext}^{M} = \left(\frac{S}{D}\right)^{k_1}\left(\frac{S}{L}\right)^{k_2}\left(\frac{d_e}{S}\right)^{k_3} \quad \text{(II.6)}$$

$$LDF_{Int}^{S} = c\left(\frac{S}{D}\right)^{k_1}\left(\frac{S}{L}\right)^{k_2} \quad \text{(II.7)}$$

$$LDF_{Ext}^{S} = \text{ Lever rule} \quad \text{(II.8)}$$

where $L$ is the span length in ft; $W_c$ is the bridge width in ft; $N_g$ is the girder number; $d_e$ is the overhang width in ft; and $D$, $k_1$, $k_2$, $k_3$, and $c$ are empirical constants (Table II.4). For design purposes, the calibrated live load distribution factors ($LDF_{calibrated}$, Eqs. II.5 to II.8) may be converted to

$$LDF_{adjusted} = \gamma_s m(LDF_{calibrated}) \quad \text{(II.9)}$$

where $LDF_{adjuisted}$ is the adjusted live load distribution factor; and $\gamma_s$ and $m$ are the design factors (Table II.4). The measured and predicted factors matched (Test and Model in Fig. II.13) and were reasonably enveloped by those determined by Fanous et al. (2011); in contrast, the wheel-load-based AASHTO factors were substantially higher. In relation to other situations (Figs. II.13(a) to (c)), the load distribution with the HSS retrofit was steady (Fig. II.13(d)), signifying that the applied truck loads were shared pertinently between the timber and HSS members.

**Table II.4**. Constants for live load distribution factors proposed by Fanous et al. (2011)

| Effect | Girder | Loading | $c$ | $D$ | | | | $k_3$ | | $\gamma_s$ | $a$ | $b$ | $m$ |
|---|---|---|---|---|---|---|---|---|---|---|---|---|---|
| | | | | SI | Cust. | $k_1$ | $k_2$ | SI | Cust. | | | | |
| Moment | Int. | S | - | 12.192 | 40 | 0.409 | 0.108 | -0.075 | -0.018 | 1.02 | 1.126 | -0.041 | 1.2 |
| | | M | - | 3.048 | 10 | 0.792 | 0.058 | -0.214 | -0.051 | 1.02 | 1.037 | -0.018 | 1.0 |
| | Ext. | S | - | 3.658 | 12 | 0.643 | 0.075 | 0.127 | 0.127 | 1.02 | 1.138 | -0.055 | 1.2 |
| | | M | - | 3.048 | 10 | 0.821 | -0.008 | 0.166 | 0.166 | 1.02 | 1.108 | -0.052 | 1.0 |
| Shear | Int. | S | 0.92 | 3.658 | 12 | 0.719 | 0.065 | - | - | 1.03 | 1.112 | -0.046 | 1.2 |
| | | M | 0.92 | 3.042 | 10 | 0.704 | -0.015 | - | - | 1.03 | 1.179 | -0.141 | 1.0 |
| | Ext. | S | - | - | - | - | - | - | - | 1.03 | 1.167 | -0.067 | 1.2 |
| | | M | - | - | - | - | - | - | - | 1.03 | 1.171 | -0.099 | 1.0 |

Int. = interior girder; Ext. = exterior girder; SI = international system of units; Cust. = US customary units

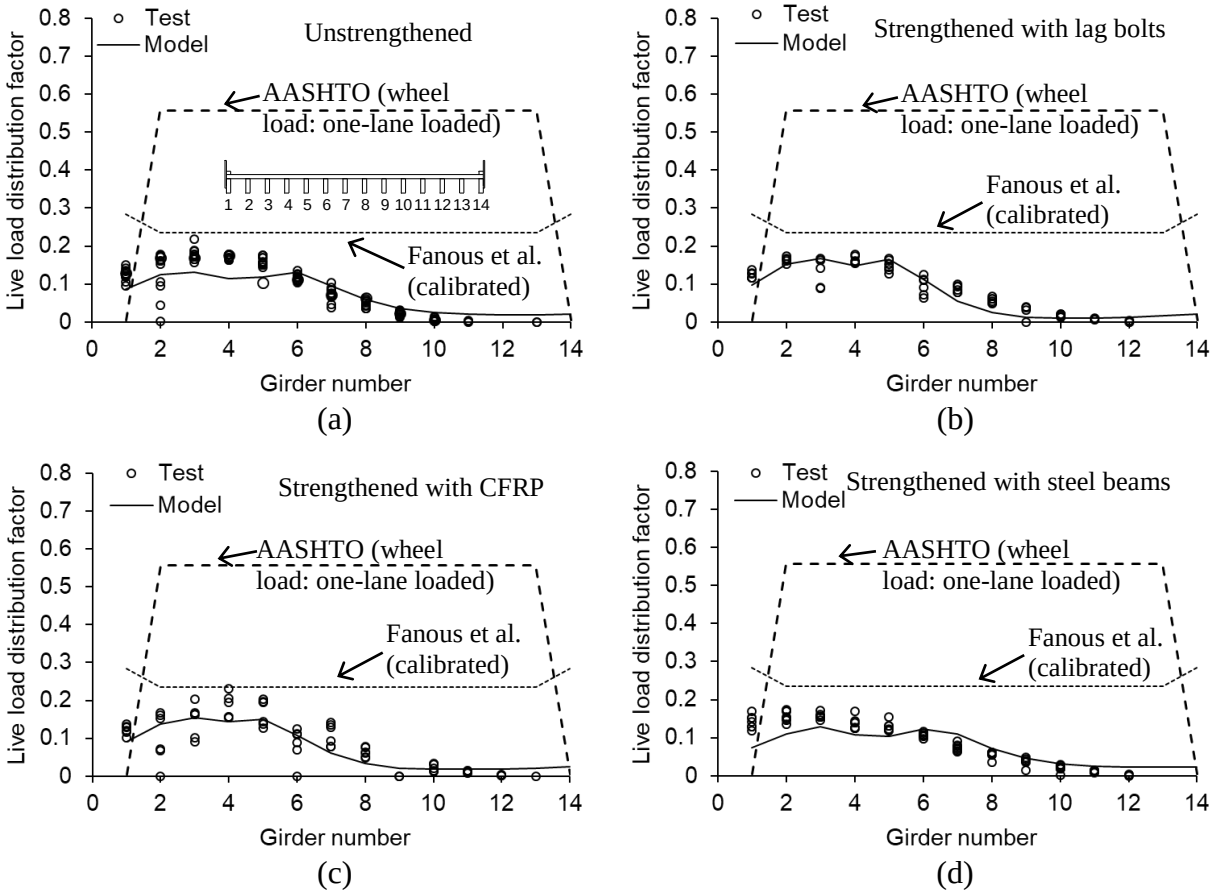


**Fig. II.13**. Live load distribution: (a) unstrengthened; (b) strengthened with lag bolts; (c) strengthened with CFRP; (d) strengthened with HSS beams

Presented in Fig. II.14 is the evaluation of the predicted load distribution factors (average values in each girder were shown for clarity). The factors gained from the finite element model clustered around the 1:1 reference line with considerable linearity (Fig. II.14(a)). As opposed to the AASHTO factors (labeled as *wheel*), the axel-based AASHTO factors (axle load/2 = wheel load) and those of Farnous et al. (2011) demonstrated better predictability (Fig. II.14(b)). The residuals of the calculated factors (i.e., distance from the 1:1 reference line) were charted in Fig. II.14(c), where the average responses of the bridge with and without strengthening are garnered. The residuals of the refined model and Farnous et al. (2011) were 0.017 and 0.121, respectively,

which outperformed their AASHTO counterparts (AASHTO(wheel) = 0.366 and AASHTO(axle) = 0.164).

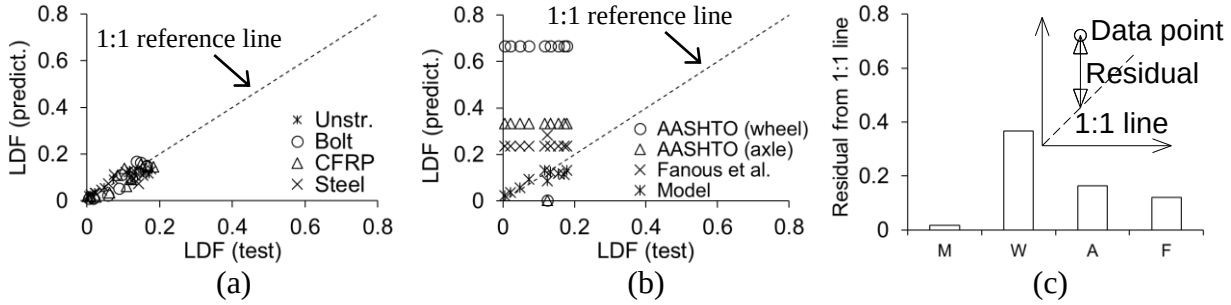


**Fig. II.14**. Comparison of live load distribution factors: (a) model vs. test; (b) unstrengthened bridge; (c) residual (M = model, W = AASHTO (wheel), A = AASHTO (axle), and F = Fanous et al.)

## II.6. PARAMETRIC INVESTIGATIONS

The outcomes of computational modeling account for the positive and negative aspects of each strengthening method, and the Colorado Department of Transportation (CDOT) selects the HSS beam option for upgrading several other timber bridges in the state. Accordingly, parametric investigations are conducted to elucidate the influence of variable HSS sizes on the deflection control of the F-22-V Bridge. Furthermore, the Colorado Permit Truck (167% heavier than the above-utilized Colorado Legal Truck) is loaded to study the serviceability of the bridge.

### II.6.1. Effects of Hollow Structural Sections

Supplementary to the default HSS configuration of 12 × 8 × 5/16, six more sections were modeled without modifying the length of the beams (24 ft), the location of retrofit (Fig. II.2(a)), and the grade of steel (ASTM A500 Grade C). Table 5 lists details about these sections: the first group (the 12 × 8 series) was focused on the wall thickness of the beams, varying from $t$ = 0.291 in. to

0.581 in., while the second group (the 5/16 series) was related to the depth and width of the beams with a constant wall thickness of $t$ = 0.291 in. In comparison with the deflection of the unstrengthened bridge, those of the bridge strengthened with the 12 × 8 series decreased by up to 35.7% (Fig. II.15(a)). In all sections, the $L$/425 limit was satisfied, whereas the relative measure of the deflections to the $L$/800 limit noticeably lessened. It should be recognized that excessive deflections can cause dislocations in the assembled timber elements and the loosening of connection bolts, thereby accelerating the degradation of the bridge over time. The stress distribution of the girders across the bridge deck at midspan is provided in Fig. II.15(b). The maximum stresses of the girders were 551 psi and 754 psi with and without the retrofit, respectively, both of which were lower than the allowable stresses for an indefinite time period ($\sigma_I$ = 1,600 psi) and for a permissible live load ($\sigma_O$ = 2,128 psi) that are specified in the CDOT Bridge Rating Manual (CDOT 2022). Unlike the wall thickness variable of the HSS beams (Figs. II.16(a) and (b)), the depth of the sections was a crucial factor that rearranged the deflection and stress values (Figs. II.16(c) and (d), respectively). The moment of inertia and the section moduli of the HSS beams ($I_x$ and $S_x$ in Table 5, respectively) were responsible for these predictions.

**Table II.5**. Sectional properties of hollow structural section (US designation)

| Size | $D$ (in.) | $W$ (in.) | $t$ (in.) | $A_c$ (in.$^2$) | $I_x$ (in.$^4$) | $S_x$ (in.$^3$) |
|---|---|---|---|---|---|---|
| 12 × 8 × 5/8 | 12 | 8 | 0.581 | 21.0 | 396 | 66.1 |
| 12 × 8 × 1/2 | 12 | 8 | 0.465 | 17.2 | 333 | 55.5 |
| 12 × 8 × 5/16 | 12 | 8 | 0.291 | 11.1 | 224 | 37.4 |
| 12 × 8 × 1/4 | 12 | 8 | 0.233 | 8.96 | 184 | 30.6 |
| 20 × 12 × 5/16 | 20 | 12 | 0.291 | 18.1 | 1,010 | 101 |
| 16 × 8 × 5/16 | 16 | 8 | 0.291 | 13.4 | 451 | 56.4 |
| 8 × 6 × 5/16 | 8 | 6 | 0.291 | 7.59 | 68.3 | 17.1 |

$D$ = depth; $W$ = width; $t$ = wall thickness; $A_c$ = cross sectional area; $I_x$ = moment of inertia; $S_x$ = section modulus

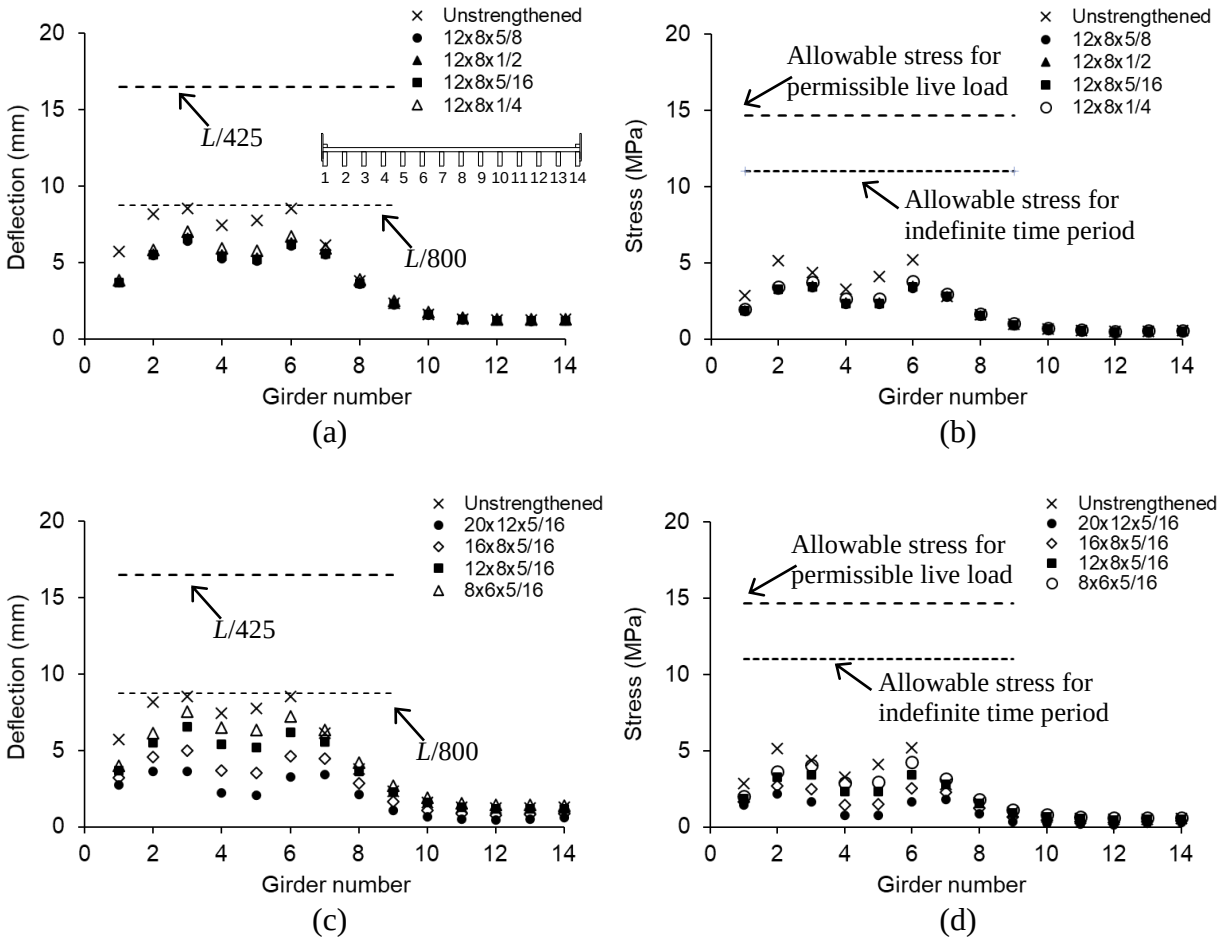


**Fig. II.15**. Effects of variable steel beams (live load-induced behavior at midspan of F-22-V, Span 1 subjected to Colorado Legal Truck (Type 3)): (a) deflection with wall thickness of HSS beams; (b) stress with wall thickness of HSS beams; (c) deflection with depth of HSS beams; (d) stress with depth of HSS beams

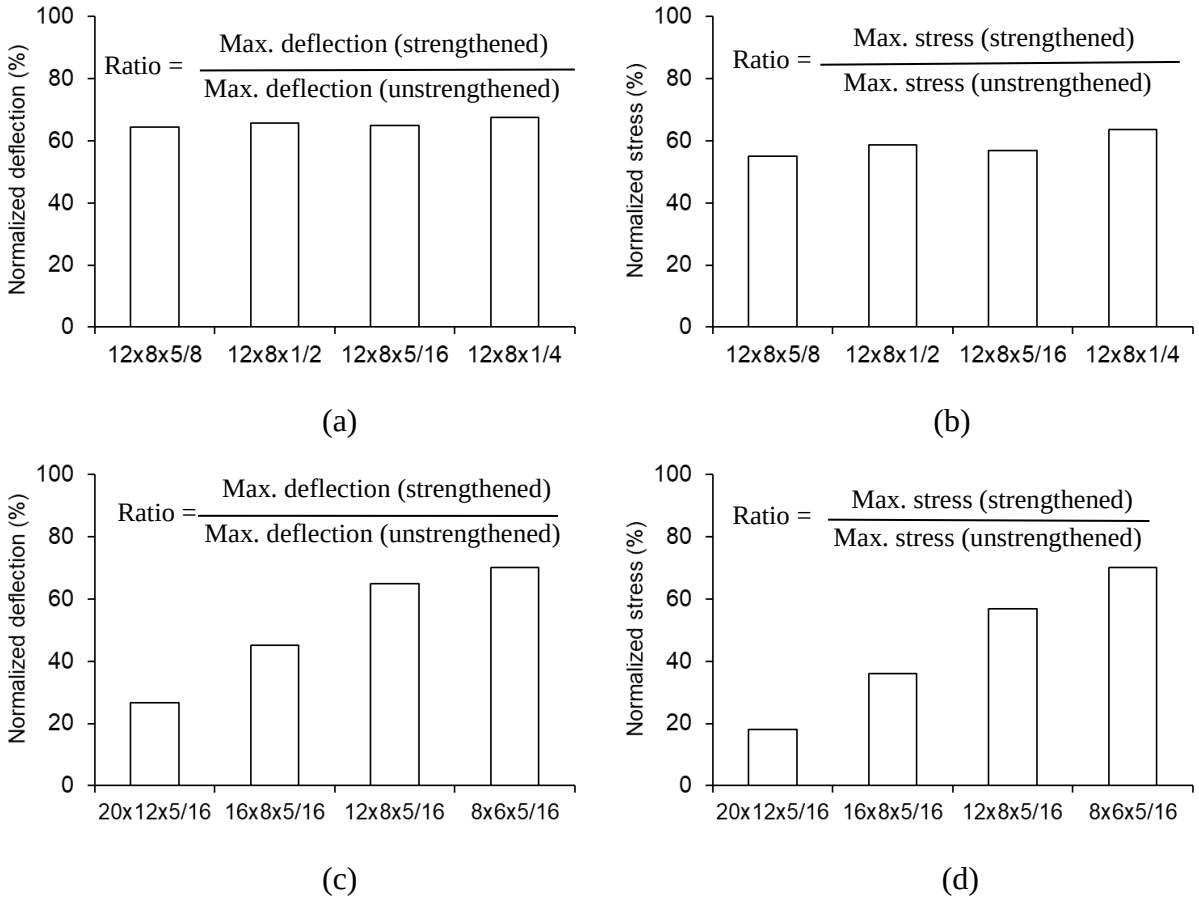


**Fig. II.16**. Effectiveness of steel beam repair (live load-induced behavior at midspan of F-22-V, Span 1 subjected to Colorado Legal Truck (Type 3)): (a) reduced deflection with wall thickness; (b) reduced stress with wall thickness; (c) reduced deflection with beam depth; (d) reduced stress with beam depth

### II.6.2. Effects of Colorado Permit Truck

Figure II.17(a) exhibits the deflection profiles of the bridge under the Colorado Permit Truck weighing 100 kips (Fig. II.3(a): $P_1$ to $P_4$ = 25 kips, each; $D_1$ = 4 ft, $D_2$ = 12 ft, and $D_3$ = 4 ft). In spite of the diminished deflections after the retrofit, the maximum value exceeded the limit of $L$/800 (the $L$/425 limit was still tolerable); hence, in order to avoid potential problems, a refined analysis seems necessary before allowing unordinary vehicles equivalent to the permit truck onto deficient timber bridges. As confirmed in Fig. II.17(b), the stresses of the girders were lower than the allowable stresses of $\sigma_I$ = 1,600 psi and $\sigma_O$ = 2,128 psi. The effectiveness of the

strengthening was akin with regard to the deflection and stress (Fig. II.17(c)); however, the serviceability requirements (Fig. II.17(a)) tended to govern the performance of the bridge, rather than the strength (Fig. II.17(b)).

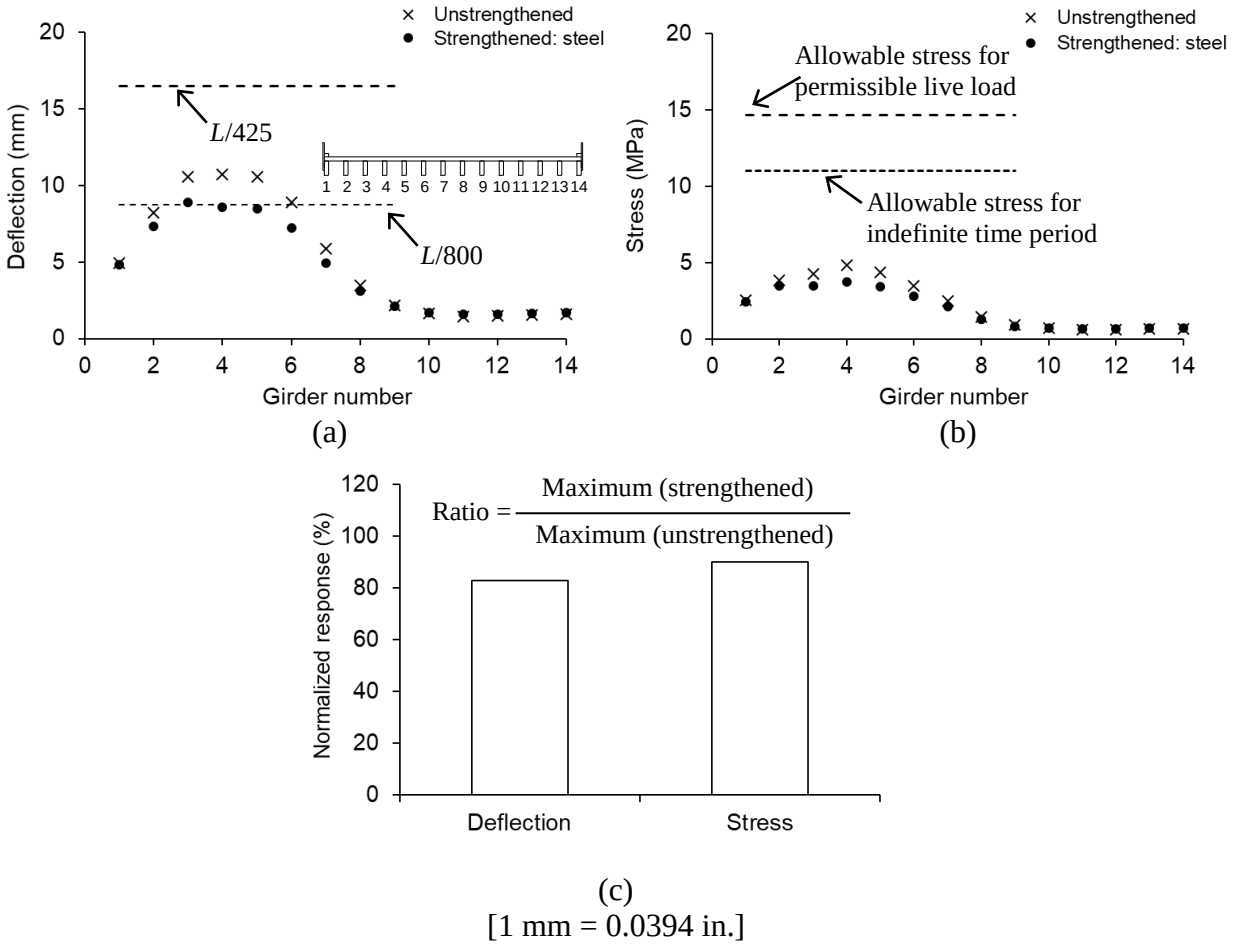


[1 mm = 0.0394 in.]

**Fig. II.17**. Effects of Colorado Permit Truck (live load-induced behavior at midspan of F-22-V, Span 1): (a) deflection; (b) stress; (c) normalized deflection and stress

## II.7. SUMMARY AND CONCLUSIONS

This part has dealt with a case study concerning the retrofit of an 83-year-old timber bridge using lag bolts, CFRP sheets, and HSS beams. The owner, the Colorado Department of Transportation (CDOT), was in need of discovering an affordable, easy to execute, and long lasting approach.

Flexural tests were carried out and finite element models were developed to examine the efficacy of strengthening under truck loadings. Emphasis was placed on deflection characteristics, suitability against the articles of the AASHTO Specifications, system reliability, stiffening efficiency, and live load distribution. Parametric analysis shed light on the repercussions of HSS-sectional properties and the Colorado Permit Truck for the serviceability and strength of the bridge. By considering these technical aspects along with financial, political, and administrative matters, a transportation agency can develop its own strategy that can facilitate the repair of deteriorated timber bridges. The following are concluded:

- The increased magnitude of the truck load raised the degree of dispersion in girder deflections, and the presence of the load above the girders affected the agreement between the measured and predicted responses. Although inappreciable (less than 0.037% of the span length of the bridge), a difference in load transfer mechanisms between the computational model and the discrete in-situ superstructure caused disparity in the flexural behavior.
- Compared with the bridge under the unloaded truck (28 kips), the probability distribution of the bridge under the loaded truck (60 kips) was wider and its peak density was lower, implying the enlarged uncertainty as the live load went up. After the strengthening of the bridge, the exceedance probability of the AASHTO deflection limits declined from 77.72% to 0.03% for $L/800$ and 5.97% to 0.00% for $L/425$.
- The reliability indices of the unstrengthened bridge system were positioned below the AASHTO design threshold of $\beta = 3.5$, while the indices of the strengthened system were greater than the demarcation value under the deflection limit of $L/425$. At the member

level, the CFRP option was more efficient than other options owing to the minimal modification of the superstructure geometry, and the stiffening efficiency of the HSS option was superior at the system level.

- The live load distribution factors predicted by the computational model were close to the measured factors with an average residual of 0.017 and the approach proposed by Farnous et al. (2011) was recommended for practice (residual = 0.121), as an alternative to the AASHTO distribution methods (residuals = 0.164 and 0.366 for the axle and wheel loadings, respectively).
- The consequences of adjusting the height of the HSS beams were pronounced in terms of decreasing the deflections and bending stresses, relative to adjusting the wall thickness; however, refined modeling was recommended for all cases when the rigorous criterion of $L/800$ was effectuated.

## II.8. REFERENCES

AASHTO. 2002. Standard specifications for highway bridges (17th edition), American Association of State Highway and Transportation Officials, Washington, D.C.

AASHTO. 2020. AASHTO LRFD bridge design specifications (9th edition), American Association of State Highway and Transportation Officials, Washington, D.C.

Balendra, T., Wilson, J.L., and Gad, E.F. 2010. Review of condition assessment and retrofitting techniques for timber bridge assets in Australia, Advances in Structural Engineering, 13(1), 171-180.

Barker, R.M. and Puckett, J.A. 2021. Design of highway bridges: an LRFD approach (4th Edition), Wiley, Hoboken, NJ.

Breyer, D. and Cobeen, K. 2019. Design of wood structures, McGraw Hill, New York, NY.

Brunetti, M., Christovasilis, I.P., Micheloni, M., Nocetti, M., and Pizzo, B. 2019. Production feasibility and performance of carbon fibre reinforced glulam beams manufactured with polyurethane adhesive, Composites Part B, 156, 212-219.

CDOT. 2022. Bridge rating manual: staff bridge branch, Colorado Department of Transportation, Denver, CO.

Chandrathilaka, E.R.K., Gamage, J.C.P.H., and Fawzia, S. 2019. Mechanical characterization of CFRP/steel bond cured and tested at elevated temperature, Composite Structures, 207, 471-477.

Christie, D. and Neill, S.P. 2022. Measuring and observing the ocean renewable energy (2nd edition), Volume 8, Elsevier, Amsterdam, The Netherlands.

Dahlberg, J., Phares, B., Bigelow, J., and Klaiber, F.W. 2012. Timber abutment piling and back wall rehabilitation and repair, Report No. IHRB Project TR-616, Bridge Engineering Center, Iowa State University, Ames, IA.

Dethlefs, R. and Martin, Z. 2009. Collapse of the Wimer Covered Timber Bridge, 5th Forensic Engineering Congress, American Society of Civil Engineers, 133-142.

Dunker, K.F. and Rabbat, B.G. 1993. Why America's bridges are crumbling, Scientific American, 268(3), 66-72.

Fanous, F., May, J., and Wipf, T. 2011. Development of live-load distribution factors for glued-laminated timber girder bridges, 16(2), 179-187.

FHWA. 1995. Recording and coding guide for the structure inventory and appraisal of the nation's bridges, Federal Highway Administration, Washington, D.C.

FHWA. 2013. Long-Term Bridge Performance (LTBP) Program, Federal Highway Administration, Washington, D.C.

Gentile, C., Svecova, D., and Rizkalla, S.H. 2002. Timber beams strengthened with GFRP bars: development and applications, Journal of Composites for Construction, 6(1), 11-20.

Halicka, A. and Slosarz, S. 2021. Strengthening of timber beams with pretensioned CFRP strips, Structures, 34, 2912-2921.

Hook, R.D., Malkus, D.S., Plesha, M.E., and Witt, R.J. 2002. Concepts and applications of finite element analysis, John Wiley & Sons, Hoboken, NJ.

Kleppe, O., Keep, H., and Dyken, T. 2013. Contribution to structural details on timber bridges, International Conference on Timber Bridges, 10 pp.

McCutcheon, W.J., Gutkowski, R.M., and Moody, R.C. 1986. Performance and rehabilitation of timber bridges, Transportation Research Record, 1053, 65-69.

Moses, J.P., Harries, K.A., Earls, C.J., and Yulismana, W. 2006. Evaluation of Effective Width and Distribution Factors for GFRP Bridge Decks Supported on Steel Girders, Journal of Bridge Engineering, 11(4), 401-409.

Nowak, A.S. and Taylor, R.J. 1986. Ultimate strength of timber-deck bridges, Transportation Research Record, 1053, 26-30.

Nowak, A.S. and Zhou, J. 1990. System reliability models for bridges, Structural Safety, 7, 247-254.

Nziengui, C.F.P., Pitti, R.M., Fournely, E., Fril, J., Godi, G., and Ikogou, S. 2019. Notched-beam creep of Douglas fir and white fir in outdoor conditions: Experimental study, Construction and Building Materials, 196, 659-671.

Ou, F.L. and Weller, C. 1986. An overview of timber bridges, Transportation Research Record, 1053, 1-12.

Palanti, S. and Terziev, N. 2022. Advanced technologies for increasing the durability of timber and extending its service life, Forests, 13, f13071015

Phares, B. 2015. Cost-effective timber bridge repairs: manual for repairs of timber bridges in Minnesota, Final Report 2015-45B, Bridge Engineering Center and National Center for Wood Transportation Structures, Iowa State University, Ames, IA.

Ranjith, S., Setunge, S., Gravina, R., and Venkatesan, S. 2013. Deterioration prediction of timber bridge elements using the Markov Chain, Journal of Performance of Constructed Facilities, 27(3), 319-325.

Rashidi, M., Hoshyar, A.N., Smith, L., Samali, B., and Siddique, R. 2021. A comprehensive taxonomy for structure and material deficiencies, preventions and remedies of timber bridges, Journal of Building Engineering, 34, 101624.

Rescalvo, F.J., Valverde-Palacios, I., Suarez, E., and Gallego, A. 2017. Experimental comparison of different carbon fiber composites in reinforcement layouts for wooden beams of historical buildings, Materials, 10, 1113.

Ribas, A.D.S. and Molina, J.C. 2021. Wooden bridges with deck of sawn board and round beams: main orientations, Australian Journal of Structural Engineering, 22(1), 1-9.

Shuraim, A.B., El-Sayed, A.K., Al-Negheimish, A.I., and Alhozaimy, A.M. 2016. Efficiency of CFRP strengthening in controlling the deflection of RC beams in a redundant structural system, Journal of Composites for Construction, 20(2), 04015054.

USDA. 2010. Wood handbook: wood as an engineering material, United States Department of Agriculture, Madison, WI.

Wu, S.Q. and Law, S.S. 2009. A stochastic finite element model with non-Gaussian properties for bridge-vehicle interaction problem, Computational Structural Engineering, 445-451, Springer Science+Business, Berlin, Germany.

Yang, H., Liu, W., Lu, W., Zhu, S., and Geng, Q. 2016. Flexural behavior of FRP and steel reinforced glulam beams: experimental and theoretical evaluation, Construction and Building Materials, 106, 550-563.

Zhu, W., Gong, M., Chui, Y.-H., and Li, L. 2021. Improved fastening designs for bridge decks made of mechanically-laminated timber, Construction and Building Materials, 266, 121166.

Zienkiewicz, O.C., Taylor, R.L., Zhu, J.Z. 2013. The finite element method its basis and fundamentals, Elsevier, Waltham, MA.

# Part III: Rating of Constructed Timber Bridges Repaired with Steel Beams

## III.1. INTRODUCTION

Timber is a nature-made and abundant material that has been a principal source for bridge construction before the advent of concrete and steel. Statistics report that more than 10,000 timber bridges were built during the 18$^{th}$ and 19$^{th}$ centuries in the United States (Kromoser et al. 2023). As far as economy is concerned, timber bridges demand 30-50% lower costs compared with concrete bridges (Tazarv et al. 2019); on the contrary, frequent maintenance endeavors are imperative to preserve the quality of timber elements (Rashidi et al. 2021). Notwithstanding many notable advantages (De Araujo 2023), timber bridges are susceptible to deterioration on account of spontaneous decay, moisture, fungi, insects, weathering, and excessive vehicular loadings (Dahlberg et al. 2012; Lokuge et al. 2019; Zhu et al. 2021). As a consequence, periodic inspections and timely rehabilitation are deemed crucial to extend the longevity of those bridges. Inadequate technical activities may cause a collapse like in the case of the Wimer Covered Timber Bridge, Rogue River, Oregon, USA (Dethlefs 2009).

Contemporary vehicular loadings tend to be heavier and longer with more axles; thus, highway bridges often encounter inordinate stresses and experience accelerated deterioration (Deng et al. 2019; Zhou et al. 2020). Previous research documents that an average service life of timber bridges is 23 to 27 years without major rehabilitation (Srikanth et al. 2022). When the extent of damage is moderate, member-level repairs may be performed (e.g., epoxy injection, fastening, splicing, and plating, Dahlberg et al. 2012); however, if the capacity of load-carrying elements is found insufficient, explicit means should be sought to address critical issues at the structure level. In contrast with replacement, repair offers a variety of benefits, namely, minimal traffic control, affordable expense, convenience, customized execution, and priority-based decision-makings (Peterson and Gutkowski 1999; Khan 2010). Additionally, from a practical standpoint, bridge professionals prefer repair techniques that are familiar, prevalent, application-oriented, easy-to-implement, and long-lasting.

Load rating is a convenient metric to assess the present state of bridges with an emphasis on identifying allowable live loads that would not adversely affect their functionality (AASHTO 2017). The intrinsic notion of load rating is drawn from a comparison between the current

capacity of a bridge and expected load magnitudes, which can figure out the restriction limit of truck weights to warrant operational requirements in a transportation network. Ratings are also beneficial in understanding the realistic conditions of bridge structures that may not necessarily be the same as those assumed when they were designed initially. Two rating levels are prescribed in the American Association of State Highway and Transportation Officials (AASHTO) Manual for Bridge Evaluation (AASHTO 2017): the Inventory level is aligned with customary design loads and the Operating level represents the maximum permissible live load to which a bridge may be subjected. Finite element modeling is commonly accepted for rating analysis (Ravazdezh et al. 2021; Sofi and Steelman 2021); while, albeit uncommon, destructive testing can be undertaken to ascertain the actual capacity of a bridge (Alkhrdaji et al. 2001). Among others that are specified in the AASHTO Manual for Bridge Evaluation (AASHTO 2017), the Allowable Stress Rating (ASR) method traditionally dominates the rating of timber bridges (CDOT 2022). Nonetheless, the fact that little guidance is available on rating repaired timber bridges leads to overly conservative evaluations by ignoring interactions between existing and newly added members (CDOT 2022). Research is necessitated to fill this identified gap in practice, so that federal and state agencies can assure reliable transportation services across the board.

This part explores the implications of steel-beam repairs for the rating of timber bridges that have served traffic loadings for over 80 years. Upon outlining field work with pictorial explanations, computational models are formulated and validated against site data. An extensive parametric study incorporating 17 live loads renders indispensable information for examining the rating factors of these bridges. A mechanics-based rating method is proposed to quantify the contribution of the repair.

### III.2. Research Significance

Degraded civil infrastructure is a primary concern in modern society and transportation authorities expend a substantial amount of resources every year (Renne et al. 2020). The necessity of an appropriate bridge management program is consistently growing. In 2022, the federal government of the United States spent $36.6 billion and subsidized $94.5 billion for states (USA Facts 2023). Proper ratings are essential in bridge management because incorrect appraisals bring about potential hazards, traffic controls, and needless repairs (Boothby and Craig 1997). Considering that the size, weight, and axle number of trucks and trailers are

archetypal factors that impinge upon the behavior and safety of bridge structures (Luskin and Walton 2001), holistic investigations are a prerequisite when developing evaluation approaches. The research aims to clarify rating mechanisms for timber bridges that are repaired with steel beams and to adduce a systematic methodology within the boundary of ASR, thereby assisting bridge engineers in gaining a new perspective on the accomplishment of sustainable built-environments.

**Table III.1**. Material properties of Douglas Fir used for modeling the F-22-V Bridge

| | $E_L$ (ksi) | $E_T$ (ksi) | $E_R$ (ksi) | $G_{LT}$ (ksi) | $G_{TR}$ (ksi) | $G_{LR}$ (ksi) | $\mu_{LT}$ | $\mu_{TR}$ | $\mu_{LR}$ |
|---|---|---|---|---|---|---|---|---|---|
| Value | 1,570 | 80 | 110 | 120 | 11 | 100 | 0.029 | 0.374 | 0.292 |

$E$ = elastic modulus; G = shear modulus; $\mu$ = Poisson's ratio; $L$ = longitudinal; $T$ = tangential; $R$ = radial

**Table III.2**. Condition rating of timber bridges

| | F-22-V (inspection year = 2019) | | | H-20-T (inspection year = 2021) | | |
|---|---|---|---|---|---|---|
| | Deck | Superstructure | Substructure | Deck | Superstructure | Substructure |
| Value | 6 | 4 | 6 | 6 | 5 | 6 |

Rating scale of Federal Highway Administration (FHWA 1995): 6 = *Satisfactory condition* (structural elements show some minor deterioration), 5 = *Fair condition* (all primary structural elements are sound but may have minor section loss, cracking, spalling or scour), and 4 = *Poor condition* (advanced section loss, deterioration, spalling or scour)

### III.3. Repair of Existing Bridges and Rating Loads

#### III.3.1. Bridge configuration

Two bridges were selected for repair, which were located in Washington County and El Paso County, Colorado, USA (F-22-V and H-20-T, respectively). The F-22-V Bridge, constructed in 1938, had 3 spans (23 ft, each) with 14 Douglas Fir girders (Figs. III.1(a) and (b)). The dimension of the girders was 6 in. in width and 20 in. in depth, spaced at 26.75 in. The H-20-T Bridge was built in 1935 and possessed 4 spans (22.5 ft, each) supported by 14 Douglas Fir girders (6 in. wide by 20 in. deep and girder spacings of 32 in.) at a skew angle of 30$^o$ (Figs. III.1(c) and (d)). Both bridges were designed to resist a two-axle truck load weighing 15 tons (HS15) and the amount of measured average daily traffic (ADT) was 720 vehicles for F-22-V and 3,800 vehicles for H-20-T. Table III.1 enumerates the mechanical properties of Douglas Fir based on the USDA Wood Handbook (USDA 2010). According to recent inspection data (Table III.2), the decks and substructures of the bridges were in satisfactory condition; however, their superstructures were rated to be poor and fair conditions. As such, the Colorado Department of

Transportation (CDOT) initiated repair projects to improve the performance of the superstructures.

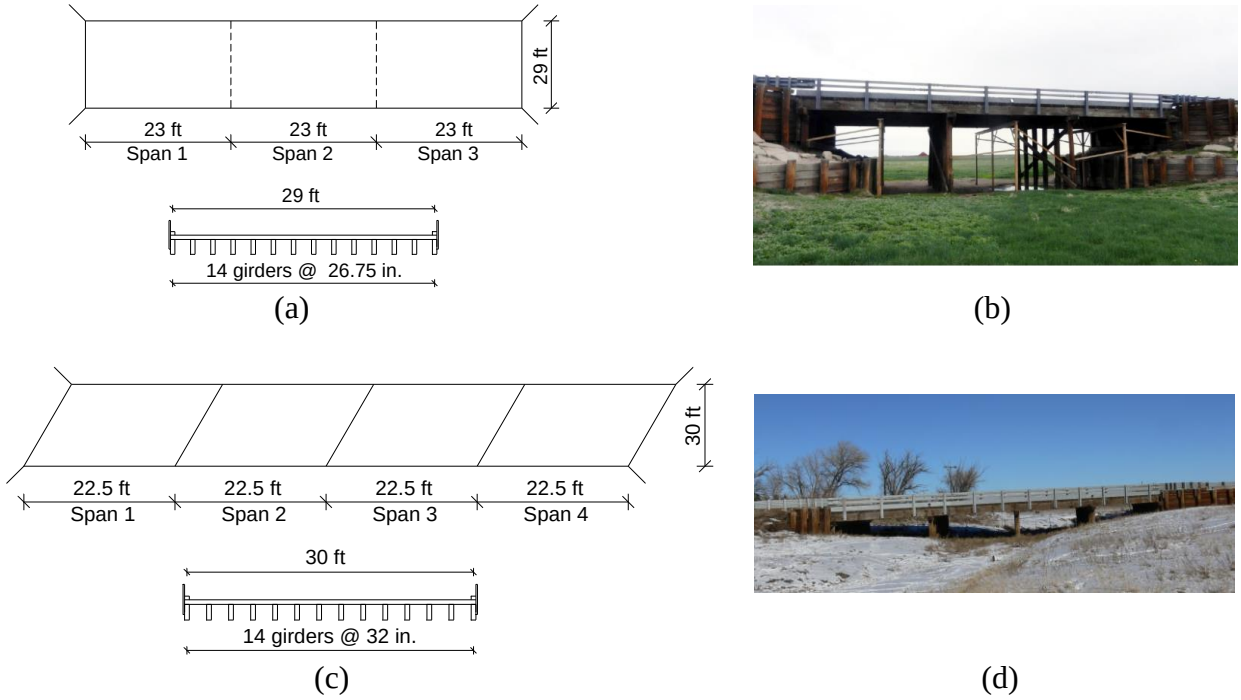


**Fig. III.1**. Constructed timber bridges in Colorado, USA: (a) dimension of F-22-V; (b) site view of F-22-V; (c) dimension of H-20-T; (d) site view of H-20-T

### III.3.2. Repair using hollow structural sections

A hollow structural section (HSS) was chosen to upgrade the capacity of the superstructures. The designation of steel HSS beams was 12×8×5/16 (12 in. deep×8 in. wide×0.29 in. thick for F-22-V) and 12×6×3/8 (12 in. deep×6 in. wide×0.35 in. thick for H-20-T), and the grade was ASTM A500C (elastic modulus ($E_s$) = 29,000 ksi, yield strength ($f_y$) = 520 ksi, and Poisson's ratio = 0.3). Figures III.2(a) to (c) depict the schematic views of the installed HSS. All beams were precut to fit the bridge spans and bent to provide a 3 in. camber at midspan. The procedure of repair work is detailed below and selected pictures are visible in Figs. III.2(d) to (g):

- Step 1: end diaphragms and cross bracings were removed
- Step 2: one HSS beam was located next to a target timber girder (Fig. III.2(d)). In addition, at least 2 steel members were allocated per travel lane

- Step 3: steel bearing blocks (HSS 9×7×5/16, 9 in. deep×7 in. wide×0.29 in. thick) were placed above pier caps (Fig. III.2(e)). Steel shim plates with a thickness of 3 mm were inserted between the longitudinal HSS beam and the bearing blocks until the beam was snug tight.
- Step 4: a 0.7 mm diameter hole was drilled through the girder at midspan and an all threaded rod (0.63 in. in diameter) was inserted through the HSS beam and the girder (Fig. III.2(f)). Nuts were snug-tightened with plate washers (2 in. ×2 in.).
- Step 5: the diaphragms and cross bracings were replaced and field-fitted to avoid a gap. These secondary structural members were then connected to the girder (Fig. III.2(g)).

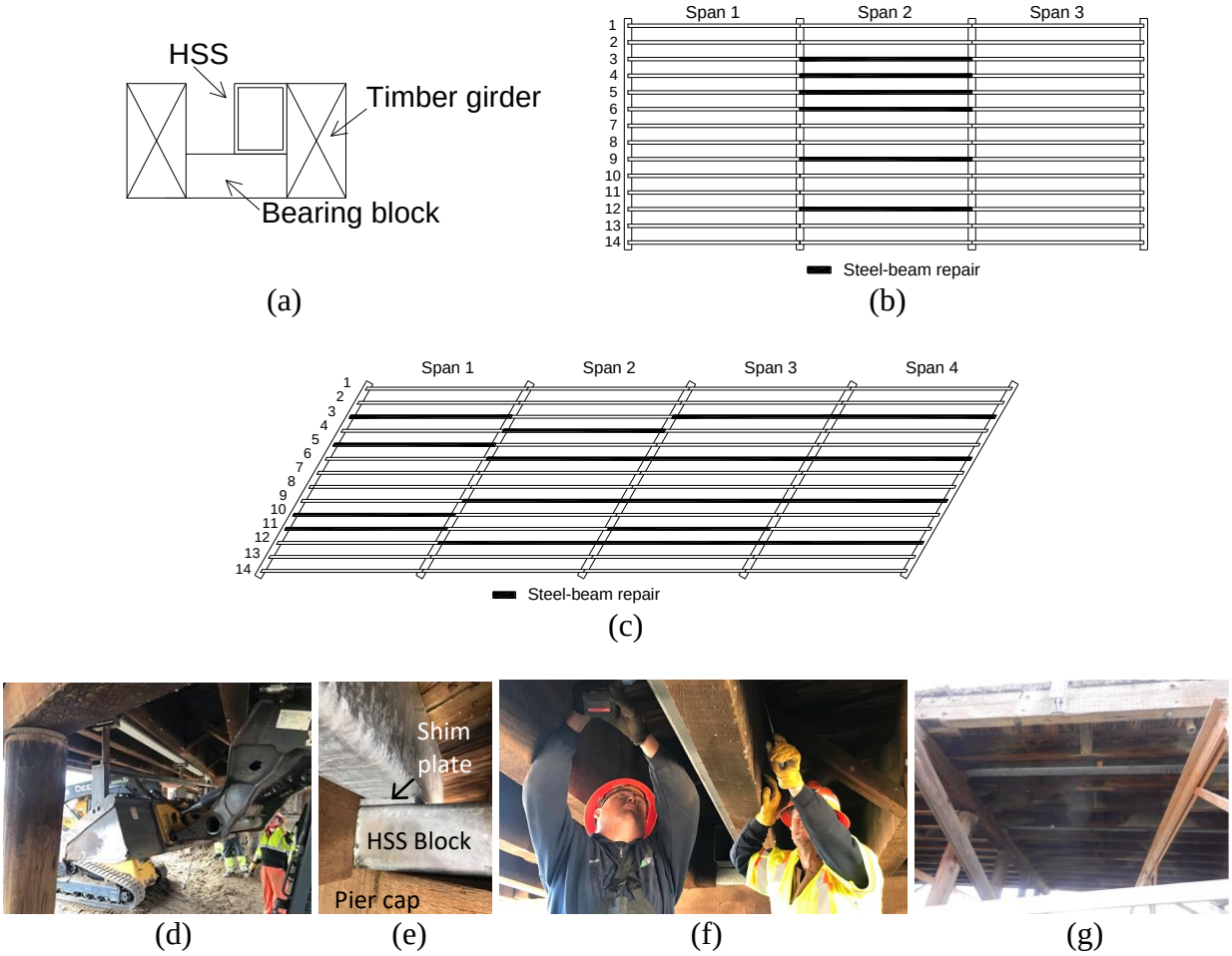


**Fig. III.2**. Repair with hollow structural sections (HSS): (a) schematic view; (b) HSS installation locations of F-22-V; (c) HSS installation locations of H-20-T; (d) lifting of HSS; (e) assembled HSS system; (f) drilling for connection; (g) completion

### III.3.3. Live load

Assorted trucks were employed to study the response and rating of the timber bridges with and without repair. A total of 17 live loads were adopted from the CDOT Rating Manual (CDOT 2022), as shown in Fig. III.3. Although the axle loads and spacing of the trucks differed in the longitudinal direction, the width of the trucks and axle gage distance were identical (10 ft and 6 ft, respectively). In the state of Colorado, three rating levels are stipulated (CDOT 2022): Design Load Rating, Legal Load Rating, and Permit Load Rating. For the Design Load Rating, HS20 and HL93 are used (Figs. III.3(a) and (b), respectively). Regarding the Legal Load Rating, Colorado Legal Trucks (Figs. III.3(c) to (e)), Interstate Legal Trucks (Figs. 3(f) to (h)), Specialized Hauling Vehicles (Figs. III.3(i) to (m)), and Fixing America's Surface Transportation Act's Emergency Vehicles (Figs. III.3(n) and (o)) are included. If a Legal Load Rating is less than the gross truck weight limit, the bridge is posted and a strengthening task can be assigned. To cover the Permit Load Rating, Colorado Permit Vehicle (Fig. III.3(p)) and Colorado Modified Tandem Vehicle (Fig. III.3(q)) are utilized. It is worth noting that the Colorado Permit Vehicle is the maximum allowable weight per axle group and is applied when new bridge members are designed for the Strength II Limit State (overload) of the AASHTO Load and Resistance Factor Design (LRFD) Bridge Design Specifications (BDS) (AASHTO 2020). The design live loads (Figs. III.3(a) and (b)) are intended to calculate the Inventory and Operating levels, while other trucks (Figs. III.3(c) to (q)) are to compute the Operating level.

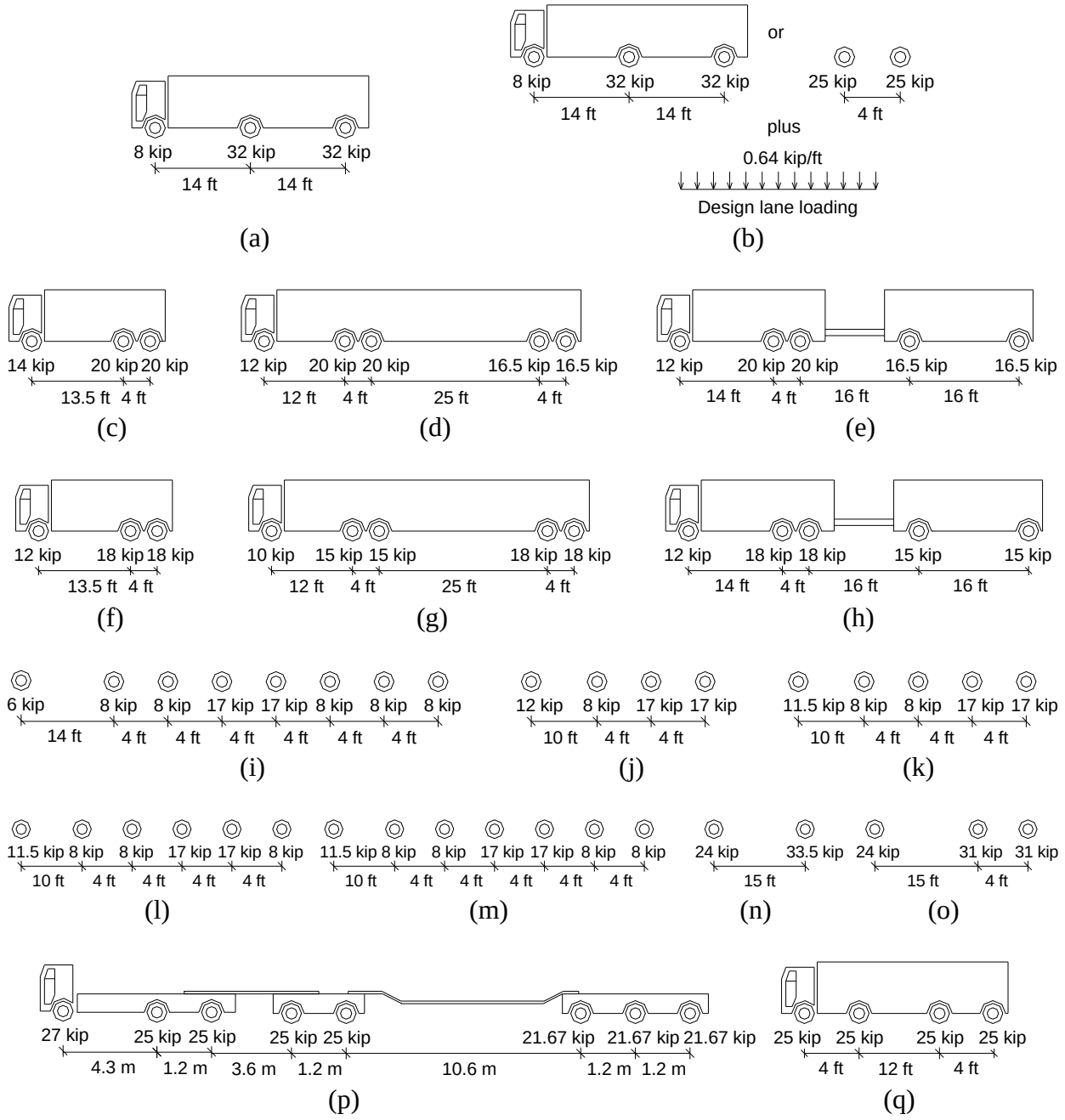


**Fig. III.3**. Live loads used for loading bridges: (a) HS20; (b) HL93; (c) Colorado Legal Type 3; (d) Colorado Legal Type 3S2; (e) Colorado Legal Type 3-2; (f) Interstate Legal Type 3; (g) Interstate Legal Type 3S2; (h) Interstate Legal Type 3-2; (i) Hauling Vehicle A; (j) Hauling Vehicle SU4; (k) Hauling Vehicle SU5; (l) Hauling Vehicle SU6; (m) Hauling Vehicle SU7; (n) Emergency Vehicle 2 (EV2); (o) Emergency Vehicle 3 (EV3); (p) Colorado Permit Vehicle; (q) Colorado Modified Tandem Vehicle

### III.4. Finite Element Modeling

#### III.4.1. Formulation

The behavior of the F-22-V and H-20-T bridges was predicted with commercial software, CSiBridge (CSI 2016). Four-node shell and two-node frame elements represented the deck and girders of the bridges, respectively, both of which had three translational and three rotational degrees of freedom per node. Because these superstructural components were connected by nails with a shank diameter of 0.24 in., local slips were likely when loaded. For this reason, linear elastic link elements were positioned between the shell and the frame elements to simulate relative displacements. The stiffness of the link elements ($K_{link}$) was taken from Eurocode 5 (CEN 2004):

$$K_{link} = \frac{\rho_t^{1.5} d}{23} \tag{III.1}$$

$$\rho_t = \sqrt{\rho_{dk} \rho_{gr}} \tag{III.2}$$

where $\rho_t$, $\rho_{dk}$, and $\rho_{gr}$ are the densities of the superstructure, deck, and girder, respectively ($\rho_{dk} = \rho_{gr}$ = 50 lb/ft$^3$ in accordance with AASHTO LRFD BDS (AASHTO 2020)); and $d$ is the diameter of the nail. This refined modeling technique differs from conventional grillage models and simplified perfect bond models (Zhou et al. 2021; Nader et al. 2023). The aforementioned material properties were input and the girders were supported by hinges and rollers. The connections between the timber girders and steel beams (the threaded rods and bearing blocks at mid- and end-spans) were reproduced by the link elements with rigid stiffness. Afterward, moving load analysis that was built upon the concept of influence line was conducted using the 17 rating live loads (Fig. III.3). Further details on the theory and developmental steps of the bridge models are available elsewhere (CSI 2016).

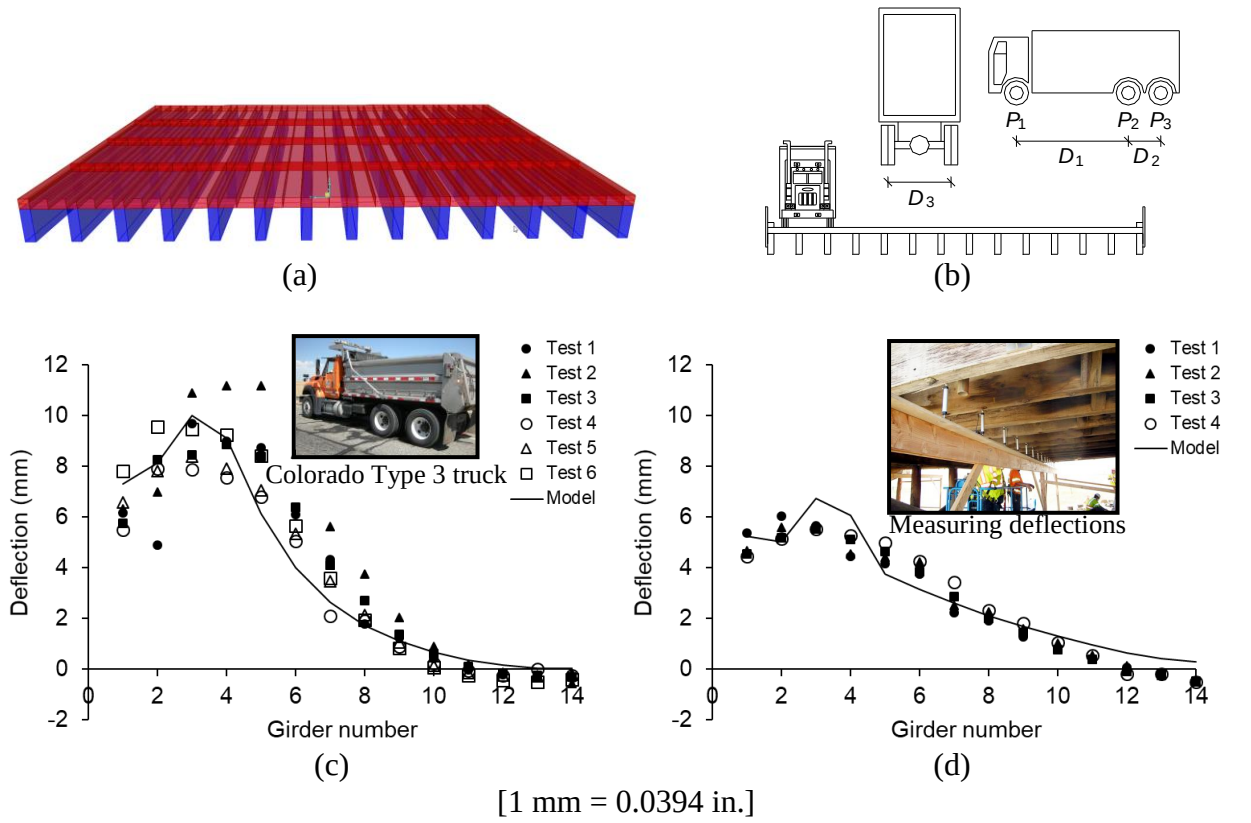


**Fig. III.4**. Finite element modeling of F-22-V: (a) bridge model; (b) loading scheme; (c) validation with unrepaired case under Colorado Type 3 truck; (d) validation with repaired case under Colorado Type 3 truck

### III.4.2. Validation

The modeling approach was validated against the load test data of F-22-V. While a concise summary is given in this section, a full description about the site work can be found in Part II. The constructed bridge model (Fig. III.4(a)) was subjected to a single Colorado Type 3 Legal truck (Fig. III.4(b)). The measured truck weight was 60 kips ($P_1$ = 15.5 kips and $P_2$ = $P_3$ = 22.25 kips; $D_1$ = 13.5 ft, $D_2$ = 4 ft, and $D_3$ = 6 ft) and it was situated to generate the maximum bending of the bridge (Fig. III.4(c), inset). The test was repeated 10 times (6 times without repair and 4 times with repair) and the bridge response was logged by linear variable displacement transducers at midspan (Fig. III.4(d), inset). The average distance between the inside curb face and the rear axle outside tire was 25.4 in. As shown in Fig. III.4(c), the deflections of the unrepaired girders underneath the loaded region (Girders 1 to 5) were greater than those of others. An analogous trend was noticed for the repaired girders (Fig. III.4(d)); however, the magnitude of the deflections was lower than their unrepaired counterparts. This observation was attributed

to the fact that the applied truck load was shared by the timber girders and the steel beams (i.e., a redistribution of the live load). Despite some discrepancies, the model prediction agreed with the site data: the average absolute margin between the measured and computed deflections of Girders 1 to 5 was 17.0% and 16.6% for the unrepaired and repaired cases, respectively.

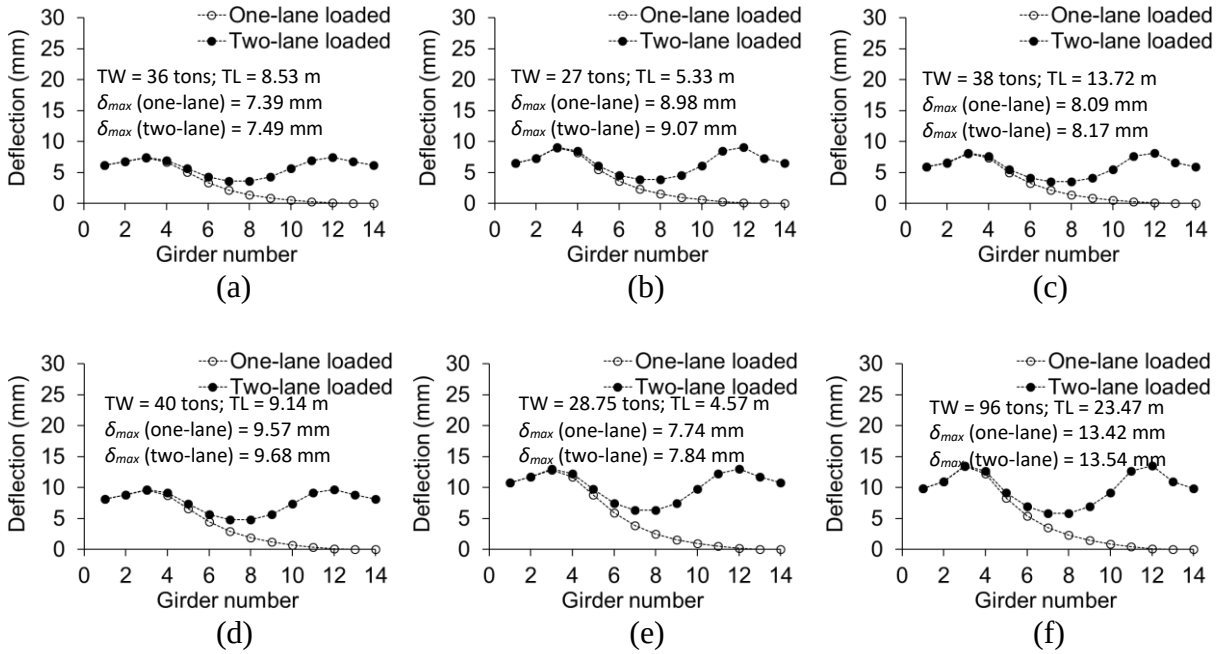


[1 mm = 0.0394 in.; 1 m = 3.3 ft]

**Fig. III.5**. Deflection profiles of unrepaired F-22-V under selected truck loads (TW = truck weight in total; TL = truck length from front to rear axles): (a) HS20; (b) Colorado Legal Type 3; (c) Interstate Type 3S2; (d) Hauling Vehicle A; (e) Emergency Vehicle 2; (f) Colorado Permit

### III.4.3. Flexural Behavior

Figure III.5 exhibits the deflection profiles of the unrepaired F-22-V bridge under selected live loads. The HS20 truck generated the maximum deflections of 7.39 mm (0.291 in.) and 7.49 mm (0.295 in.) for the one- and two-lane loaded cases, respectively (Fig. III.5(a)), and the individual configurations were dependent upon the position of the truck. Although the total weight of Colorado Legal Type 3 (27 tons) was less than that of HS20 (36 tons), the deflections increased by 21.5% and 21.1% for the one- and two-lane loaded cases, respectively (Fig. III.5(b)). This is due to the reduced distance between the front and rear axles (5.33 m (17.6 ft) for Colorado Legal Type 3 vs. 8.53 m (28 ft) for HS20), which resulted in the so-called concentrated load effect. A similar tendency was found between Interstate Type 3S2 and Hauling Vehicle A in Figs. III.5(c)

and (d), where a reduction of 33.4% in the axle-to-axle distance was responsible for the increased deflections of 18.3% and 18.5% belonging to the one- and two-lane loads, respectively. Such observations, however, are not always valid as can be seen in Figs. III.5(e) and (f). Even if the axle-to-axle distance of Emergency Vehicle 2 (4.57 m (15 ft)) was much shorter than the distance of Colorado Permit (23.47 m (77 ft)), the deflection under Colorado Permit was 173.4% higher than the instance of Emergency Vehicle 2 (13.42 mm (0.528 in.) vs. 7.74 mm (0.305 in.)) owing to a significant difference in the total weights (96 tons vs. 28.75 tons). It is, thus, recommended that sophisticated modeling be carried out when the ramifications of nonconforming features (other than the customary design loads of HS20 and HL93) are examined. The flexural responses of H-20-T with the steel beams are plotted in Fig. III.6. For facilitating discussions on the effectiveness of the repair, the predicted results were normalized to show a ratio between deflections with and without the steel beams. The responses before and after the repair entailed inappreciable variations without regard to the types of the live loads and the number of the loaded lanes. This signifies that a single methodology can be used to generate consistent evaluation outcomes for timber bridges repaired with steel sections.

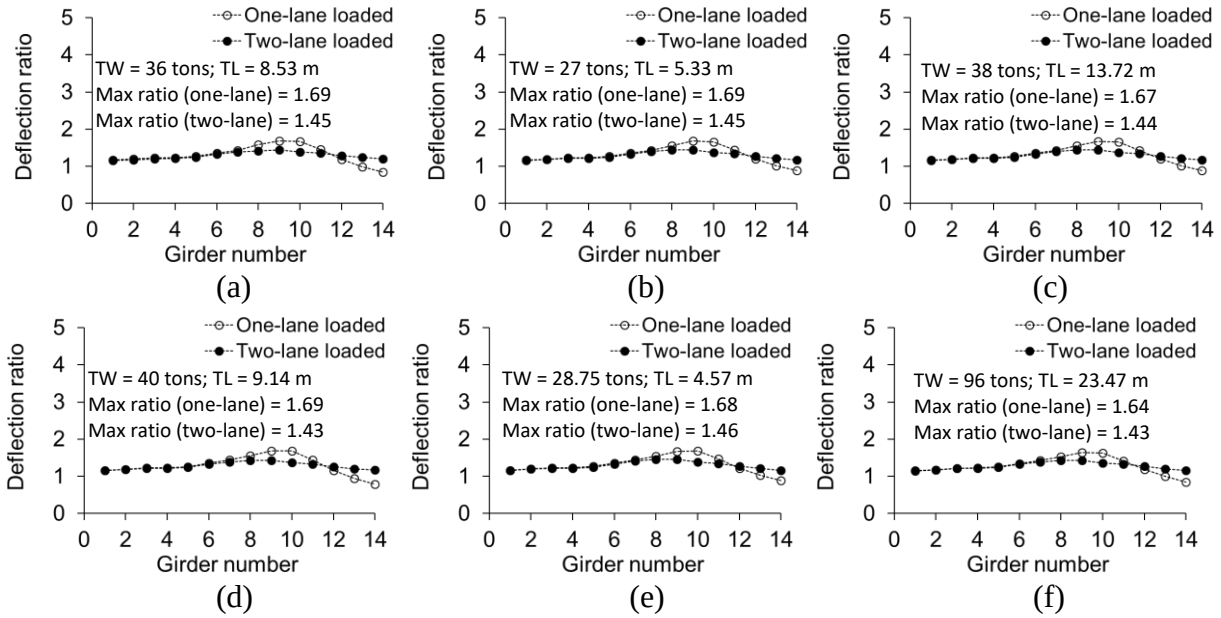


[1 mm = 0.0394 in.; 1 m = 3.3 ft]

**Fig. III.6**. Deflection ratios of H-22-T with and without steel beams under selected truck loads (TW = truck weight in total; TL = truck length from front to rear axles; ratio = deflection after repair to deflection before repair): (a) HS20; (b) Colorado Legal Type 3; (c) Interstate Type 3S2; (d) Hauling Vehicle A; (e) Emergency Vehicle 2; (f) Colorado Permit

## III.5. Rating Factors

### III.5.1. Allowable stress rating

Complying with the CDOT Rating Manual (CDOT 2022), the safe live load capacity of the timber bridges may be determined by

$$RF = \frac{C - A_1 D}{A_2 L\left(1 + I\right)} \tag{III.3}$$

where *RF* is the rating factor of the bridge; *C* is the capacity of the bridge; *D* and *L* are the dead and live load effects, respectively; *I* is the impact factor (*I* = 0% for timber bridges, AASHTO 2017); $A_1$ and $A_2$ are the dead and live load constants, respectively ($A_1 = A_2 = 1.0$ for the Allowable Stress Rating method).

### III.5.2. Capacity adjustment

The capacity adjustment factor ($\alpha_{adj}$) of the timber bridges is proposed to be

$$\alpha_{adj} = \frac{M_{rep}}{M_0} \tag{III.4}$$

where $M_{rep}$ and $M_0$ are the moment capacities of the repaired and control girders, respectively. As per the theory of bending combined with the transformed section method,

$$M_{rep} = \frac{F_r I_{rep}}{\left(h_w - y_{rep}\right)} \tag{III.5}$$

$$M_0 = \frac{F_r I_0}{y_0} \tag{III.6}$$

$$y_{rep} = \frac{b_w h_w^2 + n h_s A_s}{2\left(b_w h_w + n A_s\right)} \tag{III.7}$$

$$I_{rep} = b_w h_w \left[\left(\frac{h_w}{2} - y_{rep}\right)^2 + \frac{h_w^2}{12}\right] + \left[n A_s \left(\frac{h_s}{2} - y_{rep}\right)^2 + \frac{b_s' h_s^3}{12}\right] \tag{III.8}$$

where $F_r$ is the modulus of rupture of the timber; $I_{rep}$ and $I_0$ are the moment of inertia of the repaired and control sections, respectively; $b_w$ and $h_w$ are the width and depth of the timber girder; $n$ is the modular ratio ($n = E_s/E_w$, in which $E_s$ and $E_w$ are the elastic moduli of the steel and wood, respectively); $h_s$ and $A_s$ are the height and cross-sectional area of the steel beam, respectively; $b'_s$ is the width of the transformed steel section ($b'_s = nA_s/h_s$); and $y_{rep}$ and $y_0$ are the distance from the neutral axis to the extreme tension fiber of the girder with and without the repair, respectively. Substituting Eqs. III.5 and III.6 into Eq. III.4 yields,

$$\alpha_{adj} = \frac{I_{rep} y_0}{I_0 \left( h_w - y_{rep} \right)} \tag{III.9}$$

Therefore, the capacity of the repaired girder may be obtained from

$$M_{rep} = \frac{\left( \alpha_{adj} F_r \right) I_0}{y_0} = \frac{F_{Beff} I_0}{y_0} \tag{III.10}$$

where $F_{Beff}$ is the effective bending strength of the timber after the repair. Contemplating a relationship between the flexural strength and shear strength of timber (CEN 2003), the effective shear strength of the timber after the repair ($F_{Veff}$) may be expressed as ($F_r$ and $F_{Veff}$ are in MPa in Eq. III.11)

$$F_{Veff} = 0.2 \left( \alpha_{adj} F_r \right)^{0.8} = 0.2 \left( F_{Beff} \right)^{0.8} \tag{III.11}$$

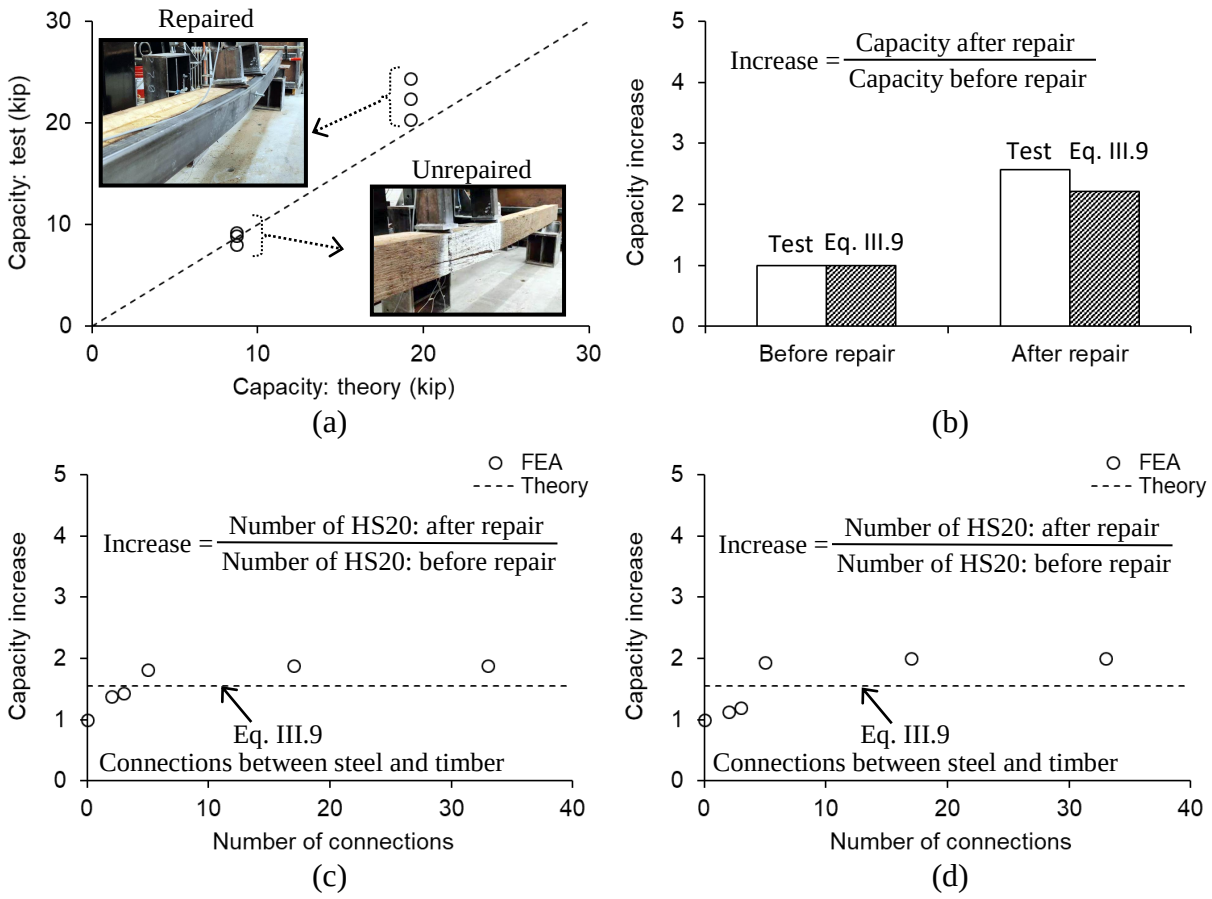


**Fig. III.7**. Flexural capacity of timber girders before and after repair (FEA = finite element analysis): (a) comparison with tests; (b) assessment with test data; (c) F-22-V; (d) H-20-T

### III.5.3. Increased capacity after repair

Prior to executing the capacity adjustment approach, its relevance was appraised. Figure III.7(a) displays test data excerpted from Part I, which loaded Douglas Fir beams with and without repair (inset pictures in Fig. III.7(a)), and predicted results from the proposed approach. For the unrepaired case, the average ultimate loads of the experimental and theoretical beams were 8.72 kips and 8.70 kips, respectively; in contrast, the calculated capacity of the repaired beam was lower than the measured capacities by 14.1%, on average. This discrepancy can be ascribed to the fact that the actual modular ratio $n$ in Eqs. III.7 and III.8 might be higher than the nominal value and that the applied load might not be uniformly distributed to the timber and steel during the test. The increased capacities of the experimental and theoretical beams after the repair were 2.56 and 2.21 times the capacities of the unrepaired beams, respectively (Fig. III.7(b)).

The efficacy of the repair for the F-22-V and H-20-T bridges is charted in Figs. III.7(c) and (d), respectively. To determine the capacity of the bridges, the weight of the HS20 truck (Fig. III.3(a)) was incrementally raised in the finite element analysis (FEA) until the maximum tensile stress of the timber girders reached the modulus of rupture. Subsequently, the number of the trucks was counted before and after the repair to attain a capacity increase ratio, as indicated in Figs. III.7(c) and (d). The ratio was contingent upon the number of connections between the timber and steel at uniform spacings (i.e., the number of the link elements delineated in Sec. III.4.1). When the number of the connections was more than five, increases in the capacity were alike between the FEA and theory (Eq. III.9), which means that full composite action took place. On the site application with three connections at both ends and midspan (Fig. III.2), the average capacity increase was 1.32 (41.9% lower than that of the five connection cases). It is hence stated that the capacity increase after the repair with at least three connections varied from 1.32 to 1.94 and, for practical ratings in the field, the capacity increase is suggested to be 10% lower than the capacity increase estimated by Eq. III.9, stemming from the difference between the theory and the lower bound value of 1.32. Therefore, including the capacity reduction factor ($\kappa$) given in Table III.3 to reflect in-situ degradation over time (MDT 2019), the adjusted nominal capacities of the repaired timber girder for rating become ($F_r$ is in MPa for Eq. III.13):

$$F_{Beff-rating} = 0.9\alpha_{adj}\kappa F_r \qquad \text{for flexure} \qquad \text{(III.12)}$$

$$F_{Veff-rating} = 0.2\left(F_{Beff-rating}\right)^{0.8} \qquad \text{for shear} \qquad \text{(III.13)}$$

**Table III.3**. Capacity reduction due to deterioration (reproduced from MDT 2019)

| Capacity range | Reduction factor | Description |
|---|---|---|
| 100% | 1.0 | Full capacity |
| 80% to 99% | 0.9 | Minor cracks; localized low grade rot; robust maintenance repair |
| 60% to 80% | 0.7 | Moderate cracks; less robust maintenance repair |
| 0% to 60% | 0.0 (remove girders from model) | Severe crack; broken; extreme rot |

### III.5.4. Strength for rating

In conformity with the CDOT rating manual (CDOT 2022), the allowable stress of the unrepaired timber girders was set to $F_r$ = 1,600 psi and 2,128 psi for the Inventory and Operating levels, respectively. These default values were multiplied by several design factors that are defined in the AASHTO Manual for Bridge Evaluation (AASHTO 2017):

$$F_B = F_r C_D C_M C_t C_L C_F C_{fu} C_i C_r \quad \text{(III.14)}$$

where $F_B$ is the adjusted flexural strength of the timber; $C_D$ is the load duration factor; $C_M$ is the wet service factor; $C_t$ is the temperature factor; $C_L$ is the stability factor; $C_F$ is the size factor; $C_{fu}$ is the flat use factor; $C_i$ is the incising factor; and $C_r$ is the repetitive use factor. As guided by the AASHTO Manual for Bridge Evaluation (AASHTO 2017), all of these factors were assigned to be 1.0 except for $C_D$ = 1.15 (two months for cumulative live load effect) and $C_F$ = 0.94 (girder depth = 20 in.). Likewise, the adjusted shear strength of the timber ($F_V$) was expressed by (AASHTO 2017)

$$F_V = F_{V0} C_D C_M C_t C_i \quad \text{(III.15)}$$

where $F_{VO}$ is the default shear strength ($F_{VO}$ = 113 psi and 150 psi for the Inventory and Operating levels, respectively, CDOT 2022). The shear capacity of the timber girder ($V_R$) was converted from Eq. III.15 (AASHTO 2002)

$$V_R = \frac{2}{3} F_V b d \quad \text{(III.16)}$$

where $b$ and $d$ are the width and depth of the girder, respectively. For the repaired bridge, the default allowable stresses for the Inventory level ($F_r$ and $F_{V0}$) were replaced by Eqs. III.12 and III.13, and those were multiplied by 1.33 for the Operating level (AASHTO 2017). Then, the rating factors of F-22-V and H-20-T were calculated using the dead and live load effects (Eq. III.3) in line with the finite element models. The densities of the timber and steel beams were 50 lb/ft$^3$ and 490 lb/ft$^3$, respectively (AASHTO 2020).

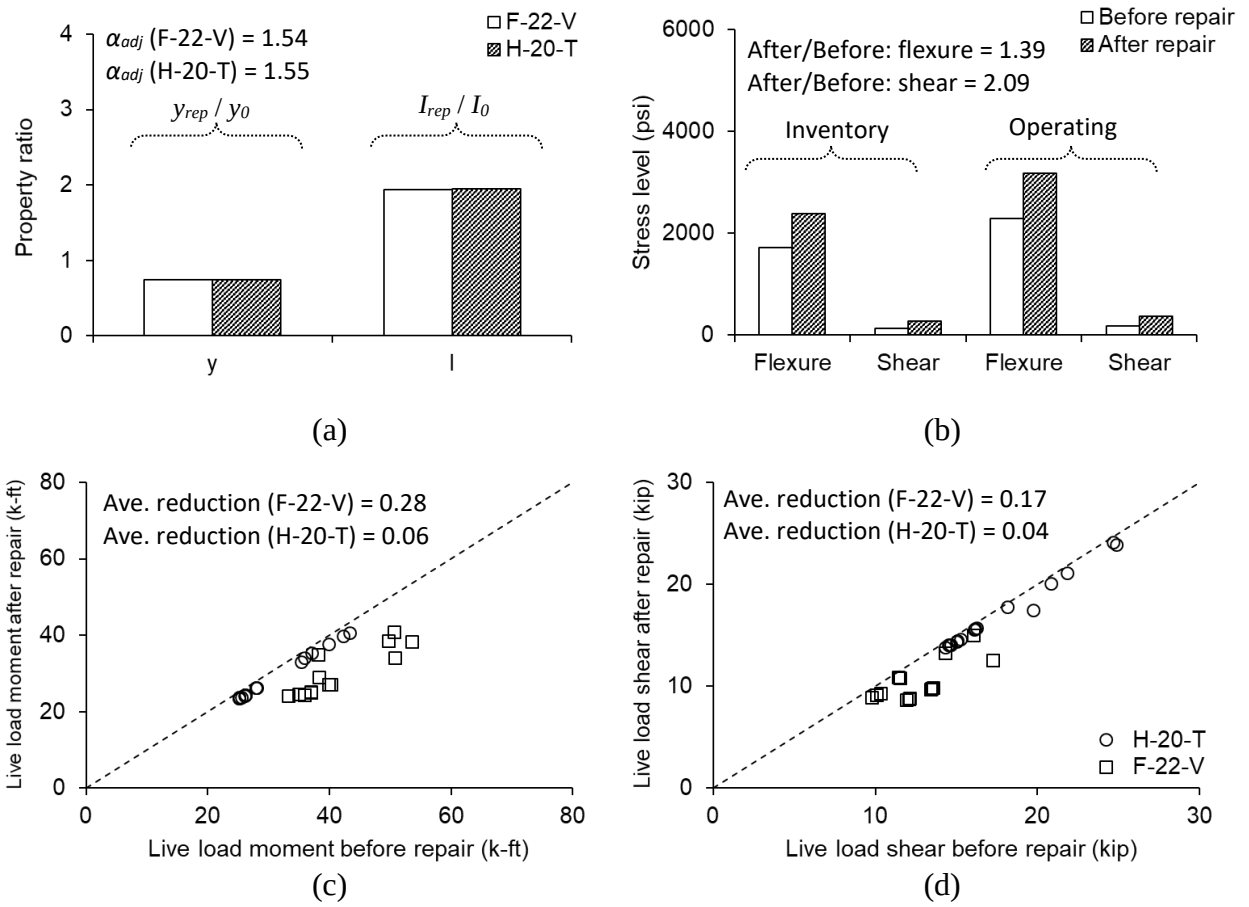


**Fig. III.8**. Consequences of repair: (a) sectional property; (b) stress level; (c) live load moment; (d) live load shear

### III.5.5. Rating calculation

The ramifications of the repair are provided in Fig. III.8. The geometric-property ratios of the two bridges were virtually identical (Fig. III.8(a)); consequently, there was an insignificant difference in their capacity adjustment factors ($\alpha_{adj}$ = 1.54 and 1.55 for F-22-V and H-20-T, respectively). The stress levels of these bridges before and after the repair are shown in Fig. III.8(b). The allowable stresses of the timber girders ($F_r$ and $F_{VO}$) increased by 1.39 and 2.09 for flexure and shear, respectively. Figures III.8(c) and (d) reveal the effects of the live loads (Fig. III.3) with and without the steel beams, which are necessary to compute rating factors. Since more girders were repaired and the steel beams were grouped in F-22-V relative to H-20-T (Fig. III.2(b)), the former experienced better load distributions than the latter; for example, the average reduction of the live load moment was 0.28 and 0.06 for F-22-V and H-20-T, respectively (Fig. III.8(c)). It should be declared that the shear values in Fig. III.8(d) are the maximum forces

collected from the finite element models, rather than design shear at a specific location away from supports (lesser of 3 times the girder depth or at the quarter span point, whichever is less, AASHTO 2002). A comprehensive comparison is made for the rating factors of the bridges with $\kappa$ = 1.0 when subjected to the Design, Legal, and Permit loads (Figs. III.9(a) to (d): Inventory and Operating levels are valid for the Design loads and only Operating is usable for the Legal and Permit loads, CDOT 2022). Regardless of the load types and rating levels, the rating factors were improved; scilicet, all factors after the repair were positioned above the one-to-one reference line. Figures III.9(e) and (f) enumerate rating ratios between the repaired and unrepaired states of the bridges. Overall, the efficacy of the repair was pronounced and F-22-V outperformed H-20-T due to the grouped placement of the steel beams (supplementary information to follow).

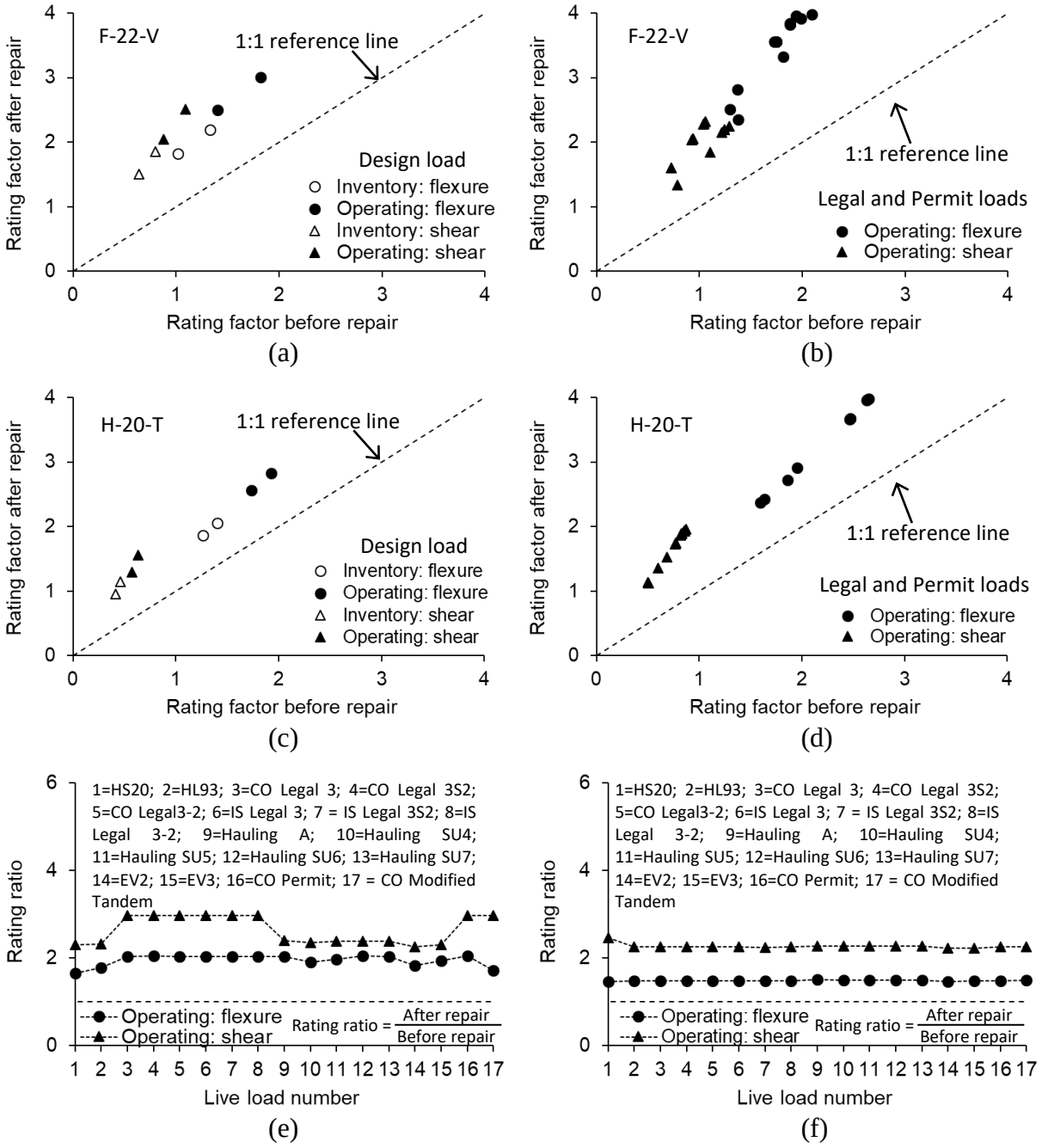


**Fig. 9**. Allowable stress rating: (a) rating factor of F-22-V with design loads; (b) rating factor of F-22-V with legal and permit loads; (c) rating factor of H-20-T with design loads; (d) rating factor of H-20-T with legal and permit loads; (e) rating ratio of F-22-V; (f) rating ratio of H-20-T

### III.6. Parametric Investigations

To supplement the findings of the numerical studies elaborated earlier, parametric investigations were conducted. For consistency and simplification, F-22-V was selected with HS20 and the

properties of the bridge were taken as the defaults, unless otherwise noted. Figures III.10(a) and (b) illustrate the effects of deterioration levels. Complying with the reduction factors listed in Table 3, the capacity of the timber girders varied from 100% to 60%. The enhanced ratings after the repair were prominent (Fig. III.10(a)) and the efficaciousness of the repair went up as the reduction factor declined (Fig. III.10(b)). This fact implies that timber bridges that have suffered considerable deterioration can be suitable candidates for upgrading their ratings with the steel sections. The influence of the steel beam size is shown in Figs. III.10(c) and (d). The first group (the $12 \times 8$ series, steel section numbers 1 to 4 in Fig. III.10(c)) was focused on the wall thickness of the beams, spanning from $t$ = 0.291 in. to 0.581 in., while the second group (the 5/16 series, steel section numbers 5 to 8 in Fig. III.10(c)) was related to the depth and width of the beams with a constant wall thickness of $t$ = 0.291 in. A wide breadth of rating factors were predicted from 2.59 to 9.60, contingent upon the size of the steel beams (Fig. III.10(c)), which corroborates that the selection of an adequate beam is instrumental for the repair method. The impact of the web thickness was marginal with an average rating increase of 1.80 and 2.33 for flexure and shear, respectively (Section numbers 1 to 4 in Fig. III.10(d)); however, that of the section size was noteworthy up to 5.27 and 4.61 for flexure and shear, respectively (Section numbers 5 to 8 in Fig. III.10(d)). The number of repaired girders was influential in rating the bridge (Fig. III.10(e): No. 1 = the first girder with steel; No. 2 = the second with steel, and so forth, Fig. III.2(b)). As the number increased from 1 to 14 (Fig. III.10(f), inset), the rating ratio steadily rose from 1.63 to 2.04 for flexure and from 2.35 to 2.54 for shear (Fig. III.10(f)). Accordingly, placing the steel beams across the entire superstructure do not seem to be necessary in practice and the designer's discretion is needed to determine the level of improvement; nonetheless, as discussed previously, grouped steel beams will benefit the performance of repaired timber bridges.

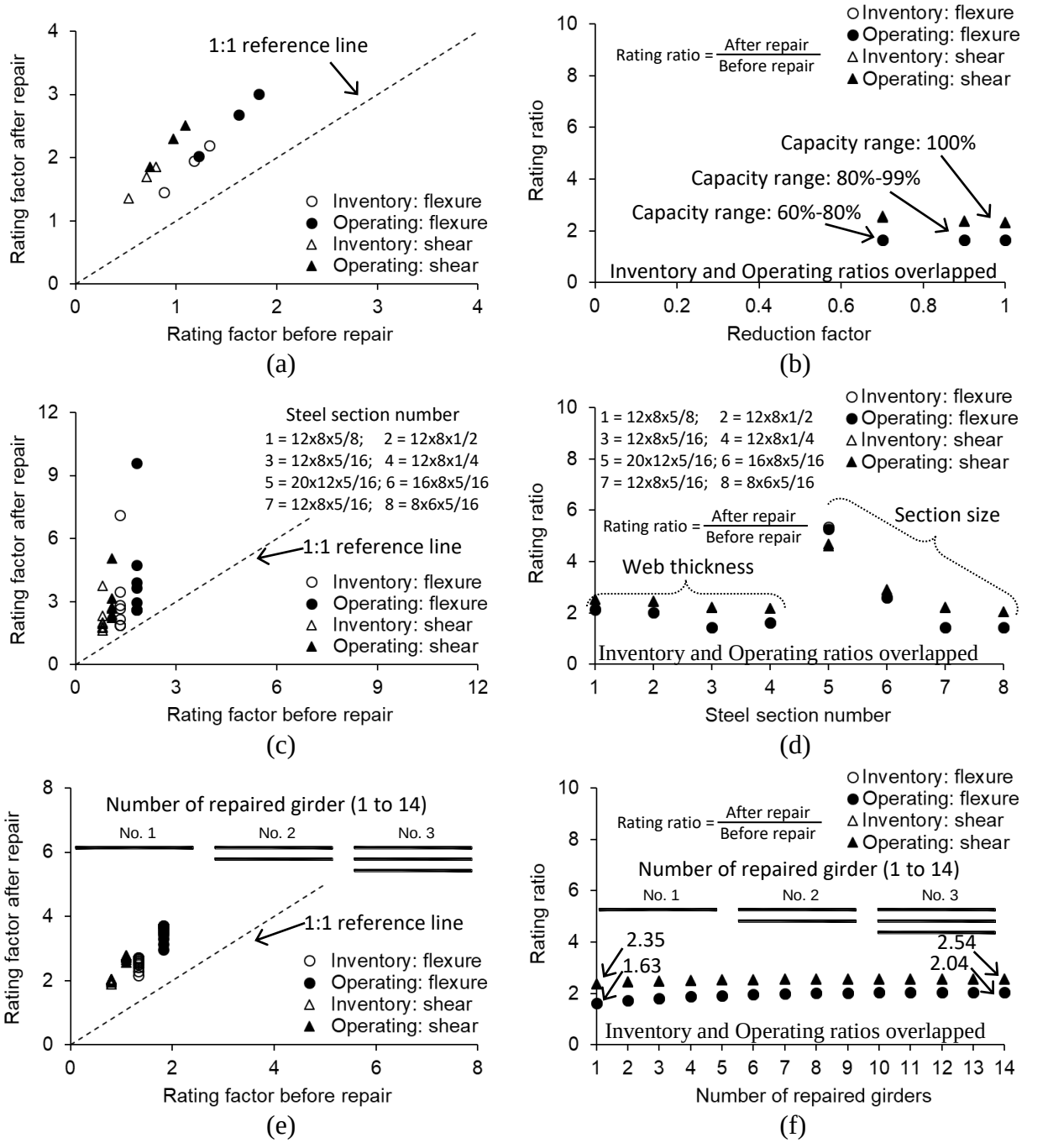


**Fig. III.10**. Parametric investigations: (a) deterioration level- before and after repair; (b) deterioration level- rating ratio; (c) steel section size- before and after repair; (d) steel section size- rating ratio; (e) steel section arrangement- before and after repair; (f) steel section arrangement- rating ratio

**III.7. Safety Analysis**

The safety level of the bridges was quantified by (Barker and Puckett 2013)

$$\beta = \frac{\ln\left(C/\left(D+L\right)\right)}{\sqrt{COV_C^2 + COV_D^2 + COV_L^2}} \quad \text{(III.17)}$$

where $\beta$ is the reliability index and $COV$ is the coefficient of variation ($C$ = capacity, $D$ = dead load, and $L$ = live load). Published literature guides that the components of Eq. III.17 for Douglas Fir bridges show lognormal distributions with the succeeding values (Bakht 1983; Nowak and Eamon 2008; Yamasaki et al. 2010; Olsson et al. 2018): $COV_c$ = 0.22, $COV_D$ = 0.089, and $COV_L$ = 0.12. The probability of failure ($P_f$) can then be inferred from

$$P_f = \Phi(-\beta) \quad \text{(III.18)}$$

where $\Phi(.)$ is the standard normal cumulative distribution. Figure III.11(a) demonstrates the reliability indexes of F-22-V and H-20-T (the Operating levels in flexure are shown, controlling traffic restrictions in most agencies, Wang et al. 2011). The degree of reliability rose owing to the steel beam repair and the probability of failure remarkably diminished by 99.2% and 96.7% for F-22-V and H-20-T, respectively. The reliability indexes and corresponding failure probabilities associated with the parametric studies are given in Figs. III.11(b) to (d). On all occasions, the use of the steel beams was more effective for the Operating levels than the Inventory levels in terms of reducing the failure probability; in other words, the repair method is expected to preclude the catastrophic collapse of decrepit timber bridges.

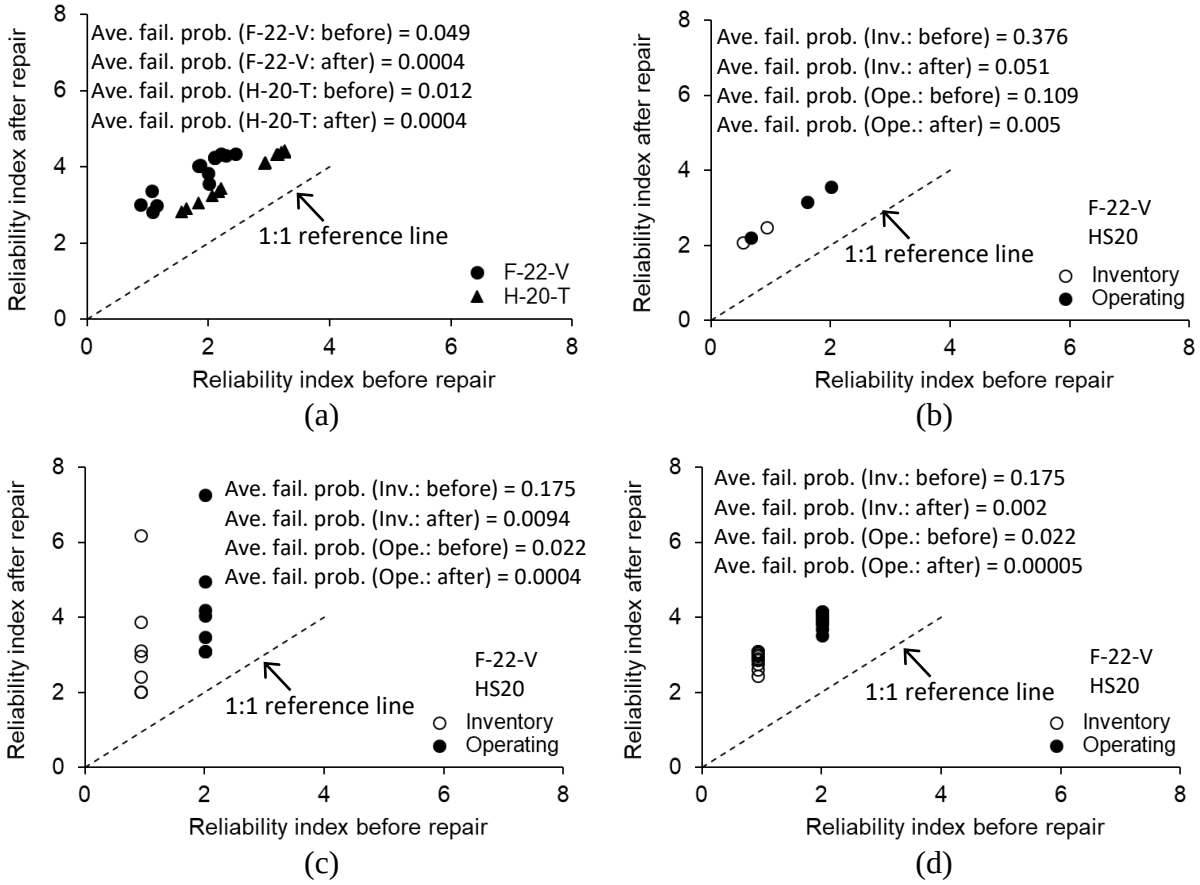


**Fig. III.11**. Safety analysis: (a) Operating level under 17 rating live loads; (b) deterioration level; (c) steel section size; (d) steel section arrangement

### III.8. Summary and Conclusions

This part has dealt with the rating of timber bridges repaired with hollow structural sections: ASTM A500C steel beams. Two bridges (F-22-V and H-20-T constructed in 1938 and 1935, respectively) were strengthened and load testing was performed with a known-weight truck of 60 kips. To calculate the rating factors of these bridges under 17 live loads specified in the CDOT Rating Manual (CDOT 2022), finite element models were developed and predicted responses were validated against in-situ data. A mechanics-based method was proposed to rate these bridges before and after the repair, including the capacity adjustment and capacity reduction factors ($\alpha_{adj}$ and $\kappa$, respectively). Through a parametric study, the implications of deterioration, section size, and beam arrangement were elucidated. The level of safety was quantified by the principle of reliability in order to deduce the probability of failure. The following are concluded:

- The deflection profiles of the bridges were dependent upon the configuration and position of the live loads and, in general, concentrated load effects alongside reduced axle spacings caused noticeable deflections. Such a propensity was maintained after installing the steel beams, denoting that an integrated approach can embrace the ratings of the timber bridges with and without the repair work.
- The capacity of the repaired girders was as high as 2.56 times that of the control girders. The number of connections between the timber girders and steel beams influenced the efficacy of the repair. For practice with at least three connections (two at supports and one at midspan), the capacity of the upgraded girder was proposed to be 10% less than the analytical capacity derived from transformed section theory.
- On the rating of F-22-V and H-20-T after the repair, the allowable stress of the constituent girders increased by 1.39 and 2.09 for flexure and shear, respectively. The effectiveness of the repair was prominent in the context of elevating the rating factors of the bridges, irrespective of the load types and rating levels.
- When the level of deterioration ascended in timber, the repair technique became more useful for ameliorating the state of the bridges within a capacity reduction factor of $\kappa$ = 1.0 to 0.7 (i.e., a capacity range of 100% to 60% for the girders). The consequences of increasing the depth of the steel sections were pronounced in raising the rating factors, relative to adjusting the thickness of the sections. The placement of grouped steel beams was recommendable to capitalize on the repair system. The repair reduced the probability of failure by 99.2% and 96.7% for the F-22-V and H-20-T bridges, respectively.

**III.9. References**

AASHTO. 2002. Standard specifications for highway bridges (17th edition), American Association of State Highway and Transportation Officials, Washington, D.C.

AASHTO. 2017. The manual for bridge evaluation (3rd edition), American Association of State Highway and Transportation Officials, Washington, D.C.

AASHTO. 2020. LRFD bridge design specifications (9th edition), American Association of State Highway and Transportation Officials, Washington, D.C.

Alkhrdaji, T., Nanni, A., Chen, G., and Barker, M. 2001. Destructive and non-destructive testing of Bridge J857 Phelps County, Missouri, Report No. CIES 99-08A, Missouri Department of Transportation, Jefferson City, MO.

Bakht, B. 1983. Statistical analysis of timber bridges, Journal of Structural Engineering, 109(8), 1761-1779.

Barker, R.M. and Puckett, J.A. 2013. Design of highway bridges: an LRFD approach, John Wiley & Sons, Inc., Hoboken, NJ.

Boothby, T.E. and Craig, R.J. 1997. Experimental load rating study of a historic truss bridge, Journal of Bridge Engineering, 2(1), 18-26.

CDOT. 2022. Bridge rating manual, Colorado Department of Transportation, Denver, CO.

CEN. 2003. Timber structures- strength classes (EN338), European Committee for Standardization, Brussels, Belgium.

CSI. 2016. CSI analysis reference manual, Computers and Structures, Inc., Berkeley, CA.

Dahlberg, J., Phares, B., Bigelow, J., and Klaiber, F.W. 2012. Timber abutment piling and back wall rehabilitation and repair, Report No. IHRB Project TR-616, Bridge Engineering Center, Iowa State University, Ames, IA.

De Araujo, V. 2023. Timber construction as a multiple valuable sustainable alternative: main characteristics, challenge remarks and affirmative actions, International Journal of Construction Management, 23(8), 1334-1343.

Deng, L., Yan, W., and Nie, L. 2019. A simple corrosion fatigue design method for bridges considering the coupled corrosion-overloading effect, Engineering Structures, 178, 309-317.

Dethlefs, R. 2009. Collapse of the Wimer Covered Timber Bridge, Forensic Engineering Congress, American Society of Civil Engineers, 133-142.

FHWA. 2022. National Bridge Inventory (NBI), Federal Highway Administration, Washington, D.C.

Khan, M. 2010. Bridge and highway structure rehabilitation and repair, McGraw Hill, New York, NY.

Kromoser, B., Spitzer, A., Ritt, M., and Grabner, M. 2023. Wooden bridges: strategies for design, construction and wood Species - from tradition to future, International Journal of Architectural Heritage, doi.org/10.1080/15583058.2023.2181719, published online: Mar 5, 2023

Lokuge, W., Wilson, M., Tran, H., and Setunge, S. 2019. Predicting the probability of failure of timber bridges using fault tree analysis, Structure and Infrastructure Engineering, 15(6), 783-797.

Luskin, D.M. and Waltron, C.M. 2001. Effects of truck size and weights on highway infrastructure and operations, Project Summary Report 2122-S, Center for Transportation Research, Austin, TX.

MDT. 2019. Interim guidance for load rating of timber bridges, Montana Department of Transportation, Helena, MT.

Nader, R.N., Tousignant, K., Smith, G., and Newhook, J.P. 2023. Evaluation of the CHBDC simplified method of analysis for transverse wood deck on wood girder bridges, Canadian Journal of Civil Engineering, In-Press

Nowak, A.S. and Eamon, C.D. 2008. Reliability analysis of plank decks, Journal of Bridge Engineering, 13(5), 540-546.

Olsson, A. Pot, G., Viguier, J., Faydi, Y., and Oscarsson, J. 2018. Performance of strength grading methods based on fibre orientation and axial resonance frequency applied to Norway spruce (Picea abies L.), Douglas fir (Pseudotsuga menziesii (Mirb.) Franco) and European oak (Quercus petraea (Matt.) Liebl./Quercus robur L.), Annals of Forest Science, 75, Article No. 102

Peterson, M.L. and Gutkowski, R.M. 1999. Evaluation of the structural integrity of timber bridges, NDT & E International, 32, 43-48.

Rashidi, M., Hoshyar, A.N., Smith, L., Samali, B., and Siddique, R. 2021. A comprehensive taxonomy for structure and material deficiencies, preventions and remedies of timber bridges, Journal of Building Engineering, 34, 101624.

Ravazdezh, F., Seok, S., Haikal, G., and Ramirez, J.A. 2021. Effect of nonstructural elements on lateral load distribution and rating of slab and T-beam bridges, Journal of Bridge Engineering, 26(9), 04021063.

Renne, J., Wolshon, B., Murray-Tuite, P., and Pande, A. 2020. Emergence of resilience as a framework for state Departments of Transportation (DOTs) in the United States, Transportation Research Part D, 82, 102178.

Sofi, F.A. and Steelman, J.S. 2021. Using committees of artificial neural networks with finite element modeling for steel girder bridge load rating estimation, Structures, 33, 533-553.

Srikanth, I., Arockiasamy, M., and Nagarajan, S. 2022. Performance of aging timber bridges based on field tests and deterioration models, Transportation Research Record, 2676(10), 315-327.

Tazarv, M., Carnahan, Z., and Wehbe, N. 2019. Glulam timber bridges for local roads, Engineering Structures, 188, 11-23.

USA Facts. 2023. What does America spend on transportation and infrastructure? Is infrastructure improving? USA Facts, https://usafacts.org/state-of-the-union/transportation-infrastructure (accessed April 15, 2023)

USDA. 2010. Wood handbook: wood as an engineering material, United States Department of Agriculture, Madison, WI.

Wang, N., O'Malley, C., Ellingwood, B.R., and Zureick, A.-H. 2011. Bridge rating using system reliability assessment. I: assessment and verification by load testing, Journal of Bridge Engineering, 16(6), 854-862.

Yamasaki, M., Sasaki, Y., and Iilima, Y. 2010. Determining Young's modulus of timber on the basis of a strength database and stress wave propagation velocity II: effect of the reference distribution database on the determination, Journal of Wood Science, 56, 380-386.

Zhou, J., Liu, Y., and Yi, J. 2020. Effect of uneven multilane truck loading of multigirderbridges on component reliability, Structural Concrete, 21(4), 1644-1661.

Zhu, W., Li, L., Gong, M., and Chui, Y.-H. 2021. On-site monitoring of the moisture content of bridge decks made of nail-laminated timbers, Journal of Structural Engineering, 147(7), 04721005.

**Appendix: Examples for Rating Timber Girders with and without Steel-Beam Repair**
(Demonstration purposes only)

## A. Repair with HSS 12×8×5/16 beam

### A.1. Bridge Data

Year built: 1938
Material: Douglas Fir
Timber properties: $E_w$ = 1,570 ksi and MOR = 7.7 ksi
Condition: minor cracks and localized low grade rot
Traffic: Two lanes
Span: 23 ft
Skew: 0°
Deck: 6 in. thick
Girder dimension: $b_w$ = 6 in. wide by $h_w$ = 20 in. deep
Girder spacing: 26.75 in.
Repair method: HSS 12×8×5/16 beam ($h_s$ = 12 in. deep × $b_s$ = 8 in wide × $t_s$ = 0.2913 in. thick; $A_s$ = 11.3 in.$^2$)
Steel beam grade: ASTM A500C ($E_s$ = 29,000 ksi and $f_y$ = 50 ksi)
Rating truck: HS20

### A.2. Section Properties

Before repair:

$$y_0 = \frac{h_w}{2} = \frac{20}{2} = 10 \text{ in.}$$

$$I_0 = \frac{b_w h_w^3}{12} = \frac{6(20)^3}{12} = 4{,}000 \text{ in.}^4$$

$$S_0 = \frac{I_0}{h_w/2} = \frac{4{,}000}{20/2} = 400 \text{ in.}^3$$

$A_w = b_w h_w = 6(20) = 120$ in.$^2$

After repair:

$$n = \frac{E_s}{E_w} = \frac{29{,}000}{1{,}570} = 18.5$$

$$y_{rep} = \frac{b_w h_w^2 + n h_s A_s}{2(b_w h_w + n A_s)} = \frac{6(20)^2 + 18.5(12)(11.3)}{2(6\times 20 + 18.5\times 11.3)} = 7.5 \text{ in.}$$

$$b_s' = n\frac{A_s}{h_s} = 18.5\frac{11.3}{12} = 17.4 \text{ in.}$$

$$I_{rep} = b_w h_w \left[ \left( \frac{h_w}{2} - y_{rep} \right)^2 + \frac{h_w^2}{12} \right] + \left[ nA_s \left( \frac{h_s}{2} - y_{rep} \right)^2 + \frac{b_s' h_s^3}{12} \right]$$

$$= 6(20) \left[ \left( \frac{20}{2} - 7.5 \right)^2 + \frac{20^2}{12} \right] + \left[ 18.5 \times 11.3 \left( \frac{12}{2} - 7.5 \right)^2 + \frac{17.4 \times 12^3}{12} \right]$$

$$= 7{,}726 \text{ in.}^4$$

$$\alpha_{adj} = \frac{I_{rep} y_0}{I_0 \left( h_w - y_{rep} \right)} = \frac{7{,}726(10)}{4{,}000(20 - 7.5)} = 1.55$$

**A.3. Load Analysis**

The following information is given for interior girders:

Flexure
Before repair: dead load ($D$) = 6.3 k-ft and live load ($L$) = 38.2 k-ft
After repair: dead load ($D$) = 8.9 k-ft and live load ($L$) = 32.0 k-ft

Shear
Before repair: dead load ($D$) = 1.1 kips and live load ($L$) = 11.5 kips
After repair: dead load ($D$) = 1.5 kips and live load ($L$) = 10.8 kips

**A.4. Allowable Stress Rating**

**A.4.1. Impact**

No impact for timber members:

$I = 0$

**A.4.2. Stresses to be used**

**A.4.2.1. Baseline stresses**

For flexure
$F_B = F_r C_D C_M C_t C_L C_F C_{fu} C_i C_r$

For shear
$F_V = F_{V0} C_D C_M C_t C_i$

$F_B$ = adjusted flexural strength of timber
$C_D$ = load duration factor ($C_D$ =1.15)
$C_M$ = wet service factor ($C_M$ =1.0)
$C_t$ = temperature factor ($C_t$ =1.0)
$C_L$ = stability factor ($C_L$ =1.0)
$C_F$ = size factor ($C_F$ = 0.94)
$C_{fu}$ = flat use factor ($C_{fu}$ =1.0)
$C_i$ = incising factor ($C_i$ =1.0)
$C_r$ = repetitive use factor ($C_r$ =1.0)

**A.4.2.2. Inventory Level Stresses**
Before repair

$F_r$ = 1,600 psi for flexure (from CDOT Rating Manual)
$F_{V0}$ = 85 psi for shear (from CDOT Rating Manual)

After repair

$F_r = F_{Beff-rating} = 0.9\alpha_{adj}\kappa F_r$ = 0.9(1.55)(0.9)(1,600) = 2,009 psi for flexure

$F_{V0} = F_{Veff-rating} = 0.2\left(F_{Beff-rating}\right)^{0.8}$ = 0.2(2,009)$^{0.8}$ = 87.8 psi for shear

**A.4.2.3. Operating Level Stresses**
Before repair

$F_r$ = 2,128 psi for flexure (from CDOT Rating Manual)
$F_{V0}$ = 113 psi for shear (from CDOT Rating Manual)

After repair

$F_r = F_{Beff-rating} = 0.9\alpha_{adj}\kappa F_r$ = 0.9(1.55)(0.9)(2,128) = 2,672 psi for flexure

$F_{V0} = F_{Veff-rating} = 0.2\left(F_{Beff-rating}\right)^{0.8}$ = 0.2(2,672)$^{0.8}$ = 110.3 psi for shear

**A.4.3. Rating Factors**
**A.4.3.1. Inventory level rating for flexure**
Before repair

$F_B = F_r C_D C_M C_t C_L C_F C_{fu} C_i C_r$ = 1,600(1.15)(1.0)(1.0)(1.0)(0.94)(1.0)(1.0)(1.0) = 1,730 psi

$M_R = F_B S_0$ = 1,730(400) = 692 kip-in. = 57.7 kip-ft

$$RF = \frac{C - A_1 D}{A_2 L\left(1+I\right)} = \frac{57.7 - 1\times 6.3}{1\times 38.2\left(1+0\right)} = 1.35$$

After repair

$F_B = F_r C_D C_M C_t C_L C_F C_{fu} C_i C_r$ = 2,009(1.15)(1.0)(1.0)(1.0)(0.94)(1.0)(1.0)(1.0) = 2,172 psi

$M_R = F_B S_0$ = 2,172(400) = 869 kip-in. = 72.4 kip-ft

$$RF = \frac{C - A_1 D}{A_2 L\left(1+I\right)} = \frac{72.4 - 1\times 8.9}{1\times 32.0\left(1+0\right)} = 1.98$$

**A.4.3.2. Inventory level rating for shear**
Before repair

$F_V = F_{V0}C_DC_MC_tC_i$ = 85(1.15)(1.0)(1.0)(1.0) = 97.8 psi

$$V_R = \frac{2}{3}F_V bd = \frac{2}{3}(97.8)(6)(20) = 7.8 \text{ kips}$$

$$RF = \frac{C - A_1 D}{A_2 L(1+I)} = \frac{7.8 - 1\times 1.1}{1\times 11.5(1+0)} = 0.58$$

After repair

$F_V = F_{V0}C_DC_MC_tC_i$ = 87.8(1.15)(1.0)(1.0)(1.0) = 100.9 psi

$$V_R = \frac{2}{3}F_V bd = \frac{2}{3}(100.9)(6)(20) = 8.1 \text{ kips}$$

$$RF = \frac{C - A_1 D}{A_2 L(1+I)} = \frac{8.1 - 1\times 1.5}{1\times 10.8(1+0)} = 0.61$$

**A.4.3.3. Operating level rating for flexure**
Before repair

$F_B = F_rC_DC_MC_tC_LC_FC_{fu}C_iC_r$ = 2,128(1.15)(1.0)(1.0)(1.0)(0.94)(1.0)(1.0)(1.0) = 2,300 psi

$M_R = F_BS_0$ = 2,300(400) = 920 kip-in. = 76.7 kip-ft

$$RF = \frac{C - A_1 D}{A_2 L(1+I)} = \frac{76.7 - 1\times 6.3}{1\times 38.2(1+0)} = 1.84$$

After repair

$F_B = F_rC_DC_MC_tC_LC_FC_{fu}C_iC_r$ = 2,672 (1.15)(1.0)(1.0)(1.0)(0.94)(1.0)(1.0)(1.0) = 2,888 psi

$M_R = F_BS_0$ = 2,888(400) = 1,155 kip-in. = 96.3 kip-ft

$$RF = \frac{C - A_1 D}{A_2 L(1+I)} = \frac{96.3 - 1\times 8.9}{1\times 32.0(1+0)} = 2.73$$

**A.4.3.4. Operating level rating for shear**

Before repair

$F_V = F_{V0}C_DC_MC_tC_i$ = 113(1.15)(1.0)(1.0)(1.0) = 129.9 psi

$$V_R = \frac{2}{3}F_V bd = \frac{2}{3}(129.9)(6)(20) = 10.4 \text{ kips}$$

$$RF = \frac{C - A_1 D}{A_2 L(1+I)} = \frac{10.4 - 1\times 1.1}{1\times 11.5(1+0)} = 0.81$$

After repair

$F_V = F_{V0}C_DC_MC_tC_i$ = 110.3(1.15)(1.0)(1.0)(1.0) = 127 psi

$$V_R = \frac{2}{3}F_V bd = \frac{2}{3}(127)(6)(20) = 10.2 \text{ kips}$$

$$RF = \frac{C - A_1 D}{A_2 L(1+I)} = \frac{10.2 - 1\times 1.5}{1\times 10.8(1+0)} = 0.81$$

**A.4.4. Summary of Rating Factors**

**Table A.1**. Summary of Allowable Stress Rating for Interior Girder

| Method | | Rating factor | | |
|---|---|---|---|---|
| | | Before repair | After repair | Increase |
| Moment | Inventory | 1.35 | 1.98 | 46.7% |
| | Operating | 1.84 | 2.73 | 48.4% |
| Shear | Inventory | 0.58 | 0.61 | 5.2% |
| | Operating | 0.81 | 0.81 | 0.0% |

Note: steel-beam repair is mainly for increasing flexural capacity rather than shear

**B. Repair with HSS 16×8×5/16 beam**

**B.1. Bridge Data**
Year built: 1935
Material: Douglas Fir
Timber properties: $E_w$ = 1,570 ksi and MOR = 7.7 ksi
Condition: minor cracks and localized low grade rot
Traffic: Two lanes
Span: 22.5 ft
Skew: 30°
Deck: 6 in. thick
Girder dimension: $b_w$ = 6 in. wide by $h_w$ = 20 in. deep
Girder spacing: 32 in.
Repair method: HSS 16×8×5/16 beam ($h_s$ = 16 in. deep × $b_s$ = 8 in wide × $t_s$ = 0.2913 in. thick; $A_s$ = 13.4 in.$^2$)
Steel beam grade: ASTM A500C ($E_s$ = 29,000 ksi and $f_y$ = 50 ksi)
Rating truck: HS20

**B.2. Section Properties**
Before repair:

$$y_0 = \frac{h_w}{2} = \frac{20}{2} = 10 \text{ in.}$$

$$I_0 = \frac{b_w h_w^3}{12} = \frac{6(20)^3}{12} = 4{,}000 \text{ in.}^4$$

$$S_0 = \frac{I_0}{h_w/2} = \frac{4{,}000}{20/2} = 400 \text{ in.}^3$$

$A_w = b_w h_w = 6(20) = 120$ in.$^2$

After repair:

$$n = \frac{E_s}{E_w} = \frac{29{,}000}{1{,}570} = 18.5$$

$$y_{rep} = \frac{b_w h_w^2 + n h_s A_s}{2(b_w h_w + n A_s)} = \frac{6(20)^2 + 18.5(16)(13.4)}{2(6\times 20 + 18.5\times 13.4)} = 8.7 \text{ in.}$$

$$b_s' = n\frac{A_s}{h_s} = 18.5\frac{13.4}{16} = 15.5 \text{ in.}$$

$$I_{rep} = b_w h_w\left[\left(\frac{h_w}{2} - y_{rep}\right)^2 + \frac{h_w^2}{12}\right] + \left[nA_s\left(\frac{h_s}{2} - y_{rep}\right)^2 + \frac{b_s' h_s^3}{12}\right]$$

$$= 6(20)\left[\left(\frac{20}{2}-8.7\right)^2+\frac{20^2}{12}\right]+\left[18.5\times13.4\left(\frac{16}{2}-8.7\right)^2+\frac{15.5\times16^3}{12}\right]$$

$$= 9{,}615 \text{ in.}^4$$

$$\alpha_{adj} = \frac{I_{rep}y_0}{I_0\left(h_w - y_{rep}\right)} = \frac{9{,}615(10)}{4{,}000(20-8.7)} = 2.13$$

**B.3. Load Analysis**

The following information is given for interior girders:

Flexure
Before repair: dead load ($D$) = 6.3 k-ft and live load ($L$) = 38.2 k-ft
After repair: dead load ($D$) = 9.4 k-ft and live load ($L$) = 25.8 k-ft

Shear
Before repair: dead load ($D$) = 1.1 kips and live load ($L$) = 11.5 kips
After repair: dead load ($D$) = 1.6 kips and live load ($L$) = 10.4 kips

**B.4. Allowable Stress Rating**

**B.4.1. Impact**

No impact for timber members:

$I = 0$

**B.4.2. Stresses to be used**

**B.4.2.1. Baseline stresses**

For flexure
$F_B = F_r C_D C_M C_t C_L C_F C_{fu} C_i C_r$

For shear
$F_V = F_{V0} C_D C_M C_t C_i$

$F_B$ = adjusted flexural strength of timber
$C_D$ = load duration factor ($C_D$ =1.15)
$C_M$ = wet service factor ($C_M$ =1.0)
$C_t$ = temperature factor ($C_t$ =1.0)
$C_L$ = stability factor ($C_L$ =1.0)
$C_F$ = size factor ($C_F$ = 0.94)
$C_{fu}$ = flat use factor ($C_{fu}$ =1.0)
$C_i$ = incising factor ($C_i$ =1.0)
$C_r$ = repetitive use factor ($C_r$ =1.0)

**B.4.2.2. Inventory Level Stresses**
Before repair

$F_r$ = 1,600 psi for flexure (from CDOT Rating Manual)
$F_{V0}$ = 85 psi for shear (from CDOT Rating Manual)

After repair

$F_r = F_{Beff-rating} = 0.9\alpha_{adj}\kappa F_r$ = 0.9(2.13)(0.9)(1,600) = 2,760 psi for flexure

$F_{V0} = F_{Veff-rating} = 0.2\left(F_{Beff-rating}\right)^{0.8}$ = 0.2(2,760)$^{0.8}$ = 113.2 psi for shear

**B.4.2.3. Operating Level Stresses**
Before repair

$F_r$ = 2,128 psi for flexure (from CDOT Rating Manual)
$F_{V0}$ = 113 psi for shear (from CDOT Rating Manual)

After repair

$F_r = F_{Beff-rating} = 0.9\alpha_{adj}\kappa F_r$ = 0.9(2.13)(0.9)(2,128) = 3,671 psi for flexure

$F_{V0} = F_{Veff-rating} = 0.2\left(F_{Beff-rating}\right)^{0.8}$ = 0.2(3,671)$^{0.8}$ = 142.2 psi for shear

**B.4.3. Rating Factors**
**B.4.3.1. Inventory level rating for flexure**
Before repair

$F_B = F_r C_D C_M C_t C_L C_F C_{fu} C_i C_r$ = 1,600(1.15)(1.0)(1.0)(1.0)(0.94)(1.0)(1.0)(1.0) = 1,730 psi

$M_R = F_B S_0$ = 1,730(400) = 692 kip-in. = 57.7 kip-ft

$$RF = \frac{C - A_1 D}{A_2 L\left(1+I\right)} = \frac{57.7 - 1\times 6.3}{1\times 38.2\left(1+0\right)} = 1.35$$

After repair

$F_B = F_r C_D C_M C_t C_L C_F C_{fu} C_i C_r$ = 2,760(1.15)(1.0)(1.0)(1.0)(0.94)(1.0)(1.0)(1.0) = 2,984 psi

$M_R = F_B S_0$ = 2,984(400) = 1,194 kip-in. = 99.5 kip-ft

$$RF = \frac{C - A_1 D}{A_2 L\left(1+I\right)} = \frac{99.5 - 1\times 9.4}{1\times 25.8\left(1+0\right)} = 3.49$$

**B.4.3.2. Inventory level rating for shear**
Before repair

$F_V = F_{V0}C_DC_MC_tC_i$ = 85(1.15)(1.0)(1.0)(1.0) = 97.8 psi

$$V_R = \frac{2}{3}F_V bd = \frac{2}{3}(97.8)(6)(20) = 7.8 \text{ kips}$$

$$RF = \frac{C - A_1 D}{A_2 L(1+I)} = \frac{7.8 - 1\times 1.1}{1\times 11.5(1+0)} = 0.58$$

After repair

$F_V = F_{V0}C_DC_MC_tC_i$ = 113.2(1.15)(1.0)(1.0)(1.0) = 130.2 psi

$$V_R = \frac{2}{3}F_V bd = \frac{2}{3}(130.2)(6)(20) = 10.4 \text{ kips}$$

$$RF = \frac{C - A_1 D}{A_2 L(1+I)} = \frac{10.4 - 1\times 1.6}{1\times 10.4(1+0)} = 0.84$$

**B.4.3.3. Operating level rating for flexure**
Before repair

$F_B = F_rC_DC_MC_tC_LC_FC_{fu}C_iC_r$ = 2,128(1.15)(1.0)(1.0)(1.0)(0.94)(1.0)(1.0)(1.0) = 2,300 psi

$M_R = F_BS_0$ = 2,300(400) = 920 kip-in. = 76.7 kip-ft

$$RF = \frac{C - A_1 D}{A_2 L(1+I)} = \frac{76.7 - 1\times 6.3}{1\times 38.2(1+0)} = 1.84$$

After repair

$F_B = F_rC_DC_MC_tC_LC_FC_{fu}C_iC_r$ = 3,671 (1.15)(1.0)(1.0)(1.0)(0.94)(1.0)(1.0)(1.0) = 3,968 psi

$M_R = F_BS_0$ = 3,968(400) = 1,587 kip-in. = 132.3 kip-ft

$$RF = \frac{C - A_1 D}{A_2 L(1+I)} = \frac{132.3 - 1\times 9.4}{1\times 25.8(1+0)} = 4.76$$

**B.4.3.4. Operating level rating for shear**

Before repair

$F_V = F_{V0}C_DC_MC_tC_i$ = 113(1.15)(1.0)(1.0)(1.0) = 129.9 psi

$$V_R = \frac{2}{3}F_V bd = \frac{2}{3}(129.9)(6)(20) = 10.4 \text{ kips}$$

$$RF = \frac{C - A_1 D}{A_2 L(1+I)} = \frac{10.4 - 1\times 1.1}{1\times 11.5(1+0)} = 0.81$$

After repair

$F_V = F_{V0}C_DC_MC_tC_i$ = 142.2(1.15)(1.0)(1.0)(1.0) = 163.5 psi

$$V_R = \frac{2}{3}F_V bd = \frac{2}{3}(163.5)(6)(20) = 13.1 \text{ kips}$$

$$RF = \frac{C - A_1 D}{A_2 L(1+I)} = \frac{13.1 - 1\times 1.6}{1\times 10.4(1+0)} = 1.11$$

**B.4.4. Summary of Rating Factors**

**Table B.1**. Summary of Allowable Stress Rating for Interior Girder

| Method | | Rating factor | | |
|---|---|---|---|---|
| | | Before repair | After repair | Increase |
| Moment | Inventory | 1.35 | 3.49 | 158.5% |
| | Operating | 1.84 | 4.76 | 158.7% |
| Shear | Inventory | 0.58 | 0.84 | 44.8% |
| | Operating | 0.81 | 1.11 | 37.0% |

Note: steel-beam repair is mainly for increasing flexural capacity rather than shear